ABSTRACT

Title of Dissertation: INTERFACIAL DEGRADATION OF COPPER
                                   WIRE BONDS IN THERMAL AGING AND
                                   CYCLING CONDITION

                                   Subramani Manoharan,
                                   Doctor of Philosophy, 2019

Dissertation directed by: Professor. Patrick McCluskey,
                                   Department of Mechanical Engineering

Copper (Cu) wire bonds have become the dominant wire material used in microelectronic packages, having replaced gold (Au) in the majority of applications. Cost saving has been the key factor to drive this transition in wire bond material, although there are other advantages to Cu such as better electrical and thermal conductivity, reduced wire sweep during transfer molding and most importantly slower intermetallic compound (IMC) formation with Al (bond pad). Although IMC layers are much thinner than for Au-Al bonded joints, growth of second phase, Cu_9Al_4, due to exposure to high temperature leads to interfacial separation, which is exacerbated under thermal cycling condition ultimately leading to failure of the joint.

Part I of this dissertation aims at addressing the effect of combined loading (thermal aging and cycling) on the reliability of Cu wire bonded devices using a unique long dwell thermal cycling profile that accelerates growth of different IMC phases ($CuAl_2$ and Cu_9Al_4) and accelerates failure due to CTE mismatch between epoxy mold compound, die and Cu wire bond. Unlike many of the

studies presented in literature, the test vehicle in this study are made of commercial off-the-shelf (COTS) parts, where a multitude of factors vary from one another, such as wire diameter, wire bond and bond pad characteristics, etc., the combination of which play a significant role in the life time of these devices and is not fully captured by first-principal models. Hence, a data-based life estimation method is developed, to aid in part selection based on initial bond characteristics. Critical parameters of wire bond that contribute to reliability are identified, the most significant of which is Al bond pad thickness, which controls the growth of IMC and influences time for Cu_9Al_4 IMC phase formation.

Second part of this work is focused entirely on the Al bond pad thickness. Part II-A focuses on the qualitative comparison of pad thickness effect on the quality of initially formed bond through use of bond shear analysis and the effect of bond interface aging on bond shear analysis. Test vehicle consists of three pad thicknesses namely, 0.5 µm, 1 µm and 4 µm, over which Cu wirebonds with four different thermosonic bond recipes are made. Results from Part II-A provide guidelines for bond comparison using bond shear analysis. Part II-B focuses on the effect of bond pad thickness on the reliability of Cu wire bonds under isothermal aging at 175°C and 200°C for 1000 hours and 650 hours respectively. Test vehicle in this study consists of 0.675 µm and 3 µm pad thickness on silicon die in 20 leaded 5x5 QFN package. Wire bonds with one thermosonic bonding recipe are made on all the 90 packages used in the study. Electrical resistance and cross-sectional analysis are used to derive failure times, which is in turn used to build empirical relationship between pad thickness and time to failure. Result from this study shows longer time to failure for wire bonds on 3 µm pad compared to 0.675 µm pad due to delay in Cu_9Al_4 formation.

INTERFACIAL DEGRADATION OF COPPER WIRE BONDS IN THERMAL
AGING AND CYCLING CONDITION

By

Subramani Manoharan

Dissertation submitted to the Faculty of the Graduate School of the

University of Maryland, College Park, in partial fulfillment

of the requirements for the degree of

Doctor of Philosophy

2019

Advisory Committee:

Professor. Patrick McCluskey, Chair

Adjunct Professor. Stevan Hunter

Professor. Abhijit Dasgupta

Professor. Hugh Bruck

Professor. Peter Sandborn

Professor. Mohamad Al-Sheikhly, Dean's Representative

Table of Contents

List of Figures

List of Tables

1. Copper wire bonded interconnection in Microelectronic packages – Literature Review

Wire bonding is the preferred first level interconnection (connection between die and lead) in microelectronic devices and has existed for more than 50 years. Greater than 90% of the semiconductor packages used wire bonding as of 2013 [1]. The alternative to wire bonding is flip chip attach which provides higher I/O capability, but increases the cost, especially due to set-up of infrastructure [2], hence wire bonding has continued to be the dominant first level interconnection method. Bonding of wire as thin as 18µm on bond pads is a micro welding process that results in a robust joint between the different materials as shown in Figure 1.1. Thermosonic bonding process is widely used today, which involves application of temperature and ultrasonic energy on a ball formed on the end of a wire which is pressed at pre-determined force against the substrate (bond pad). Temperature during bonding is maintained between 150ºC-220ºC [3]. The combination of ultrasonic energy, force and temperature softens the wire and pad metallization, forming a metallurgical bond between them [4].
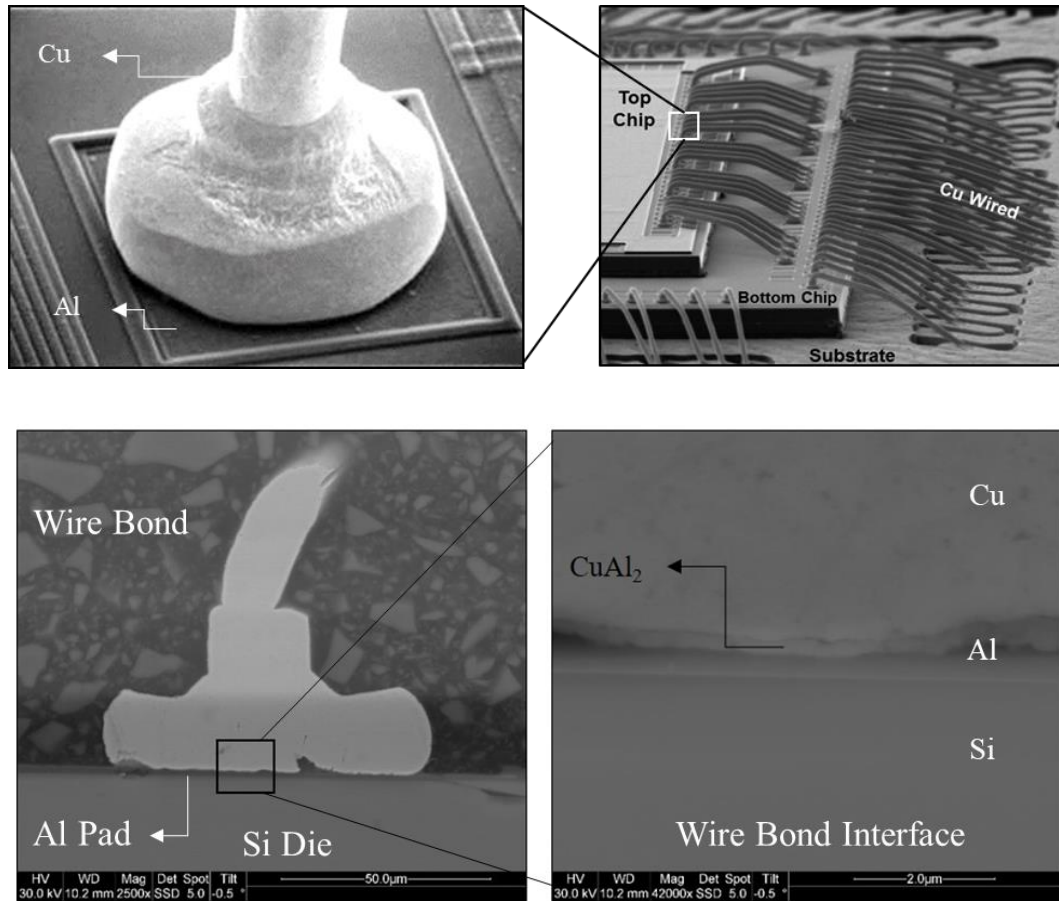
Figure 1.1 Wire bond in microelectronic devices.

Gold was the preferred choice of wire material due to its resistance to oxidation and corrosion, however with the significant increase in its price since mid-2000s, alternative options have gained popularity. Specifically, Cu is a viable material, primarily due to its low cost. Figure 1.2, shows change in wire bond material trend worldwide from 2010 until 2017, where Au wire-bonded devices have reduced from 82% to 16%. Cu and Palladium (Pd) coated Cu (PCC) has replaced Au, rising from 13% in 2010 and to 67% in 2017 [5][6].
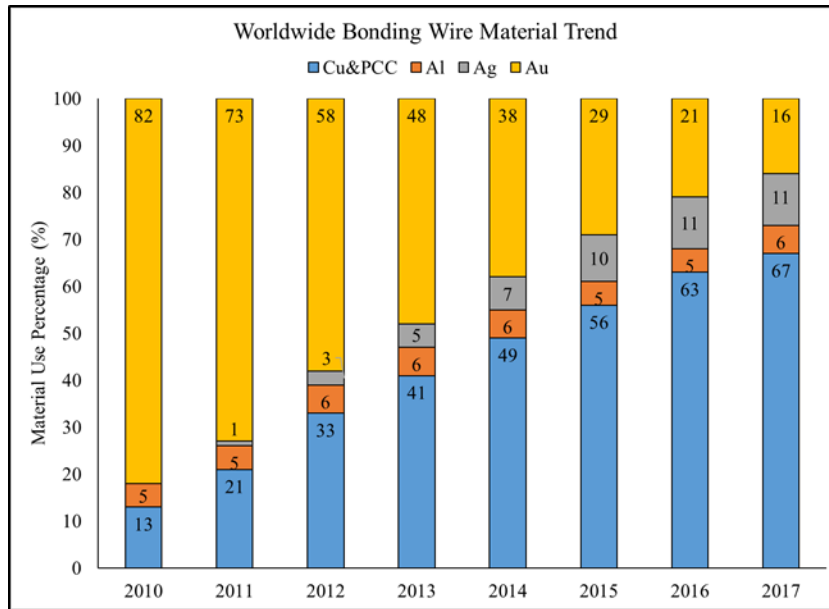
Figure 1.2: World Wide Wire Bonding Trend [5][6].

Wire cost comparison was performed between a 99.99% Cu and 99.99% Au wire (10,000 ft) for three different diameters, 18µm, 25.4µm and 50.8µm. Cost savings for OEMs from switching to Cu were calculated to be 12%, 66% and 85% respectively [7]. However, Cu has several challenges in manufacturing due to its inherent material properties such as increased hardness and high potential for oxidation, and with reliability, especially under thermal aging and thermal cycling conditions. Palesko and Vardaman [8] reported cost for a 31x31mm semiconductor package with 624 I/Os to be $2.19 when assembled with Cu wirebonds compared to $2.65 when assembled with Au. Additionally, a package size-wise cost savings between Au and Cu wire bonds and a competitive technology, flip chip bonding, was presented as shown in Figure 1.3. This shows higher cost savings with flip chip interconnection for large I/O devices such as microprocessors, where I/O greater than 1024 favors flip chip over Au wire bond, however, Cu wire bond is still the cheapest first level interconnection method for package size until as big as 45x45m with 1936 I/Os.

Several family of devices fall within this category due to which majority of the OEMs are converting to this (Cu wire bond) cost saving technology.
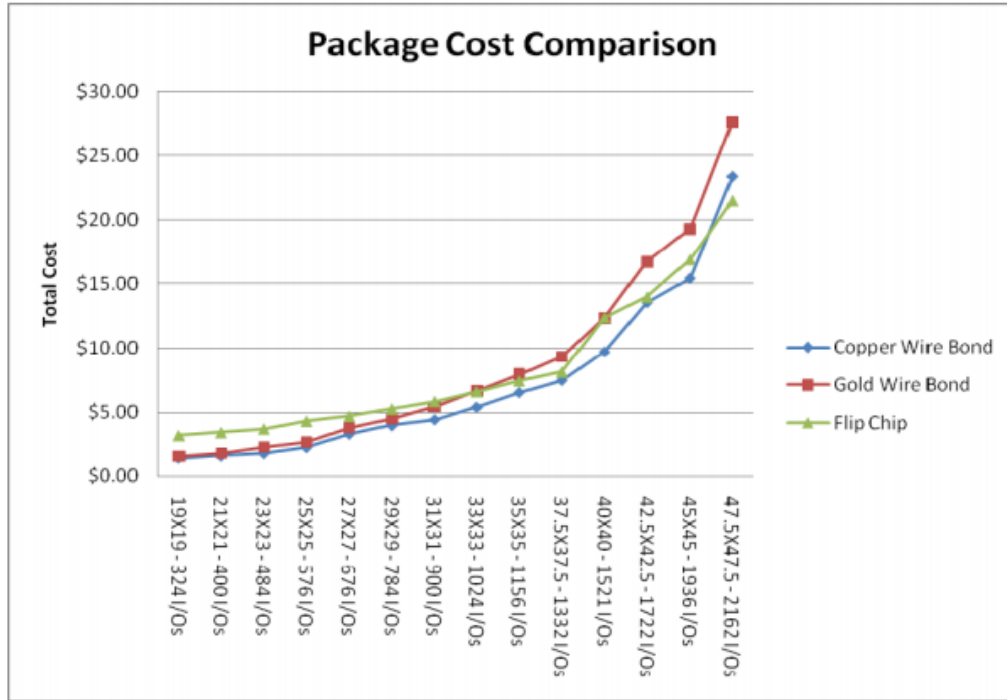
Figure 1.3: Cu vs Au Total Package Cost Comparison [8].

1.1. Comparison between Cu and Au Wire Bond Material

Cu wire bonding is now widely accepted as a replacement for Au, mainly driven by cost savings, although there are other advantages to Cu such as better electrical resistivity (1.7 vs 42.2 $\mu\Omega - cm$) and thermal conductivity (400 vs 320 W/mK), slower intermetallic compound (IMC) formation and reduced wire sweep during transfer molding as shown in **Error! Not a valid bookmark self-reference.**. Automotive, industrial and aerospace market segments, however, are still reluctant to adopt Cu wire bonded products due to perceived risks of wire and bond pad cracks during manufacturing, the potential for corrosion of the IMC and interfacial cracking, and in general due to a lack of understanding about its reliability in harsh conditions.

Table 1.1: Physical Property Comparison between Cu and Au [3].

Physical Properties	Cu	Au
Atomic Weight	63.55	196.96
Crystal Structure	FCC	FCC
Reaction Rate for IMC Formation w/ Al @150°C[5]	1.878×10^{-16} cm^2/s	1.1×10^{-14} cm^2/s
Electrical Resistivity	1.7 μΩ-cm	2.2 μΩ-cm
Young's Modulus	130 GPa	78 GPa
Ultimate Tensile Strength[7]	210 MPa	100 MPa
Thermal Conductivity	400 W/mK	320 W/mK
Density	8.92 g/cm^3	19.3 g/cm^3
Melting Temp.	1085°C	1064°C
CTE	16.5×10^{-6} /K	14.2×10^{-6} /K

Cu-Al IMC growth occurs at a much slower rate than Au-Al, by a factor of up to 100 for certain temperature conditions [9]. Compared to Au-Al bonds, theslower inter-diffusion rate of Cu and Al is caused by atomic size difference and electronegativity between Cu and Al. This leads to thinner Cu-Al IMCs compared to Au-Al IMCs, as shown in Figure 1.4, yet several studies have reported the failure at the interface due to growth of Cu-Al IMCs which poses a reliability concern.
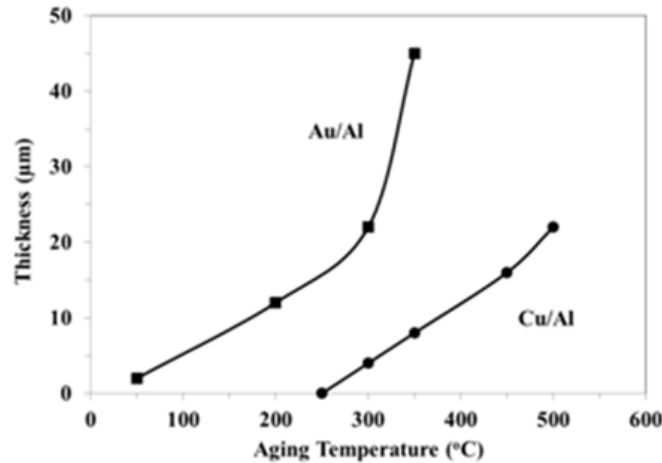
Figure 1.4: IMC thickness between Au-Al and Cu-Al (right) [10][11].

While some failures can be attributed to poor process control, such as under pad metallization cracks, they can be often prevented by carefully optimizing bonding parameters. Majority of failures occur during use condition, of which crack at wire bond neck region has been reported to be a critical concern in thermal cycling applications. Change in temperature causes expansion or contraction of all materials within the package, at differing rates due to thermal mismatch, leading to stress build up potentially causing failure of wire bond interconnections. Temperature swings can occur during different storage or use conditions in the life cycle of a device, for example, in airplanes during take-off and cruise, in industrial tools, in automotive or commercial devices. CTE mismatch between adjoining materials such as encapsulant, wire, die, die attach material and substrate causes a global deformation of the package imparting stress to the wire bond, consisting of axial, flexural and shear components. Vandendevelde,, et al. [12] showed that Cu (16 ppm/°C) wire bonds have higher susceptibility to failure than Au (14 ppm/°C) wire bonds due to a greater CTE mismatch with 'green' mold compound material (7-9 ppm/°C). Depending on the global package deformation and local deformation within the wire, one of these stresses becomes dominant, determining the failure mode. Eng, et. al., studied geometrical aspects of wire indicating that stress in wire bond is maximum at the neck near ball bond and heel, where there is a change in cross-sectional area. However, with exposure to high temperature, interfacial changes occur at the bi-metallic joint, through growth of IMC which could change failure site.

1.2. Micro-scale Ultrasonic Bonding in Microelectronic Packages

Ultrasonic wire bonding is the process of using ultrasonic energy combined with force and temperature over a period of few milli-seconds to form a weld between the wire and pad. Figure 1.5 shows the typical bonding cycle.

1.2.1. Thermosonic Bonding Process of Cu Wire

The bonding process with Cu wire starts with an electric flame off (EFO) process, where a high voltage difference is created between a metal wand and the tip of wire (held by capillary). Electric breakdown of air gap between the wand and wire tip leads to a high current spark which rises temperature of the wire tip and thereby melts it to form a spherical ball, known as the free air ball (FAB). To prevent oxidation of the Cu FAB a continuous supply of forming gas (95% N2 and 5%H2) is constantly supplied at a specific flow rate. It is important to inhibit oxidation at this stage to form a symmetric FAB and ensure adhesion of ball bond [13]. The next step in the bonding cycles is the process of ball bond formation, which is done by the descent of capillary (carrying the FAB) to the desired location and application of ultrasonic energy and bonding force on a heated substrate (usually Al). Ultrasonic energy softens the FAB, lowering flow stress, leading to plastic deformation of its shape and causes breakage of native oxide (~5nm thick on Al pad) [37]. Optimizing the energy used is very critical to form a good bond and has been studied in detail elsewhere [14]-[17]. Bonding force ensures coupling of ultrasonic energy between FAB and bond pad that leads to the bond formation. High bonding force is needed with Cu due to its increased hardness compared to Au but may also lead to pad damage by cracking it or cause cracks in the circuitry beneath the pad [18]. A low bonding force on the other hand causes lack of transmission of the ultrasonic energy between FAB and pad leading to a non-stick on pad

7

(NSOP) condition, where the bond is not formed [19]. Bonding temperature can be varied depending on pad material, thickness and wire thickness and is usually between 150ºC and 220ºC [3][19].

Upon completion of the first bond (ball bond) formation, the capillary rises to follows a pre-defined path to form the wire loop and descends to form the second bond (wedge bond). This is done through a similar process as mentioned above with an additional in-plane shearing movement by the capillary that shears the bond after its formation to separate the wedge bond and the wire connecting it through the capillary. Bond formation cycle is presented in Figure 1.5, which shows the different steps [1]. Some of the failure modes due to non-optimized bonding parameters are also presented.

S. No.	Failure Mode	Common Cause
1	BOAC cracks - Failure in the metallization layers under the pad	Non-optimized parameters Weak pad design
2	Excessive aluminum splash	Non-optimized parameters
3	Electrical shorting	Non-optimized parameters Contamination Wire sweeping
4	Ball bond lift off - Failure at the die-bond interface	Non-optimized parameters Contaminated pad Pad corrosion
5	Ball bond neck break - Failure around the neck of the bond	Non-optimized parameters Incorrect wire looping Die-to-package delamination due to molding
6	Break at mid-wire - Failure at wire loop	Wire nicks or damage Tight wire looping Wire sweeping
7	Break at wedge bond - Failure at substrate bond interface	Contamination Non-optimized parameters Oxidized pad Damaged pad

Figure 1.5: Thermosonic Ball-Wedge Bonding Process (left) and some failure modes due to non-optimized bonding parameters (right) [1][20].

1.2.2. Adhesion between Cu and Al through Initial Intermetallic Compound Formation (IMC)

Both Cu and Al have high oxidation potential and readily reacts with oxygen which has the highest reduction potential to form an oxide layer. Enthalpy of formation of Al_2O_3 was found to be -399.04±0.24 kilocalories under standard conditions. Thus, bonding between Cu and Al requires breaking the oxide layer and promote atomic inter-diffusion to form solid solution. This is done by using ultrasonic power in the bonding operation as described above. Bonding conditions generate temperature as high as 465ºC at the interface that promotes atomic flux between both Cu and Al, causing the formation of a solid-solid solution and a thin intermetallic compound region [21]. Xu, H., et. al. found three interfaces between Cu and Al right after bond formation, namely, $Cu-Al_2O_3-Al$, $Cu-CuAl_2-Al$ and just Cu-Al, of which bond adhesion was reported to be contributed by the $CuAl_2$ region [22]. Thus, a larger area of $CuAl_2$ was attributed to greater shear strength of the bond that is generally considered to yield high reliability. Initially formed $CuAl_2$ can grow in thickness with exposure to higher temperature through diffusion of Cu in to Al and extended periods of exposure can cause emergence of new phases such as Cu_9Al_4. Growth of these IMCs at the expense of Al pad consumption leads to reduction in strength of the bond.

1.3. Intermetallic Compound (IMC) Growth and Nucleation of New Phases at Elevated Temperature

Annealing of the Cu-Al joint at elevated temperature leads to formation of new phases as shown in the Cu-Al phase diagram (Figure 1.6). Different IMC phases can form depending on the atomic % Cu diffusing into Al and temperature conditions.
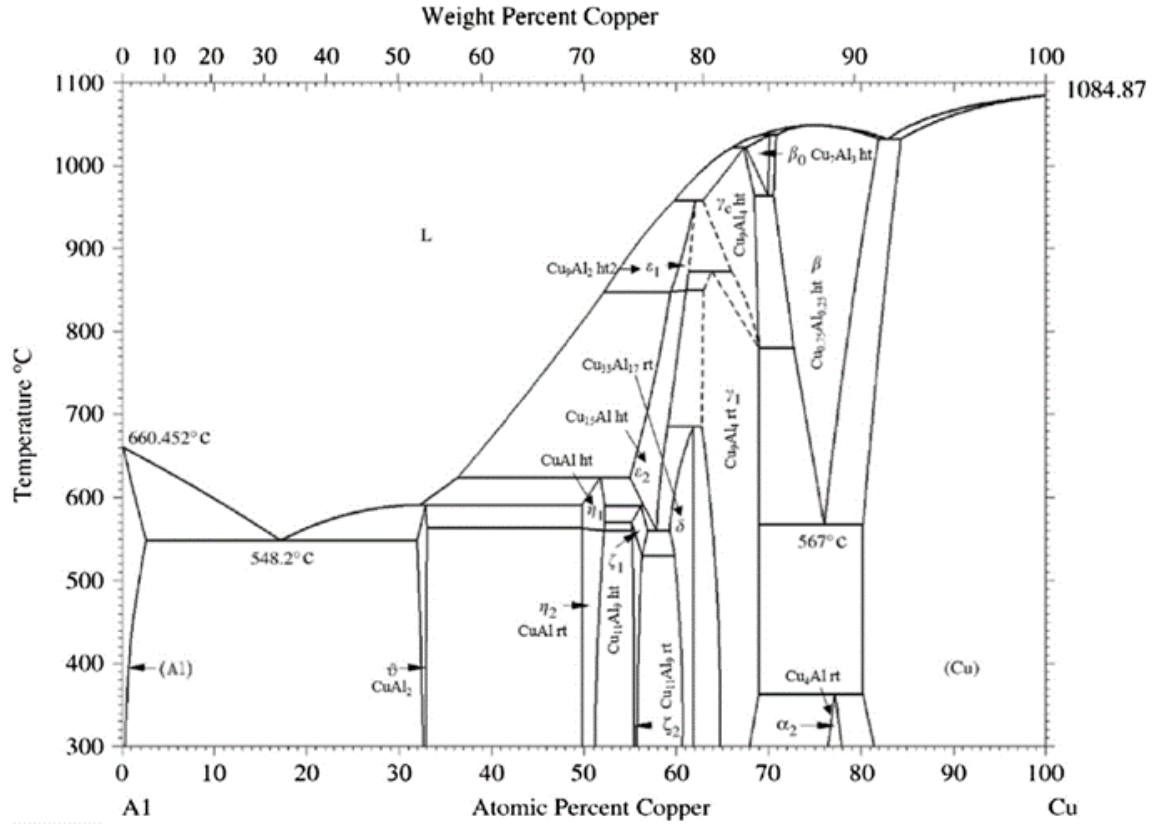
Figure 1.6: Cu-Al Phase Diagram.

Haidara et al., [24] studied different Cu to Al thickness ratios which led to formation of different end IMC phases as shown in Table 1.2. In the case of wire bonds in microelectronic devices, where Al is limiting, CuAl and Cu_9Al_4 have been reported widely as the subsequent phase to $CuAl_2$, of which CuAl is reported to be an intermediate un-stable phase and the termination phase has been agreed in literature to be Cu_9Al_4.

Table 1.2: IMC Phase Formation with Different Cu:Al Thickness Ratio [24].

Cu/Al thickness ratio	Atomic percentage Cu	Sequence of phase formation	End phases at 400°C	Stable phases at 400°C from the phase diagram
0.29	29	$Al_2Cu \backslash Al_4Cu_9$	$Al_2Cu + Al$	$Al_2Cu + Al$
0.56	44	$Al_2Cu \backslash Al_4Cu_9 \backslash AlCu$	$Al_2Cu + AlCu$	$Al_2Cu + AlCu$
0.71	50	$Al_2Cu \backslash Al_4Cu_9 \backslash AlCu$	$AlCu$	$AlCu$
0.87	55	$Al_2Cu \backslash Al_4Cu_9 \backslash AlCu \backslash Al_3Cu_4$	$AlCu + Al_3Cu_4$	$AlCu + Al_3Cu_4$
1.07	60	$Al_2Cu \backslash Al_4Cu_9 \backslash AlCu \backslash Al_3Cu_4$	Al_2Cu_3	Al_2Cu_3
1.26	64	$Al_2Cu \backslash Al_4Cu_9 \backslash AlCu \backslash Al_4Cu_9$	Al_4Cu_9	$Al_2Cu_3 + Al_4Cu_9$
1.58	69	Al_2Cu / Al_4Cu_9	Al_4Cu_9	Al_4Cu_9
2.38	77	Al_2Cu / Al_4Cu_9	$Al_4Cu_9 + (Cu)$	$Al_4Cu_9 + (Cu)$

Cu diffusion into Al dominates the IMC growth process leading to formation of CuAl$_2$ until most of the Al beneath the bond is consumed. Further Cu diffusion into CuAl$_2$ leads to formation of Cu$_9$Al$_4$, which is the final phase that exists after extended annealing times. Growth rate and activation energy of these IMC phases have been investigated by several researchers and fall within the range of $1.97 \times 10^{-9}\ m^2/s$ [20] to $1.63 \times 10^{-4}\ m^2/s$ [21] and 44.38 kJ/mol [22] to 129.29 kJ/mol [21] respectively, based on temperature and dopant material present in wire. In a temperature range between 200ºC and 600ºC, several reactions are possible between Cu and Al as listed in the following equations [28].

$$4Al + 9Cu = Cu_9Al_4 \quad \Delta G_1°(J/mol) = -33400 + 2.2T \tag{2}$$

$$2Al + Cu = CuAl_2 \quad \Delta G_2°(J/mol) = -77100 + 2.3T \tag{3}$$

$$Al + Cu = CuAl \quad \Delta G_3°(J/mol) = -20496.8 + 1.6T \tag{4}$$

$$Al + 3Cu = Cu_3Al_2, \quad \Delta G_4°(J/mol) = -20137.8 + 1.6T \tag{5}$$

$$Al + 3Cu = Cu_3Al, \quad \Delta G_5°(J/mol) = -19653 + 3.2T \tag{6}$$
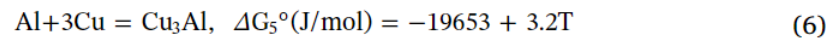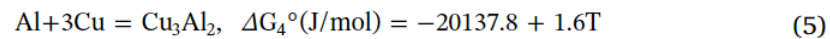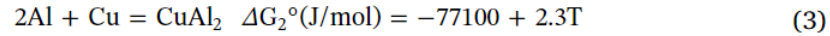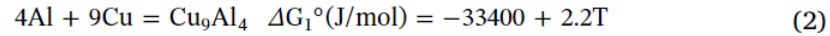
The Gibbs free energy values of these IMCs follows an increasing order from CuAl$_2$, Cu$_9$Al$_4$, CuAl, Cu$_3$Al$_2$ and Cu$_3$Al, which signifies the order for formation of these IMCs at

the Cu-Al interface. And out of these, $CuAl_2$ and Cu_9Al_4 are the phases that have been predominantly observed in the Cu-Al wire bonded interface.
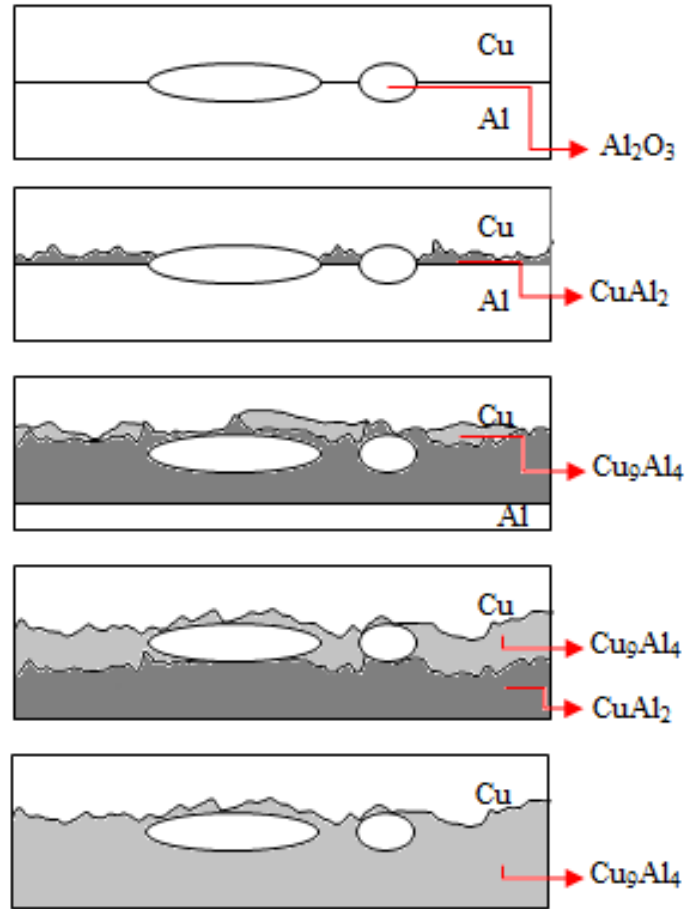
Figure 1.7: Sequence of IMC formation in Cu-Al interface [20,21,22,28].

A schematic of the IMC formation process, in cross-section view, is shown in Figure 1.7. Electrical resistance increases due to growth in thickness of the various IMC layers as these IMCs have high resistivity, ultimately leading to loss in device functionality. Thicker IMCs are known to reduce shear strength with easy fracture at the interface, due to its brittle nature, leading to an open circuit. Following section discusses the reliability concerns and mechanism of failure in detail.

1.4. Reliability Concerns in Cu-Al Bond Interface

Reliability concern due to interfacial changes with growth of IMCs are presented below, specifically under thermal aging and thermal cycling condition.

1.4.1. Risk of Lattice Mismatch at Interface due to Nucleation of γ—Phase

Grain level characterization was performed to show structure of different phases of IMCs as presented in Table 1.3. Cu and Al exists as a face centered cubic (FCC) structure, while the IMCs that form by combination of the two take different forms in order to reach stability. $CuAl_2$, the first phase, exists as a body centered tetragonal (BCT) structure. CuAl, the intermediate phase, forms an orthorhombic structure and Cu_9Al_4, the final phase in ball bond-bond pad system, forms a cubic in the form of γ-brass structure.

Table 1.3: Cu-Al IMC Characteristics [25][26][27].

	Designation	Crystal Structure	Lattice Constant(s)	Density	Composition
$CuAl_2$	θ	BCT	6.06Å/4.87Å	4.27	33 at.% Cu
CuAl	η	Ortho	6.95Å/4.16Å	5.31	50 at% Cu
Cu_3Al_4	ξ	Rhomb γ-brass	(7.07 / 4.08 / 10.02)Å	~6.86	~55 at.% Cu
Cu_4Al_3	δ	Ortho γ-brass	n/a	n/a	~60 at. % Cu
	ϵ	γ-brass variant	n/a	n/a	~55-60 at. % Cu
Cu_9Al_4	γ	γ-brass	8.704Å	6.86	69 at. % Cu
$Cu_{\sim 10}Al_{\sim 1}$	β	BCC	2.95Å	6.86	~70-80 at. % Cu
$Cu_{\sim 10}Al_{\sim 1}$	α_2	FCC	(3.65-3.68)Å	~7.25 -7.43	~88-91 at. % Cu

Li, J., et al. obtained XRD peaks for $CuAl_2$ as d(310)=1.9200A, d(112)=2.1156A, d(110)=4.2869A, d(202)=1.8935A and lattice parameters were calculated to be a = 6.06A and c=4.87A.

Similarly inter-planar spacing for Cu_9Al_4 were found to be, d(330)=2.0518A, d(552)=1.1844A, d(211)=3.5559A. Using these, the lattice parameter for Cu_9Al_4 cubic phase is to be a = 8.70642A.

From the above, a higher mismatch is evident between Cu_9Al_4 and Cu compared to all other interfaces that are present in the wire bonded joint. Higher lattice mismatch leads to poor interfacial strength at this interface which is susceptible for failure. This is exasperated in thermal cycling condition, where additional stress due to CTE mismatch exists which can cause failure at this interface.

1.4.2. Loss of Bond Adhesion of due to Growth of γ-Phase (Cu_9Al_4)

To understand the relationship between IMC phase, thickness and failure at the bonded interfaces, Lassnig, et. al., performed mechanical fatigue tests on thermally aged copper wire bonds on Al pad [31]. Cu bonds were made using thermosonic bonding on Al pad and the wire is cut carefully. Surface treatment of the bond is performed with ethanol and a SnPb solder sphere of 400μm diameter is placed on the bond in preparation for mechanical fatigue test as shown in Figure 1.8. This ensured good adhesion between solder bump and bond. This set-up is thermally aged for at 200ºC for up to 2000 hours. Three conditions are used for the study, namely, as bonded (condition A), 200 hours (condition B) and 2000 hours of aging (condition C). In condition A, IMCs were reported to be as thin as few tens of nanometers, however with condition B the IMCs were much thicker and predominantly

CuAl$_2$ phase. Condition C, showed CuAl$_2$, CuAl and Cu$_9$Al$_4$ phase with Cu$_9$Al$_4$ much thicker than in condition B. These changes in IMC phases and thickness can affect failure significantly.
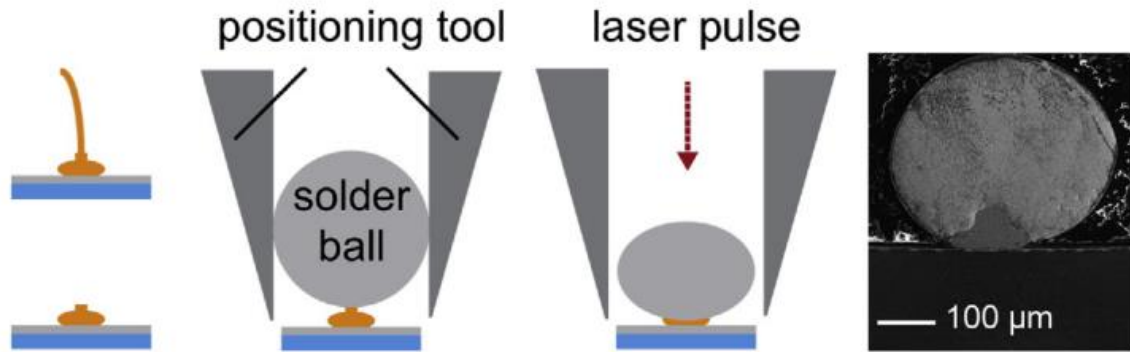
Figure 1.8: Mechanical fatigue specimen preparation [31].

Mechanical fatigue study was conducted through displacement loading at 20Hz that causes a shear stress at the bonded interface. It can be represented as shown in equation A,

$$\tau = (m.a)/A \qquad \text{(A)}$$

Where, 'm' denotes active mass above the bond, 'a' is the acceleration of the test cycle and 'A' is the bonding area. Results from this study is shown in Figure 1.9, where, the same applied stress, causes early failure with condition C compared to B and A. This is attributed to the newer IMC phases and its thickness.
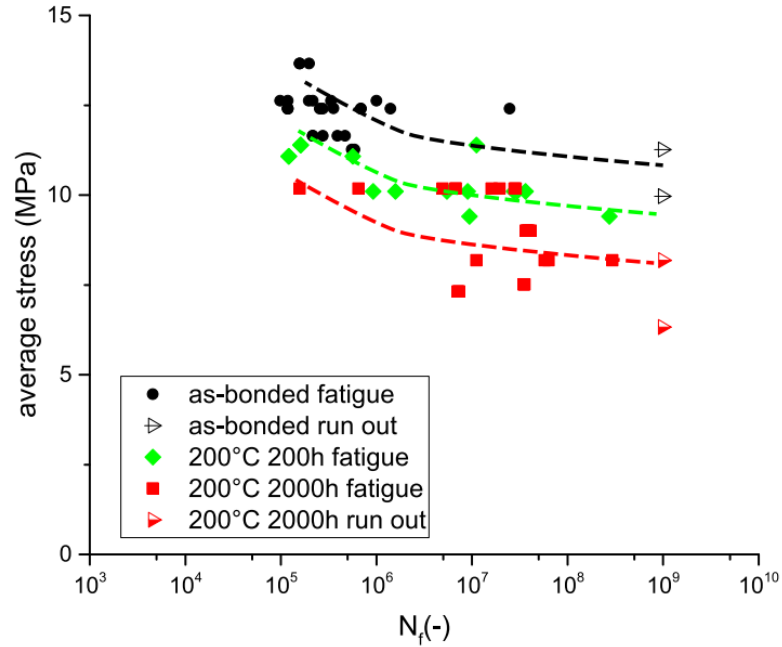
Figure 1.9: S-N curve obtained from experimental result [31].

In addition, fractographic analysis was performed on these failed bonds which showed failure predominantly in Al pad region at the un-aged condition. At condition B (200 hours at 200ºC), crack initiates and initially propagates through the Al pad but deflects to interface between $CuAl_2$ and Cu_9Al_4. At the highly aged condition C (2000 hours at 200ºC), crack initiates through Al and grows through interface between Cu_9Al_4 and Cu, finally it was found to deflect to CuAl IMC. These are summarized in Figure 1.10. This study shows severity of Cu_9Al_4 phase through the reduction in mechanical fatigue cycles.
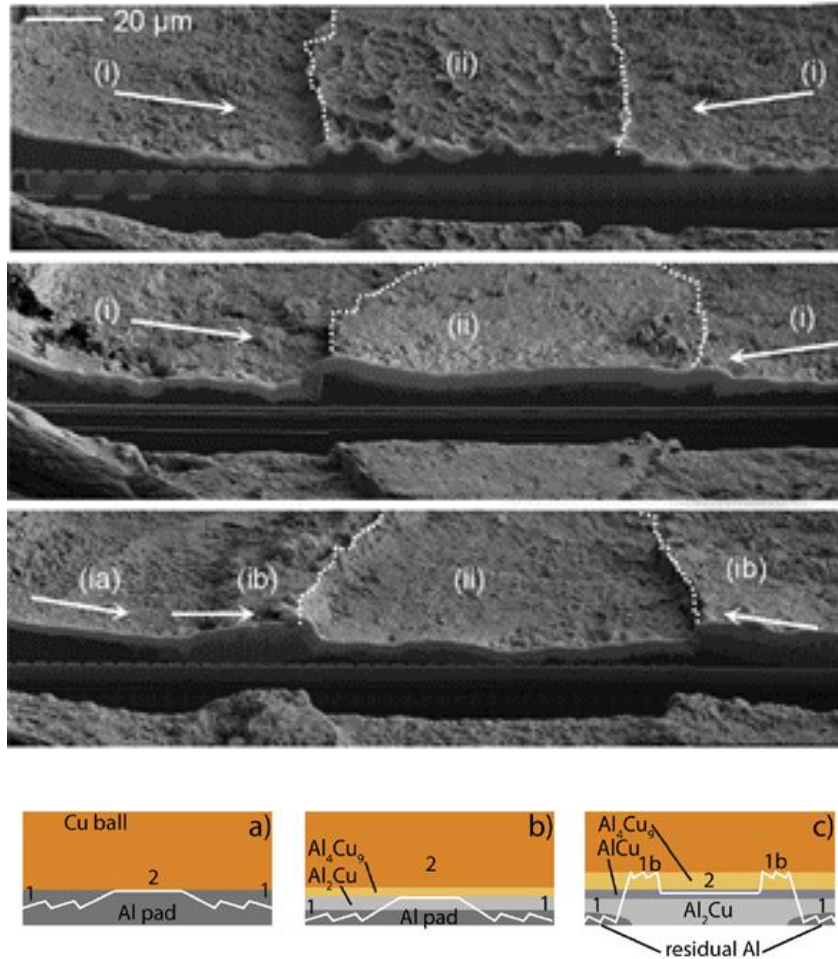
Figure 1.10: Fractograph of the mechanical fatigue analysis [31].

In another study, by Kouters, M.H.M, et.al., Cu-Al interface strength was found through a four-point bending test on thermally aged Cu-Al specimen at a maximum of 500°C up to 1225 hours [32]. The aged specimen was attached to steel carriers for performing four point bending study to identify weakest interfacial strength in the Cu-Al intermetallic system. Initiation of crack was found to occur at the pre-defined notch in the $CuAl_2$ region (for 100 to 200μm), which propagates in CuAl layer (region I) that has the lowest fracture toughness out of all IMC phases. Finally, the crack jumps to interface between Cu and Cu_9Al_4 (region II). Figure 1.11, shows cross-section of fractured region.
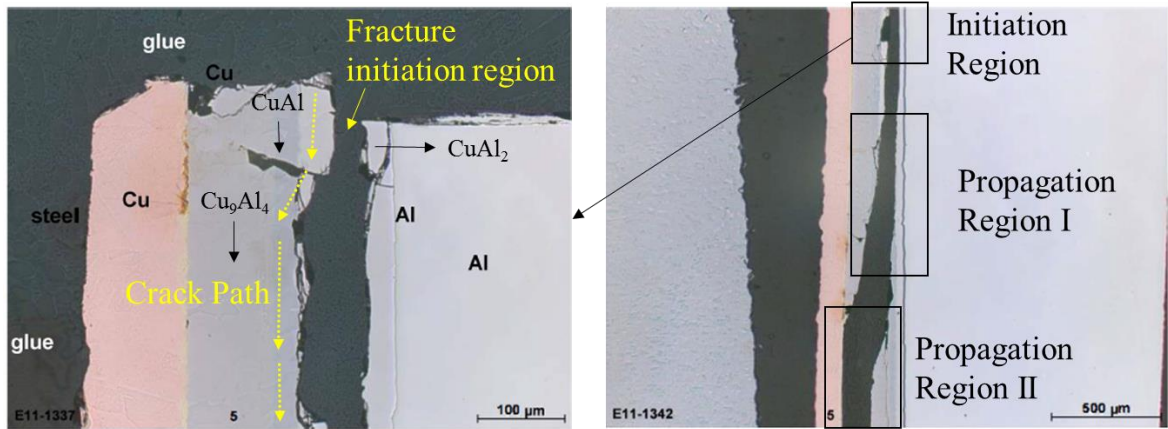
Figure 1.11: Cross-sectional analysis of fractured region [32].

Thus, the above studies indicate the severity of Cu_9Al_4 IMC phase, which can reduce strength of joint causing failure, making it the detrimental phase that forms between Cu and Al.

1.4.3. Electrical Resistance Increase due to γ-Phase (Cu_9Al_4)

In addition to mechanical degradation of interfacial strength due to Cu_9Al_4 phase formation, electrical resistance has also been shown to rise sharply due to the poor conductivity of Cu_9Al_4. F.W.Wulff, et al., [33] showed resistivity of each possible phase in Cu-Al pair as shown in Table 1.4. Out of the five possible IMCs that can form, Cu_9Al_4 has the maximum resistivity that causes a high resistance at the wire bond-bond pad interface.

Table 1.4: Cu-Al IMC Phase Characteristics [33].

Phase	At. % Cu	Resistivity ($\mu\Omega$ cm)	Density (g/cm^3)
Al	0 – 2.84	2.4	2.7
$CuAl_2$	31.9 – 33	7.0 – 8.0	4.63
CuAl	49.8 – 52.3	11.4	2.7
Cu_4Al_3	55.2 – 56.3	12.2	NA
Cu_3Al_2	59.3 – 61.9	13.4	NA
Cu_9Al_4	62.5 – 69	14.2 – 17.3	6.85
Cu	80.3 – 100	2.0	8.93

1.5. Potential Mechanism of Failure in Copper Wire Bonds

Interfacial separation has been reported in Cu wire bonds caused due to different reasons as suggested by different authors. Although the mechanism is still debated, the location of separation has been unanimously agreed to propagate between Cu_9Al_4 and Cu, making it detrimental phase of IMC between Cu bond and Al pad.

1.5.1. Volume reduction due to growth of Cu_9Al_4

IMC growth-related void formation was observed after exposure to 250ºC after 4 hours [1]. The location was identified to be in-between the IMC layer and bottom of the Cu ball surface, occurring towards the outer periphery of the ball bond. With increase in aging time these cavities were found to grow towards the center of the bond. 81 hours of aging was reported to cause a continuous layer of separation at the bond interface. The cause of such a separation was identified as IMC growth that is developed due to reactive diffusion. Volume reduction due to growth of Cu_9Al_4, results in micro-cracks and voids. In the ball bond-bond pad case, the IMC initiates at the bond periphery hence the separation occurs at the periphery and grows towards the center of the bond.

Another study [2] reported the crack formation with growth of Cu_9Al_4 phase. This was found to be caused by the diffusion of large Al atoms (184pm) in to Cu lattice, thereby expanding the inter-planar distances to accommodate the Al. At about ~31-37.5% atomic % Al, Cu_9Al_4 formation is preferred as presented in the phase diagram (77% APF vs 74% APF for FCC Cu), leading to reduced volume and interfacial separation.

Formation of voids in the bond interface of Cu-Al is at a much lower frequency and volume in the case of Au-Al bonds. With Cu-Al, voids are not present in the as-bonded state and only nucleate after prolonged annealing and are in the order of tens of nanometer. Formation of these voids have been attributed due to the volume reduction resulting from different IMC phase formation [1-3].

Molar volume change due to different phase formation can be calculated using [3,4],

$$V_m = \frac{V_c N_a}{Z}$$

Where,

Vm $\rightarrow$ molar volume of phase,

Vc $\rightarrow$ volume of unit cell

N_a $\rightarrow$ Avogadro constant, $6.022 \times 10^{23} mol^{-1}$

Z $\rightarrow$ No. of formula weights per unit cell

Table 1.5, shows the volume reduction in percentage for the two phases of Cu-Al IMC that grows at the interface. $CuAl_2$ growth shows a very minimal change in volume due to which voids are not formed throughout the time of it being the dominant phase.

Cu_9Al_4 shows significant volume shrinkage which results in voids in the order of tens of nanometer. These voids have been reported to grow with extended annealing during transformation of $CuAl_2$ to Cu_9Al_4.

Table 1.5 Volume Reduction for Different IMC Phases.

Reaction	Volume Change (%)
$Cu + 2Al \rightarrow CuAl_2$	-0.3
$9Cu + 4Al \rightarrow$	-4.4
$2CuAl_2 + 7Cu \rightarrow Cu_9Al_4$	-4.3

1.5.2. Corrosion resulting from chlorine ions present in mold compound.

Wire bond corrosion has been reported in packages with encapsulant that have a high absorption and halogen content. In most use conditions, moisture is not controlled and hence corrosion of ball bond interface is an important contributor to the overall wire bond failure. In one of the studies done by Gan et al., wire bond corrosion was observed under uHAST condition and was reported to be contributed by $CuAl_2$ and Cu_9Al_4 formation, which reacts with moisture resulting in a hydrogen embrittlement-induced cracking [5]. The proposed mechanism is shown in Figure 1.12.
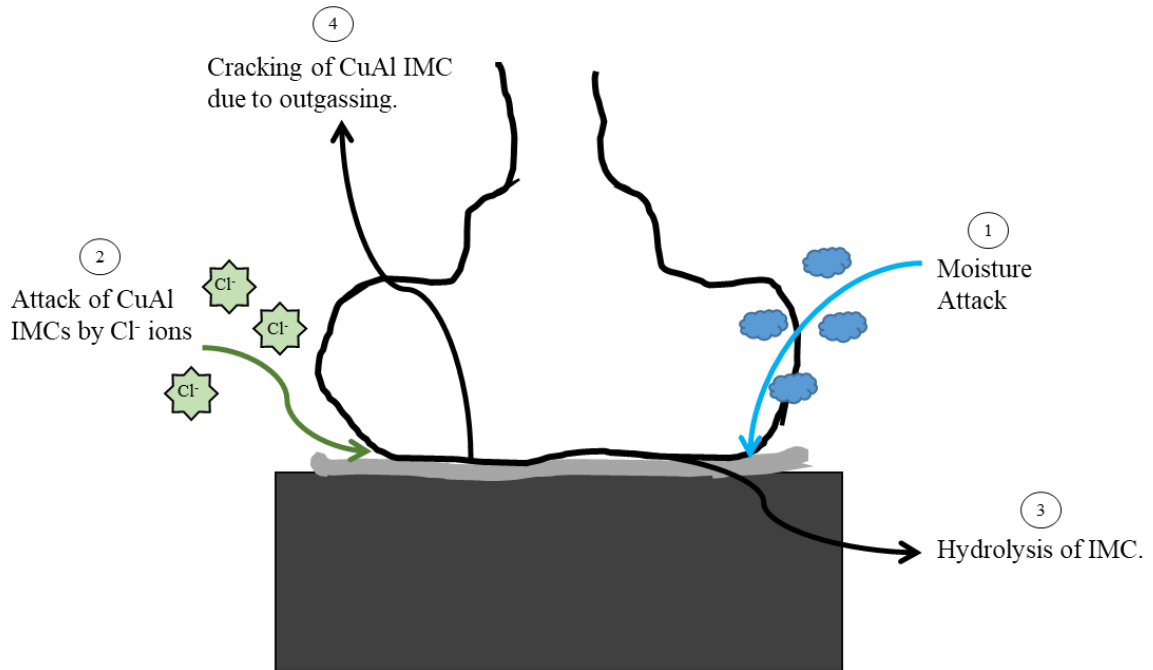
Figure 1.12: Mechanism of Corrosion in Cu Wire Bonds.

Reaction of moisture with CuAl IMCs is shown below, which results in H_2

$$Cu_9Al_4 + 4O_2 + H_2O \rightarrow 4Al + 9CuO + H_2$$

$$4CuAl_2 + \frac{1}{2}O_2 + H_2O \rightarrow 4Al + 2CuO + H_2$$
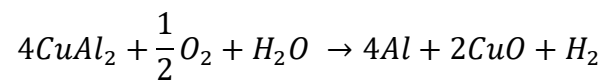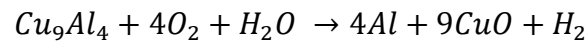
Hydrogen formed as a by-product of the reaction tries to move from the interface results in cracking of the brittle IMCs. Chlorine ions can also react with the IMCs resulting in $AlCl_3$ whose hydrolysis reaction results in Al_2O_3, which forms the corroded interface.

$$Cu_9Al_4 + 12Cl^- \rightarrow 4AlCl_3 + 9Cu$$

$$CuAl_2 + 6Cl^- \rightarrow 2AlCl_3 + Cu$$

$$2AlCl_3 + 3H_2O \rightarrow Al_2O_3 + 6HCl$$
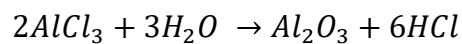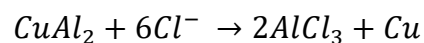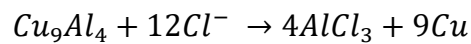
These reactions leads to cracking of the wire bond at the periphery which is the site of initial reaction and propagates towards the center of the bond causing a complete failure.

1.5.3. Oxidation of IMC

Oxidation induced cracking have also been reported as a potential cause of the failure of the Cu rich (Cu_9Al_4) IMC. An energy dispersive spectroscopy (EDS) line scan was performed by Lall et al., who identified presence of oxygen at that region. Source of oxygen has been reported to be either due to outgassing of resin in encapsulant at high temperature, or due to broken polymer chains [6].

1.6. Reliability of Cu Wire Bonds under Thermal Aging and Cycling Conditions

Several studies on IMC formation and failure under different isothermal aging conditions have been performed, results of which indicates Cu_9Al_4 formation to lead to weak interface. These failures can be exasperated under thermal cycling conditions, such as those experienced in actual use. Thermal cycling causes expansion and contraction of materials within a package causing a global deformation that results in warping of package, and a local deformation at the EMC-die interface caused by mismatch in CTE between EMC and die, as shown in Figure 1.13. A greater mismatch is expected on the ball bond side, due to the larger difference in CTE of encapsulant compared to that of die.
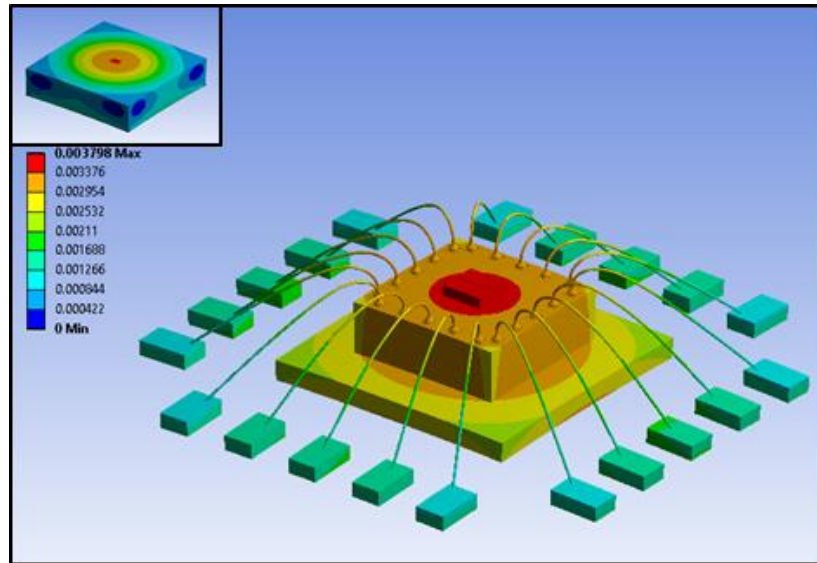
Figure 1.13: Deformation of package due to CTE mismatch of adjoining package materials.

Vandevelde, B., et.al., performed finite element analysis (FEA) on Cu wire bonds attached to Al pads encapsulated with low CTE green compound material [12]. The difference in CTE was reported to cause high stress at the wire bond neck region, which is the area of change in cross-sectional area. Thus failure was said to be localized at this region in Cu wire bonds under thermal cycling as shown in Figure 1.14.
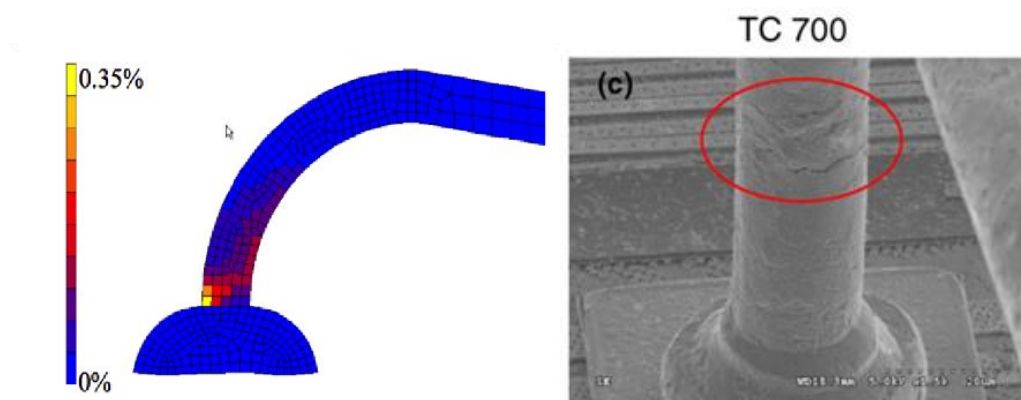
Figure 1.14: Stress concentration at wire neck under thermal cycling (left). Failure at wire neck region after 700 cycles from -60°C to 175°C (right) [12].

Fan, H., et al., listed three dominant factors that leads to wire neck failure:

1. CTE mismatch between epoxy mold compound (EMC), Cu wire and lead frame (LF).

2. Adhesion between EMC and Cu wire. (Poor adhesion led to delamination of EMC from Cu wire which was shown to be a critical factor for increase in stress at wire neck region).

3. Wire neck shape – larger loop provided lower stress as compared to smaller loop.

Experimental results from their study showed wire neck crack at 400 cycles with a particular encapsulation material.

Chan, M., et.al., reported an increase in electrical resistance of about 1.75Ohms after 700 thermal cycles from -65ºC to 175ºC [34]. Failure analysis showed crack in the wire neck region as predicted by the previously shown study.

Gan, C.L., et al., [35] reported higher life time for Cu wire bonds compared to Au from thermal cycling experiment performed between -40ºC to 150ºC as per JESD22-A104. A significant effect of mold compound type was also visible which proved results from previously reported studies. Figure 1.15 shows the Weibull failure time distribution for Cu and Au wire bonds.

Weibull Plot (TC Wearout Reliability)

Legend:
- ▲ Au_EMC A
- ■ Cu_EMC A
- ◆ Au_EMC B
- ● Cu_EMC B

$y = 8.3182\ln(x) - 80.609$
$R^2 = 0.9317$
$y = 11.431\ln(x) - 110.29$
$R^2 = 0.9467$
$y = 7.2266\ln(x) - 71.126$
$R^2 = 0.8612$
$y = 8.347\ln(x) - 82.541$
$R^2 = 0.9129$
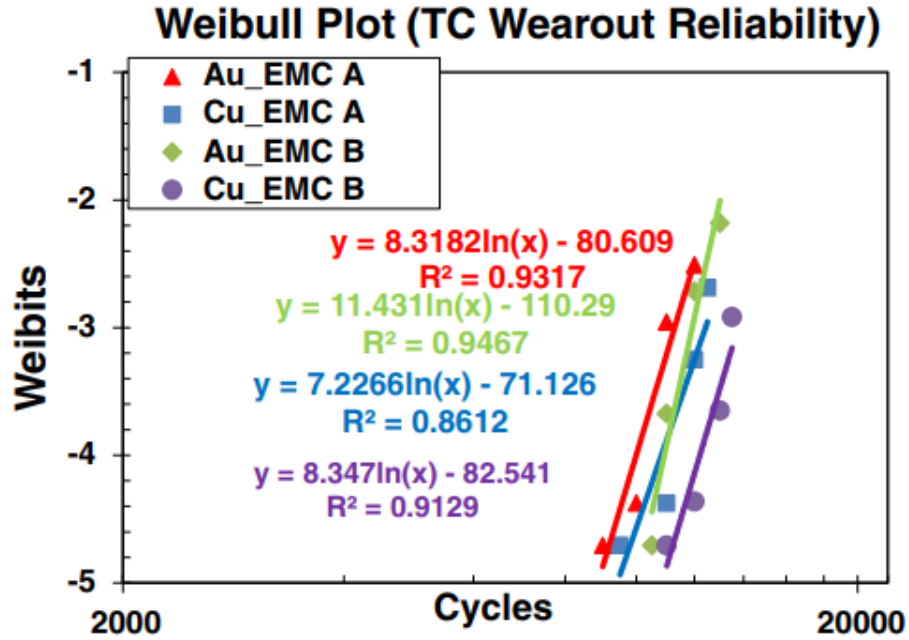
Figure 1.15: Comparison of TCT Reliability between Au and Cu Wire Bonds [35].

Cracks were observed at the interface between Cu-Al IMC and Cu bond after 9500 thermal cycles from -40ºC to 150ºC as shown in Figure 1.16 [35]. This is due to the change at the interface due to the growth of IMCs.
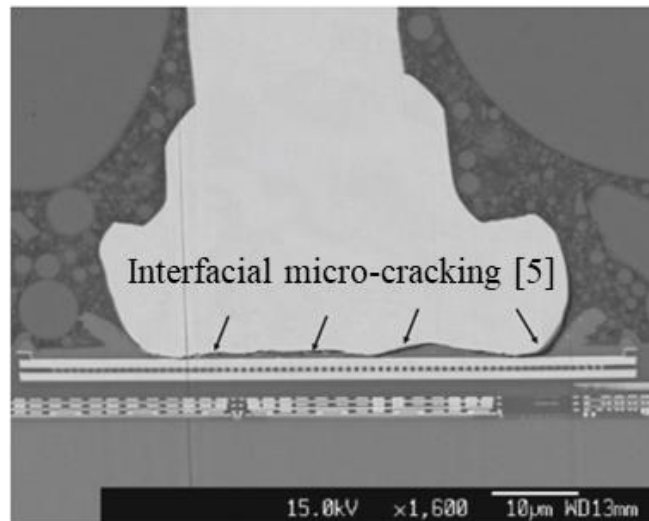
Figure 1.16: Interfacial micro-cracks after 9500 cycles from -40°C to 150°C [35].

This is one of the few studies that report interfacial failure due to growth of IMCs under thermal cycling condition. Although failure region was reported no further assessment as to mechanism and exact location was found, which is necessary to prevent it. From these thermal cycling studies and from IMC growth related interface weakening at high temperature aging, it can be identified that the failure mode shifts from the wire neck cracking to interface region due to IMC growth and hence it is necessary to consider a combination of thermal aging and thermal cycling stress (as a device would experience in actual use condition) for reliability assessment.

1.7. Research Objectives

Studies in literature points to two critical failure mechanisms, namely, IMC growth at elevated temperatures that causes weakening of the interface and failure of Cu wire bond in thermal cycling condition due to mismatch in CTE between EMC, Cu wire and LF. However, in reality these stresses happen concurrently which has not been studied. With growth of IMCs, failure could dominate at the interface rather than at wire neck. One study, (done by Gan, C.L., et al., [35]) shows this type of failure when wire neck failure was prevented by using low mismatch EMC. Literature suggests Cu_9Al_4-Cu to be the weak region due to mismatch in lattice parameters and IMC induced cavity formation, making it susceptible for failure under thermal cycling condition. With the knowledge from literature the following gaps were identified and are studied in this thesis.

1. Lack of study on Cu wire bond reliability under a combination of thermal aging and thermal cycling condition (as a device would experience in actual use condition).

2. Critical factors that contribute to reliability of copper wire bonds in microelectronic packages have not been identified as most of the studies in literature are performed

with test coupons/devices where only effect of few parameters have been studied. EMC material, wire material and wire bond process parameters have been widely studied, while bond pad characteristics and wire geometry have been mentioned sparsely in literature.

3. Due to use of test coupons/devices in the above mentioned studies, a failure estimation model for use with commercially available off the shelf (COTS) device is absent.

4. Wire bond damage due to interface degradation is studied by bond shear assessment, but needs a robust decapsulation method to access the wire bonds that does not degrade the bond due to the decapsulation process.

5. Although shear force analysis is widely used, parameters affecting its result is not studied in detail, especially bond pad thickness and aging condition, which are necessary for comparison of bonds.

6. Bond pad thickness controls the amount of Al present for reaction to form IMCs, but its effect on wire bond reliability is not studied in detail.

1.8. Research Approach

With defining the research objectives, a research approach as described in Figure 1.17 was formulated. This study will consist of two parts, where Part I will focus on studying a combination of thermal aging and cycling reliability of Cu wire bonded COTS parts, development of decapsulation technique and building a data based failure estimation model for COTS parts that can be used with knowledge of initial wire bond characteristics.

Part II of the study will focus on understanding the effect of one of the parameter (bond pad thicknes) from the multitude of variables present in COTS parts. Bond pad

thickness was identified to be a critical parameters and, its effect on initial bond shear analysis is evaluated in Part II-A. Additionally, effect of aging of bonds on shear analysis is also studied as part of this study. Part II-B focuses on the effect of bond pad thickness on the reliability of Cu wire bonds due to delay in Cu_9Al_4 phase formation. Chapter 3 to 6 of this thesis is dedicated to Part I study and Chapter 7 and 8 discusses results from Part II study.
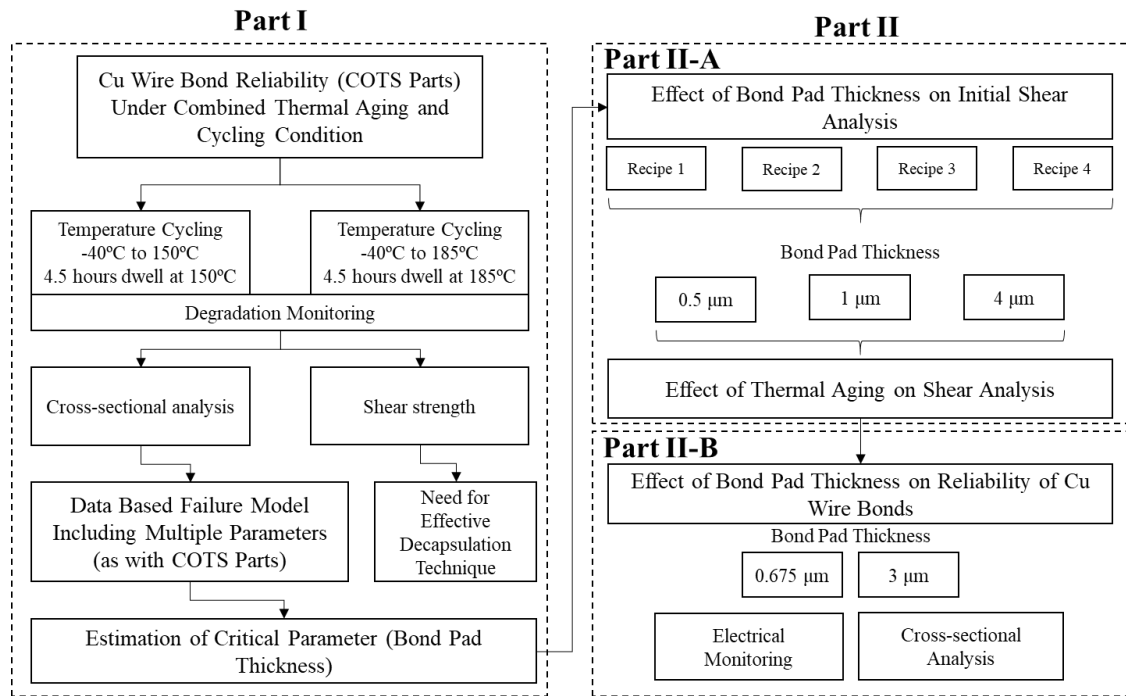
Figure 1.17: Research Approach

1.9. Reference

[1] Chauhan, P. S., Choubey, A., Zhong, Z., & Pecht, M. G. (2014). Copper wire bonding. In Copper Wire Bonding (pp. 1-9). Springer, New York, NY.

[2] Elenius, P., & Levine, L. (2000). Comparing flip-chip and wire-bond interconnection technologies. Chip Scale Review, 4(6).

[3] England, Luke, and Tom Jiang. "Reliability of Cu wire bonding to Al metallization." 2007 Proceedings 57th Electronic Components and Technology Conference. IEEE, 2007.

[4] Li, H., Chen, W., Dong, L., Shi, Y., Liu, J., & Fu, Y. Q. (2018). Interfacial bonding mechanism and annealing effect on Cu-Al joint produced by solid-liquid compound casting. Journal of Materials Processing Technology, 252, 795-803.

[5] Schneider-Ramelow, M., & Ehrhardt, C. (2016). The reliability of wire bonding using Ag and Al. Microelectronics Reliability, 63, 336-341.

[6] Schneider-Ramelow, M., Geißler, U., Schmitz, S., Grübl, W., & Schuch, B. (2013). Development and status of Cu ball/wedge bonding in 2012. Journal of electronic materials, 42(3), 558-595.

[7] Rutkowski, E., & Sampson, M. J. (2015). Body of knowledge (BOK) for copper wire bonds.

[8] Palesko, C. A., & Vardaman, E. J. (2010, June). Cost comparison for flip chip, gold wire bond, and copper wire bond packaging. In 2010 Proceedings 60th Electronic Components and Technology Conference (ECTC) (pp. 10-13). IEEE.

[9] Kim, H. J., Lee, J. Y., Paik, K. W., Koh, K. W., Won, J., Choe, S., ... & Park, Y. J. (2003). Effects of Cu/Al intermetallic compound (IMC) on copper wire and aluminum pad bondability. IEEE Transactions on Components and Packaging Technologies, 26(2), 367-374.

[10] F.W. Wulff, C.D. Breach, D. Stephan, Saraswati, and K.J. Dittmer, SEMICON Semi Technology Symposium (Singapore: 2005).

[11] A. Bischoff and F. Aldinger, IEEE Proc. Electron. Compon. Conf. (1984), p. 411.

[12] Vandevelde, Bart, and Geert Willems. "Early Fatigue Failures in Copper Wire Bonds inside Packages with Low CTE Green Mold Compounds." 2012 4th Electronic System-Integration Technology Conference (2012).

[13] P. Liu, L. Tong, J. Wang, L. Shi, and H. Tang, "Challenges and developments of copper wire bonding technology," Microelectronics Reliability, vol. 52, pp. 1092–1098, 2012.

[14] Z. W. Zhong, H. M. Ho, Y. C. Tan, W. C. Tan, H. M. Goh, B. H. Toh, and J. Tan, "Study offactors affecting the hardness of ball bonds in copper wire bonding," Microelectronic Engineering, vol. 84, pp. 368–374, 2007.

[15] H. Huang, A. Pequegnat, B. Chang, M. Mayer, D. Du, and Y. Zhou, "Influence of superimposed ultrasound on deformability of Cu," Journal of Applied Physics, vol. 106, pp. 113514–113516, 2009.

[16] Y. Tian, C. Wang, I. Lum, M. Mayer, J. P. Jung, and Y. Zhou, "Investigation of ultrasonic copper wire wedge bonding on Au/Ni plated Cu substrates at ambient temperature," Journal of Materials Processing Technology, vol. 208, pp. 179–186, 2008.

[17] S. Hong, C. Hang, and C. Wang, "Experimental research of copper wire ball bonding," in Electronic Packaging Technology, 2005 6th International Conference on, 2005, pp. 1–5.

[18] T. K. Lee, C. D. Breach, and W. L. Chong, "Comparsion of Au/Al and Cu/Al in wirebonding assembly and reliability," in Microsystems, Packaging, Assembly and Circuits Technology Conference (IMPACT), 2011 6th International, 2011, pp. 234–237.

[19] H. Chu, J. Hu, L. Jin, and Y. Jie, "Defect analysis of copper ball bonding," in Electronic Packaging Technology & High Density Packaging, 2008. ICEPT-HDP 2008. International Conference on, 2008, pp. 1–3.

[20] M. T. Labs, "Wire bonding semiconductor packaging."

[21] H. Xu, C. Liu, V. V. Silberschmidt, Z. Chen, and V. L. Acoff, "Effect of ultrasonic energy on nanoscale interfacial structure in copper wire bonding on aluminium pads," Journal of Physics D-Applied Physics, vol. 44, Apr 13, 2011.

[22] Xu H., Qin I., Clauberg H., Chylak B. and Acoff V.L., "New Observation of Nanoscale Interfacial Evolution in Micro Cu-Al Wire Bonds by in-situ High Resolution TEM Study," Scripta Materialia.

[23] Murray JL. The aluminium-copper system. Int Met Rev 1985;30:211e33.

[24] Haidara, Fanta, Marie-Christine Record, Benjamin Duployer, Dominique Mangelinck. "Investigation of reactive phase formation in the Al-Cu thin film systems." Surface & coatings Technology. 206. pp.3851-3856 (2012). In-situ TF/TF XRD sequence study.

[25] Massalski, T. B. "The Al-Cu (Aluminum-Copper) system. Bulletin of Alloy Phase Diagrams." V.1. I.1. pp. 27-33 (March 1980).

[26] R. P. Jewett and D. J. Mack, "Further Investigation of Copper-Aluminium Alloys in the Temperature Range below the ϯ ⇋ ϯϯ □ □은 Eutectoid." J. Inst. Metals, 92, 59(1963).

[27] Daams, J.L., C. Villars, P. van Vucht, J.H.N. Atlas of Crystal Structure types for Intermetallic Phases Vol.3. ASM International. (1991).

[28] ZHAO, H., WANG, D., QIN, J., & ZHANG, Y. (2011). Research Progress on Bonding Mechanism and Interface Reaction of Cu/Al Laminated Composite [J]. Hot Working Technology, 10.

[29] Hang, C. J., Wang, C. Q., Mayer, M., Tian, Y. H., Zhou, Y., & Wang, H. H. (2008). Growth behavior of Cu/Al intermetallic compounds and cracks in copper ball bonds during isothermal aging. Microelectronics reliability, 48(3), 416-424.

[30] Mishler, M.C., (2015). Interface Reaction Induced Stress Development in Al thin filmCu bulk plate Diffusion Couple (Thesis Dissertation). University of Texas, Arlington, TX.

[31] Lassnig, A., Pelzer, R., Gammer, C., & Khatibi, G. (2015). Role of intermetallics on the mechanical fatigue behavior of Cu–Al ball bond interfaces. Journal of Alloys and Compounds, 646, 803-809.

[32] Kouters, M. H. M., Gubbels, G. H. M., & Ferreira, O. D. S. (2013). Characterization of intermetallic compounds in Cu–Al ball bonds: Mechanical properties, interface delamination and thermal conductivity. *Microelectronics Reliability*, *53*(8), 1068-1075.

[33] F. W. Wulff, C. D. Breach, D. Stephan, Saraswati, and K. J. Dittmer, "Characterisation of intermetallic growth in copper and gold ball bonds on aluminium metallization," in Electronics Packaging Technology Conference, 2004. EPTC 2004. Proceedings of 6th, 2004, pp. 348–353.

[34] Chan, M., Tan, C. M., Lee, K. C., & Tan, C. S. (2016). Non-destructive degradation study of copper wire bond for its temperature cycling reliability evaluation. Microelectronics Reliability, 61, 56-63.

[35] Gan, C. L., Francis, C., Chan, B. L., & Hashim, U. (2013). Extended reliability of gold and copper ball bonds in microelectronic packaging. *gold Bulletin*, *46*(2), 103-115.

[36] Eng, T. C., Jeat, P. Y., & Fonseka, G. (2007, December). QFN wire bond dilemma-stress neck & stress heel. In Electronics Packaging Technology Conference, 2007. EPTC 2007. 9th (pp. 192-195). IEEE.

[37] H. Xu, C. Liu, V. V. Silberschmidt, S. S. Pramana, T. J. White, and Z. Chen, "A reexamination of the mechanism of thermosonic copper ball bonding on aluminium metallization pads," Scripta Materialia, vol. 61, pp. 165–168, Jul 2009.

[38] Xu, H., Liu, C., Silberschmidt, V. V., Pramana, S. S., White, T. J., Chen, Z., & Acoff, V. L. (2011). Behavior of aluminum oxide, intermetallics and voids in Cu–Al wire bonds. Acta Materialia, 59(14), 5661-5673.

[39] Xu, H. (2010). Thermosonic ball bonding: a study of bonding mechanism and interfacial evolution (Doctoral dissertation, Loughborough University).

[40] Lall, P., Deshpande, S., Nguyen, L., & Murtuza, M. (2016). Microstructural indicators for prognostication of copper–aluminum wire bond reliability under high-temperature storage and temperature humidity. IEEE Transactions on Components, Packaging and Manufacturing Technology, 6(4), 569-585.

2. Au vs Cu Wire Bond Reliability under Thermal Aging Condition

A pilot study is performed, prior to addressing the research gaps mentioned in Chapter 1, to strengthen the need to assessing Cu wire bond reliability. This study compares Au and Cu wire bonds on Al bond pad in COTS parts through isothermal thermal aging study conducted at three different temperatures.

2.1. Introduction

Diffusion of Cu in to Al is reported to be much slower than that of Au in Al, thereby leading to lesser IMC formation. Though a lot of work has been done in the past on Au-Al and Cu-Al systems [1]-[5], they have been restricted to bulk material or wire bonding done in laboratory conditions, which are different from COTS parts in terms of material, process and assembly. Additionally, growth constants and activation energy reported in the literature [6]-[13] form a wide range and is dependent on several factors such as bonding parameters, wire dopant material, etc., which makes it necessary to have a comparison between a Cu and Au bonded device, manufactured by the same OEM where package and process parameters will be the same . This is done through obtaining the same device, with date codes before the conversion to Cu (Au wire bonded device) and after the conversion was made (Cu wire bonded device). Hence minimal variation between the devices are expected and results will give a one-to-one comparison between Cu-Al and Au-Al wire bond-bond pad pairs, under accelerated isothermal aging condition.

2.2. Au-Al IMCs formation

According to the Au-Al phase diagram, five different IMC phases can be developed [15]. They are Au_5Al_2, Au_4Al, Au_2Al, $AuAl_2$ and AuAl. Out of these the predominant one is the

AuAl$_2$ that is purple in color and hence the name 'purple plague' is associated with the IMC formation in Au-Al system. Though these IMCs are not thermodynamically unstable, their brittle nature can cause formation of cracks due to thermal expansion and relaxation of mold compound causing failure. Another failure mode is the crack formation by coalescence of Kirkendall voids which are predominant in the Au-Al system caused due to the difference in the rate of diffusion of Au in to Al and Al into Au. Both of the above condition leads to an open circuit failure.

Upon bonding by thermosonic process of two 'ideal' metals with no oxide layers gold will diffuse into aluminum to form Au$_5$Al$_2$ IMC, which will be the first IMC as shown in Figure 2.1. However, in reality oxide layers exist on the aluminum pad and these break due to ultrasonic, giving way for diffusion to occur between Au and Al at certain region. Diffusing species of Au into Al forms AuAl$_2$ and the diffusing species of Al into Au forms Au$_4$Al. Thus, the IMC formation depends on the concentration of atoms. With aging, different IMC phases grow depending on temperature and time. In the current work, the IMC growth measurements are done considering IMC as a whole instead of separate phases. This is due to the fact that phase marking is tedious and would not be consistent with different aging times.

A detailed analysis of IMC growth at Cu-Al interface is discussed in Chapter 1.
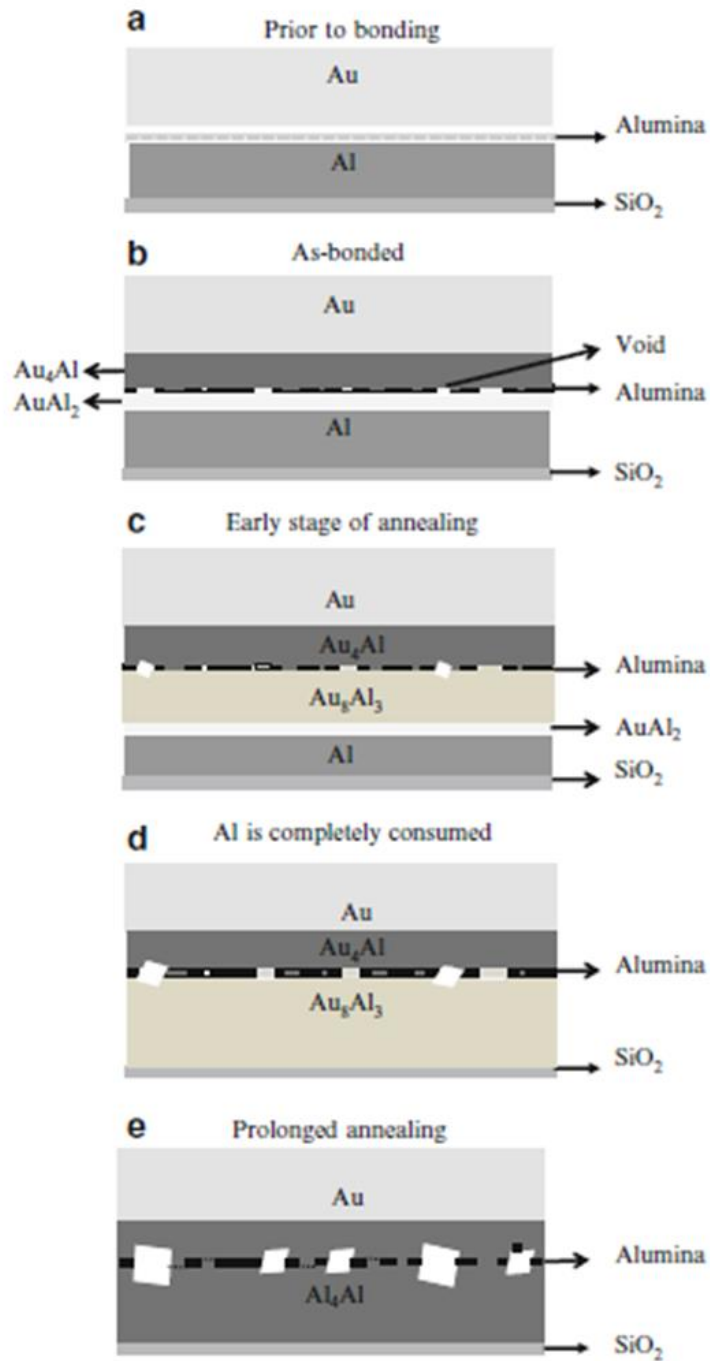
Figure 2.1: Au-Al Intermetallic Compound Formation [15].

2.3. Test Vehicle and Design of Experiment

Though a lot of work has been done in the past on Au-Al and Cu-Al pair comparison, they have been restricted to bulk material or wire bonding done in laboratory conditions, which are different compared to those in COTS parts. This work is done to identify growth constant and activation energy for commercially available off-the-shelf parts (COTS) with gold wire bond and copper wire bond. Both these parts were manufactured by the same OEM and do not contain any other changes apart from bond wire material. To account for the change in bond wire material, the manufacturer uses additional markings that signifies use of copper wire bond. In both cases, the wire diameter and ball bond dimensions are almost the same.

Purpose of this work is to be able to find the intermetallic compound thickness at a given time and temperature of aging and provide a relationship to compare Cu-Al and Au-Al IMCs. Under normal working conditions these intermetallic compounds will not grow sufficiently to make a prediction model in a short time, especially not Cu-Al IMCs. Thus the failure mechanism, intermetallic compound formation, was accelerated under temperature conditions that were higher than the normal use condition. Two different temperature conditions were chosen for this study to get enough data to be able to develop a growth prediction model as shown in Figure 2.2. 150ºC, 185ºC and 200ºC were chosen as the accelerated conditions as higher temperature could cause a drift in the failure mechanism of the Au-Al system. It has been reported that Kirkendall voids can coalesce to form cracks at low aging times at temperature of >200ºC. Formation of crack will break the path for diffusing atoms, halting the growth of IMCs. To prevent this and provide an

environment for continuous growth of intermetallic, like in the case of usage conditions, these two temperature conditions were chosen for isothermal aging.

Eight devices of each, copper and gold wire bonded parts were tested at each temperature. Devices were put in separate chambers for aging at different conditions. Thus a total of 16 devices were placed in one chamber, which were taken out at 100 hours, 200 hours, 400 hours and 800 hours. At each interval, two devices were taken out for cross sectioning, to identify the IMC thickness at different aging times.
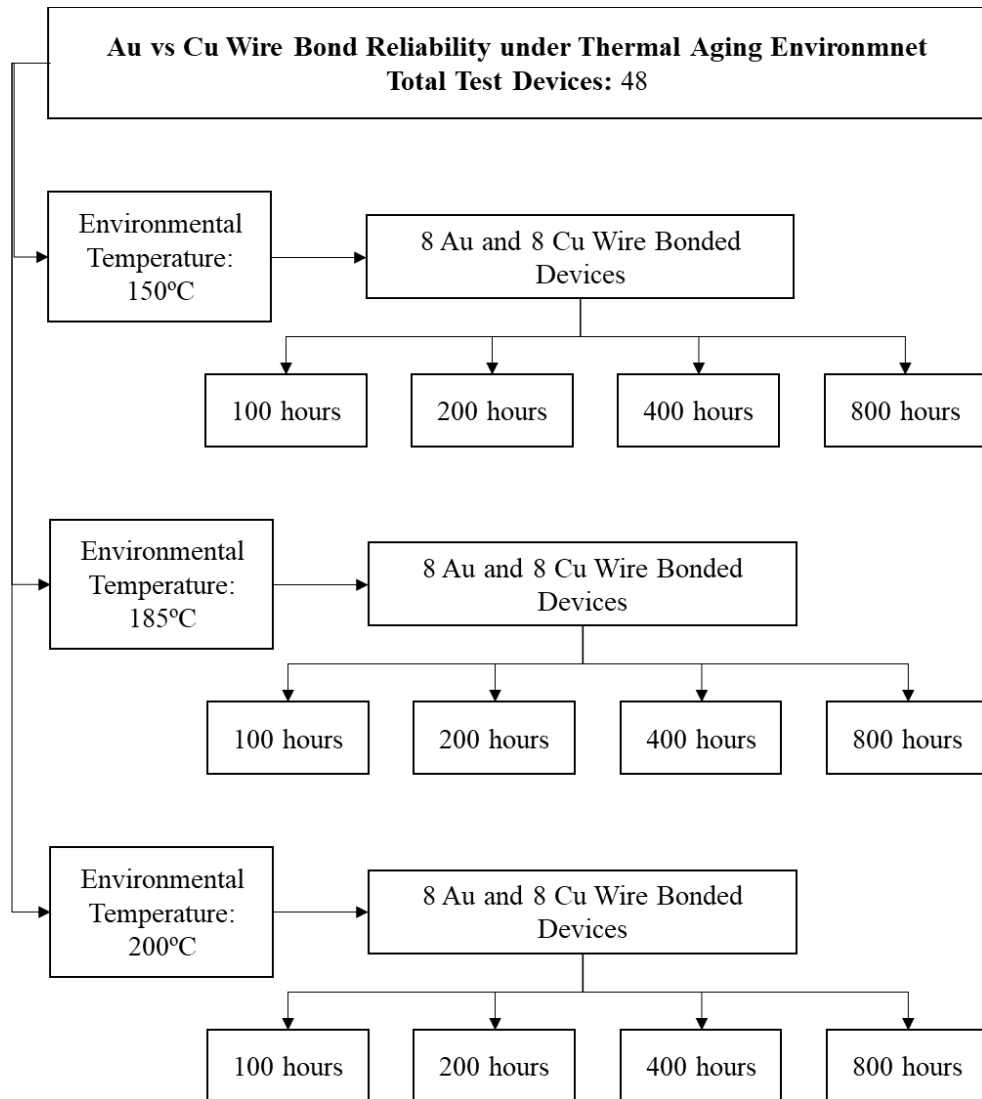
Figure 2.2 Design of Experiment (DOE) for Au vs Cu Wire Bond Reliability Study.

Devices that were taken out for failure analysis, were cut with a diamond tip circular saw to get close to the die and then potted with epoxy resin and hardener to prepare the specimen for cross sectioning. The potted specimen was allowed to cure for 12 hours after which they went through grinding with grit paper no. 400, 600, 800 and 1200. At this point the wire bonds were visible. Next, diamond suspension of particle size 3 micron, 1 micron, 0.25 micron and 0.05 micron were used to polish the specimen to remove all surface scratches that would exist from the grinding process. At the end of the polishing step, the specimen was free of cracks and had a surface roughness of 50 nm. Care was taken throughout the process to prevent introduction of cracks due to the cross-sectioning method itself. Also, the force in each of these steps were kept minimum to prevent shear of the intermetallic compounds. These specimens were imaged in a scanning electron microscope at different magnification going up to 25000X. At this magnification, it was possible to observe features in the order of few micro-meters. Images obtained showed no signs of IMC shearing or cracking due to the metallographic specimen preparation method as shown in Figure 2.3.
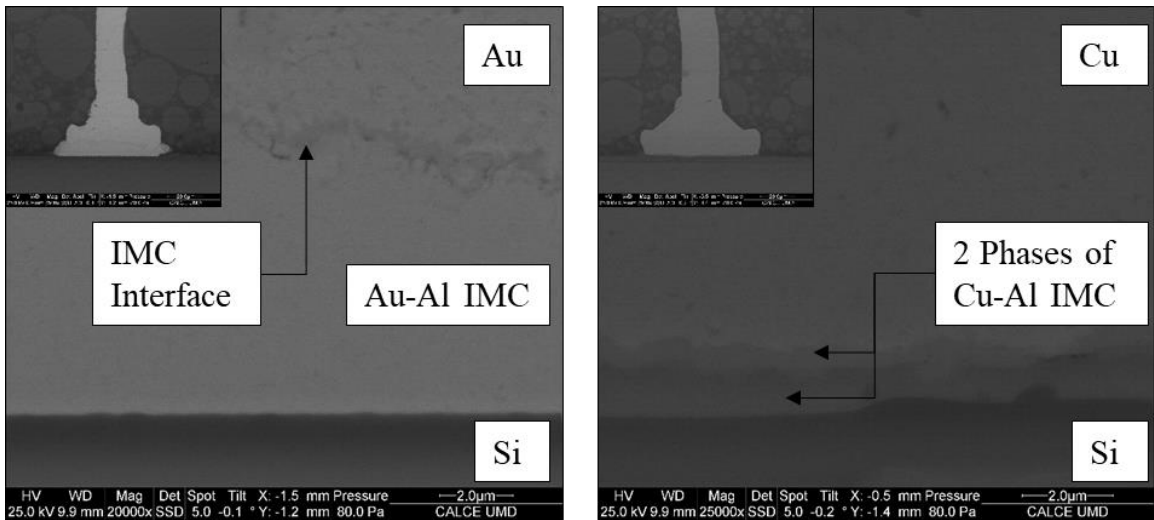
Figure 2.3 Au-Al system (left) and Cu-Al system (right) aged at 185C for 800 hours.

In case of Cu-Al system the IMCs are comparatively thinner and hence magnification of up to 25000X is used to locate them. Images obtained at different aging times for three temperature conditions were used for IMC thickness measurement. First, the area of the IMC was measured and then the length over which area measurement was taken was identified. Dividing the area by the length gave the average thickness of IMC in the ball bond-bond pad interface. More detail about the measurement process is given in Chapter 4, Section 4.2.

Table 2.1 and Table 2.2 shows the IMC thickness obtained for three different temperatures at four different aging times each. Growth in IMC thickness can be seen with aging time for a particular aging temperature and also higher IMC thickness at the same time for increasing aging temperature is observed. Time and temperature are two critical parameters that affect IMC formation.

Table 2.1 Au-Al IMC thickness measured for different temperature at different times.

Aging Time	Au-Al IMC Thickness		
	At 150°C	At 185°C	At 200°C
Un-Aged	815.0		
100 Hours	2996.6	4227.3	4394.9
200 Hours	5246.9	6007.8	7681.1
400 Hours	6371.7	7882.1	8316.2
800 Hours	6991.6	8891.3	-

Table 2.2 Cu-Al IMC thickness measured for different temperature at different times.

Aging Time	Cu-Al IMC Thickness		
	At 150°C	At 185°C	At 200°C
Un-Aged	~Few Tens of Nanometers		
100 Hours	186.2	509.1	779.6
200 Hours	255.7	629.0	1061.6
400 Hours	426.7	933.7	1469.4
800 Hours	610.2	1153.2	-

Arrhenius equation is a physics of failure model that can be used to model the IMC growth and develop a model to predict time to growth of IMC at a different temperature. Two parameters that are to be found from this model are the growth constant and the activation energy. The growth constant will be different at different temperatures, which will then be used to find the activation energy. IMC growth follows a parabolic relationship, where,

$$x = K \times t^{0.5} \qquad\qquad \text{(Eq. 1)}$$

x → Intermetallic compound thickness

K → Growth constant

t → time

Arrhenius relationship is given by,

$$K = Ce^{-E/kT} \qquad\qquad \text{(Eq. 2)}$$

C → constant,

E → Activation energy,

k → Boltzman Constant,

T → Absolute temperature in Kelvin

2.4. Result of Isothermal Aging

2.4.1. Au-Al Interfacial IMC

Using the Arrhenius equation as shown above, following graph (Figure 2.4) was plotted to

find the best fit to obtain line equation for which the slopes would give the growth constant.
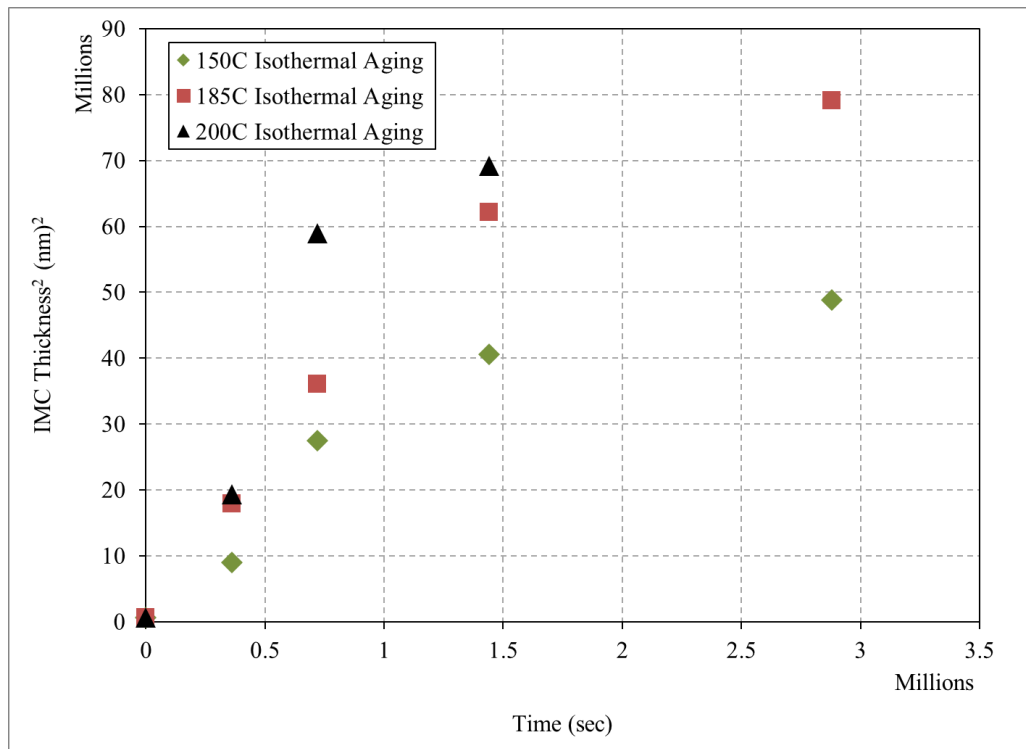
Figure 2.4 Au-Al IMC^2 Vs Time plot for 150°C, 185°C and 200°C.

Slop of these plots show an increase with the aging temperature which is expected as higher

temperature provides more energy for diffusion which in turn leads to more IMC

formation.
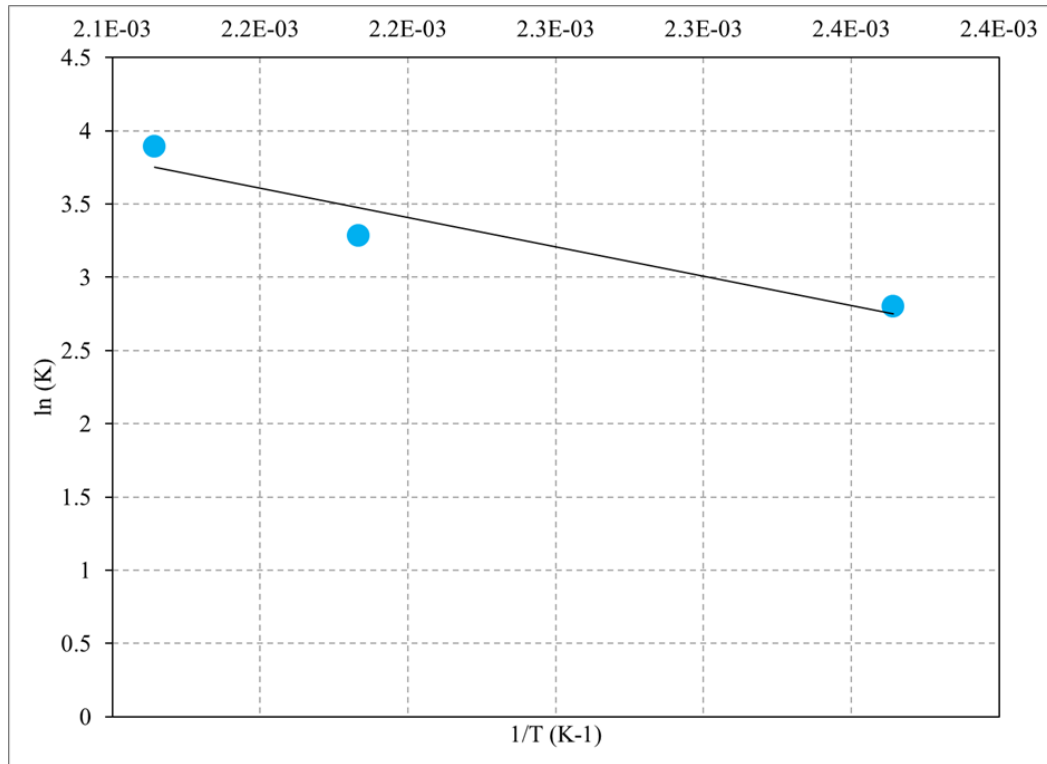
Figure 2.5 Plot to find the activation energy for Au-Al IMC.

Growth constant is related to the activation energy by equation 2. By rearranging the terms,

$$\ln(K) = \frac{-E_a}{R}\left[\frac{1}{T}\right] + \ln(Z) \qquad\qquad\text{(Eq. 3)}$$

This is in the form of,

$$y = mx + b \qquad\qquad\text{(Eq. 4)}$$

Hence, ln(K) vs 1/T plot (Figure 2.5) is made to find the slope which would lead to finding the activation energy. The values of the obtained growth constants and activation energy for the formation of Au-Al IMCs are shown in Table 2.3. These values lie within the range shown in literature, however, they are closer to the lower limit indicating that the actual

IMC growth in plastic encapsulated microelectronic devices are much higher than in the test vehicles that are mainly reported in the literature.

2.4.2. Cu-Al IMC

Similar to the Au-Al system, the Cu-Al IMC thickness were measured and tabulated as shown in Table 2.2 and their growth constants were found by finding the slope of the line for the IMC vs time plot. Figure 2.6 shows the parabolic nature of this curve, which is expected.
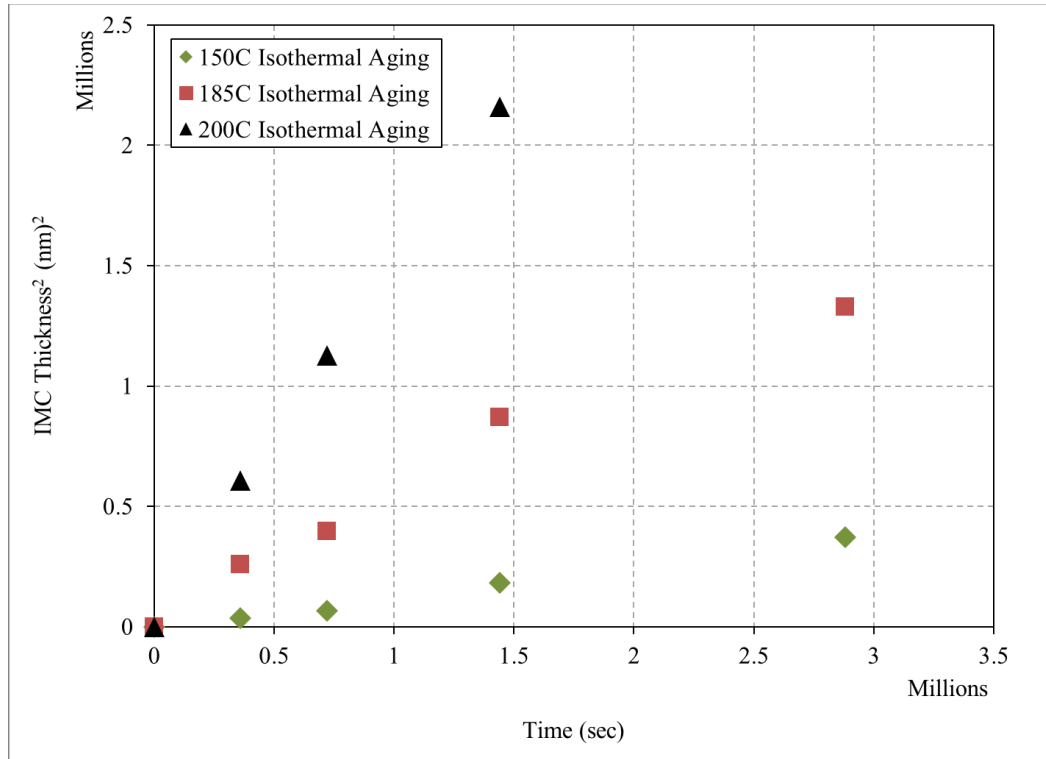
Figure 2.6 Cu-Al IMC^2 Vs Time plot for 150°C, 185°C and 200°C.

Using equation 3 and 4 we can obtain the activation energy from the growth constants at different temperature.
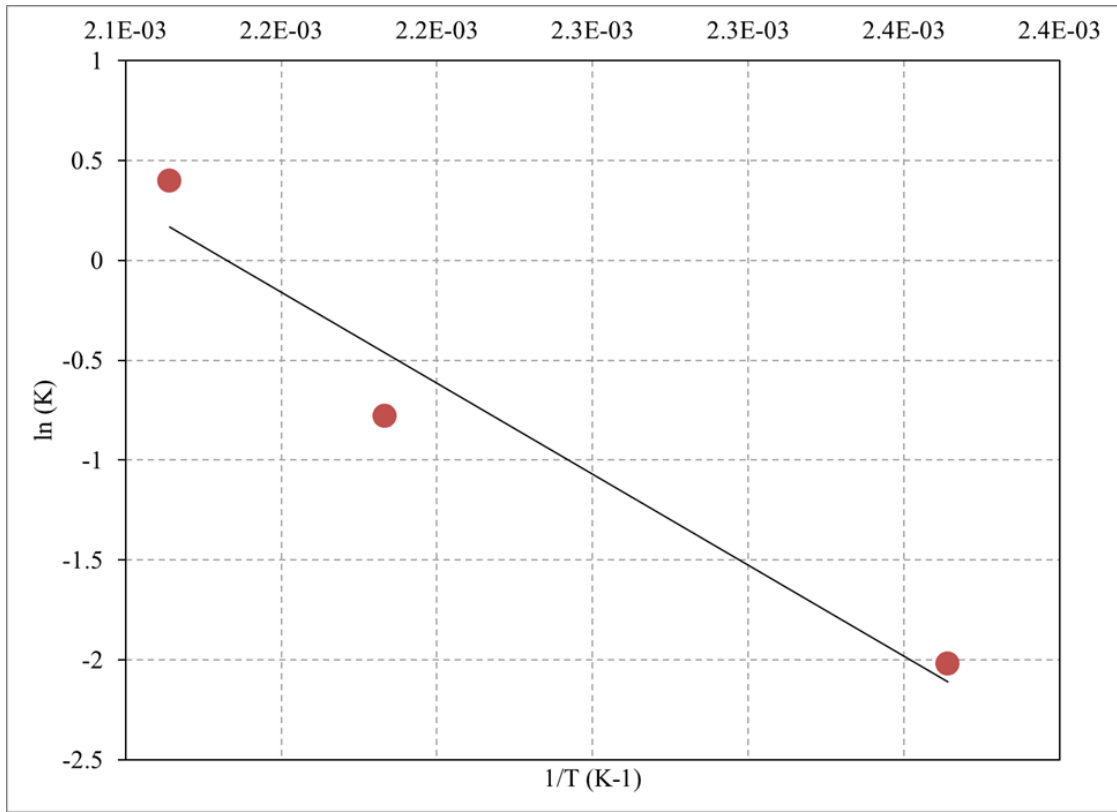
Figure 2.7 Plot to find the activation energy for Cu-Al IMC.

Slope of Au-Al is one order of magnitude higher than that of Cu-Al IMCs. With lower IMCs growing, the reliability of copper wire bonded devices would be higher for thermal aging conditions. Table 2.3, shows the comparison between Au-Al and Cu-Al kinetics.

Table 2.3: Comparison between Au-Al and Cu-Al IMC Kinetics.

Wire Bond Material	Slope at 150°C	Slope at 185°C	Slope at 200°C	Q (eV)
Gold (Au)	16.495	26.637	49.114	0.346
Copper (Cu)	0.132	0.458	1.486	0.784

Activation energy comparison shows that Cu-Al requires a higher energy, almost double, than that of Au-Al IMCs. E_a for Cu-Al is reported as between 60 to 129 kJ/mol [16]. This study showed $E_a = 75.7$ kJ/mol, which falls closer to the lower limit of the reported range, similar to the case of Au-Al IMC. This is attributed to studying the actual COTS parts with

copper and gold variant. So this study includes all the variations that would occur from devices that are manufactured by an OEM, unlike that done under laboratory conditions. Figure 2.8, Figure 2.9 and Figure 2.10 shows representative images of Au-Al and Cu-Al interface obtained at different aging conditions.
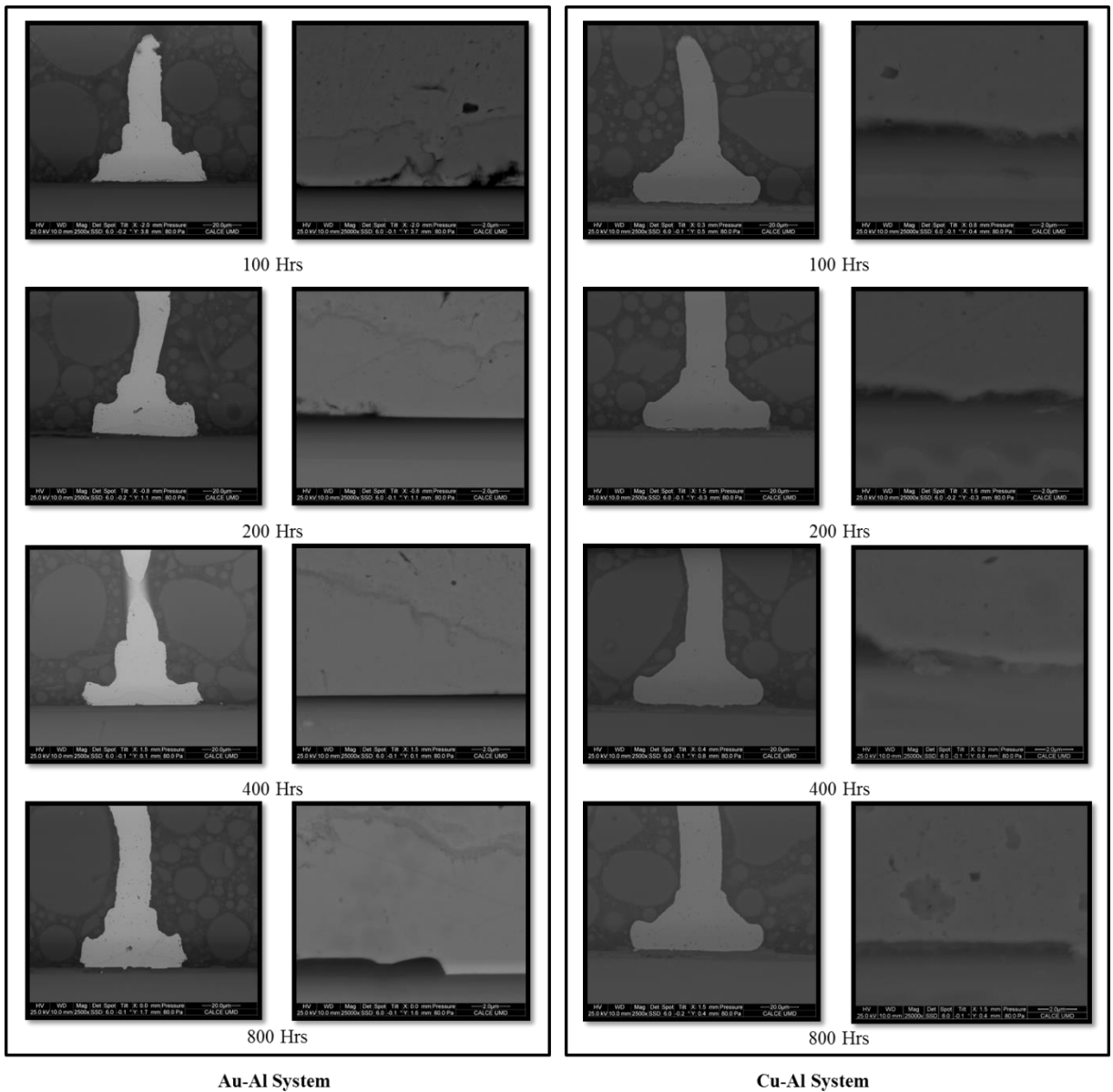
Figure 2.8: Representative images of Au wire boned and Cu wire bonded devices aged for different times at 150°C.

Au-Al System

Cu-Al System

Figure 2.9: Representative images of Au wire boned and Cu wire bonded devices aged for different times at 185°C.

100 Hrs

200 Hrs

400 Hrs

Au-Al System

100 Hrs

200 Hrs

400 Hrs

Cu-Al System
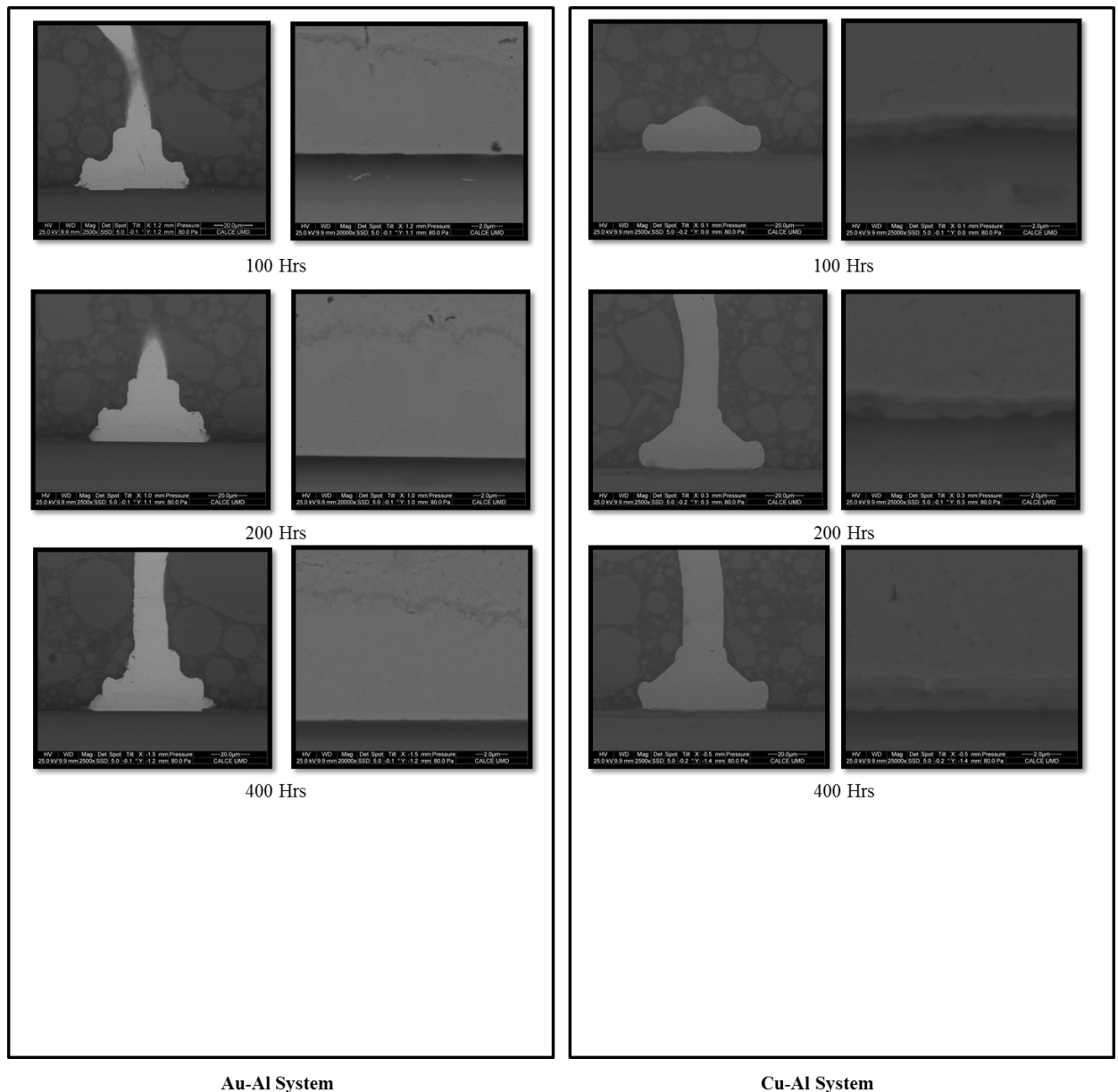
Figure 2.10: Representative images of Au wire boned and Cu wire bonded devices aged for different times at 200ºC.

In addition to IMC thickness measurements, these interfaces were examined for damage due to IMC growth. Kirkendall voiding in Au-Al joints have been widely reported, but was not observed in this study even at the maximum aging time of 800 hours in three of the temperature conditions. Cu-Al IMCs were found to be much thinner at all aging times than Au-Al, however, Cu-Al interface also showed signs of failure through interfacial separation

between Cu_9Al_4 and Cu as shown in Figure 2.11 which can act as stress concentration sites under thermal cycling condition leading to propagation of it resulting in an open circuit failure. Hence is important to assess Cu wire bond reliability under a combination of thermal aging and thermal cycling condition.
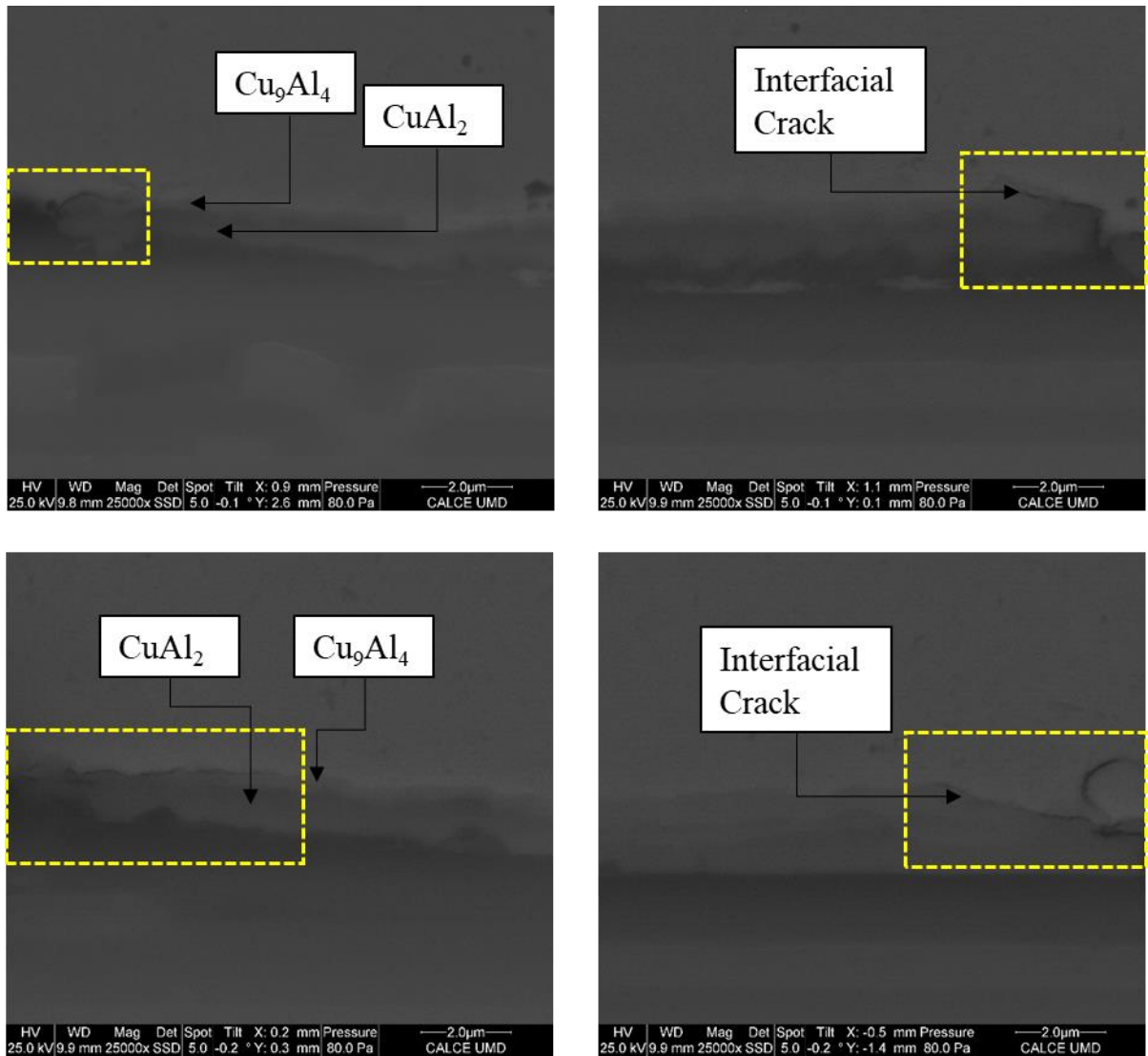
Figure 2.11: Interfacial Crack in Cu-Al Joints.

2.5. Summary

This study shows the comparison between Au-Al and Cu-Al wire bond-bond pad joints at accelerated isothermal aging condition. IMC growth rate was found to be slower with Cu

than with Au due to the slower diffusion rate of Cu in Al. IMC thickness measurements were performed at different time intervals and used along with Arrhenius equation to calculate activation energy for Au-Al and Cu-Al IMCs, which was found to be 33.4 KJ/mol and 75.7 KJ/mol respectively. Although Cu-Al has a higher activation energy, which results in thinner IMC compared to Au-Al joint, interfacial separation between Cu_9Al_4 and Cu was identified that could grow with further aging and under thermal cycling condition, leading to open circuit failure. Hence a detailed analysis of Cu-Al joint reliability is necessary to enable its use in extreme use conditions.

2.6. References

[1] Hannech, E. B., Lamoudi, N., Benslim, N., & Makhloufi, B. (2003). Intermetallic Formation in the Aluminum–Copper System. Surface Review and Letters, 10(04), 677-683. doi:10.1142/s0218625x03005396.

[2] Leong, G. C., & Uda, H. (2013). Comparative reliability studies and analysis of Au, Pd-coated Cu and Pd-doped Cu wire in microelectronics packaging. PloS one, 8(11), e78705.

[3] Jiang, Y., Sun, R., Yu, Y., Wang, Z., & Chen, W. (2010). Formation and Growth of Intermetallic Compounds in Cu–Au and Au–Al Systems for Copper on Gold Bonding. IEEE Transactions on Electronics Packaging Manufacturing, 33(3), 228-235.

[4] Wulff, F. W., Breach, C. D., Stephan, D., & Dittmer, K. J. (2004, December). Characterisation of intermetallic growth in copper and gold ball bonds on aluminium metallization. In Proceedings of 6th Electronics Packaging Technology Conference (EPTC 2004)(IEEE Cat. No. 04EX971) (pp. 348-353). IEEE.

[5] Jang, G. Y., Duh, J. G., Takahashi, H., & Su, D. (2006). Solid-state reaction in an Au wire connection with an Al-Cu pad during aging. Journal of electronic materials, 35(2), 323-332.

[6] H. Xu, C. Liu, V. V. Silberschmidt, S. S. Pramana, T. J. White, and Z. Chen, "A reexamination of the mechanism of thermosonic copper ball bonding on aluminium metallization pads," Scripta Materialia, vol. 61, pp. 165–168, Jul 2009.

[7] H. Xu, C. Liu, V. Silberschmidt, and Z. Chen, "Growth of intermetallic compounds in thermosonic copper wire bonding on aluminum metallization," Journal of Electronic Materials, vol. 39, pp. 124–131, 2010.

[8] H. Xu, C. Liu, V. V. Silberschmidt, S. S. Pramana, T. J. White, Z. Chen, and V. L. Acoff, "Behavior of aluminum oxide, intermetallics and voids in Cu–Al wire bonds," Acta Materialia, vol. 59, pp. 5661–5673, 2011.

[9] T. C. Wei and A. R. Daud, "The effects of aged Cu-Al intermetallics to electrical resistance in microelectronics packaging," Microelectronics International, vol. 19, pp. 38–43, 2002.

[10] R. Pelzer, M. Nelhiebel, R. Zink, S. Wöhlert, A. Lassnig, and G. Khatibi, "High temperature storage reliability investigation of the Al–Cu wire bond interface," Microelectronics Reliability.

[11] J. Onuki, M. Koizumi, and I. Araki, "Investigation of the reliability of copper ball bonds to aluminum electrodes," Components, Hybrids, and Manufacturing Technology, IEEE Transactions on, vol. 10, pp. 550–555, 1987.

[12] H. J. Kim, J. Y. Lee, K. W. Paik, K. W. Koh, J. H. Won, S. H. Choi, J. Lee, J. T. Moon, and Y. J. Park, "Effects of Cu/Al intermetallic compound (IMC) on copper wire and aluminum pad

bondability," in Electronic Materials and Packaging, 2001. EMAP 2001. Advances in, 2001, pp. 44–51.

[13] H.-J. Kim, J. Y. Lee, K.-W. Paik, K.-W. Koh, J. Won, S. Choe, J. Lee, J.-T. Moon, and Y.-J. Park, "Effects of Cu/Al intermetallic compound (IMC) on copper wire and aluminum pad bondability," Components and Packaging Technologies, IEEE Transactions on, vol. 26, pp. 367–374, 2003.

[14] C. L. Gan, E. Ng, B. Chan, F. Classe, T. Kwuanjai, and U. Hashim, "Wearout Reliability and Intermetallic Compound Diffusion Kinetics of Au and PdCu Wires Used in Nanoscale Device Packaging," Journal of Nanomaterials, vol. 2013, 2013.

[15] Chauhan, P. S., Choubey, A., Zhong, Z., & Pecht, M. G. (2014). Copper wire bonding. In Copper Wire Bonding (pp. 1-9). Springer, New York, NY.

[16] Marz, Benjamin, Stefan Scheibe, Andreas Graff, and Matthias Petzold. "Growth Behaviour of Gold-aluminum Intermetallic Phases (IMP) in Temperature Aged Ball Bonds Observed by Electron Backscatter Diffraction." 3rd Electronics System Integration Technology Conference ESTC (2010): n. pag. Web.

3. Design of Experiment, Test Equipment and Monitoring Systems

Objective of the experimental work was to understand the behavior of Cu-Al interface in wire bonded assemblies in extreme temperature long-dwell thermal cycling condition that is a combination of thermal aging and thermal cycling, where electronic packages are subjected to long time at maximum temperature at every thermal cycle. This chapter describes the experiment and different devices used in Part I study, including, electrical in-situ monitoring method, printed circuit board (PCB) design and fabrication and experimental set-up.

3.1. Design of Experiment

With the focus on studying the effect of thermal aging and thermal cycling on reliability of Cu wire bonds, as they would experience in real-life applications, a unique long dwell thermal cycling profile was designed to be used for accelerated experiment. The cycle would involve a ramp-up to high temperature, long dwell time at high temperature, ramp-down to low temperature, dwell at low temperature and ramp-up to room temperature. Such an environmental condition would lead to growth of IMCs at Cu-Al interface during high temperature dwell and cause thermally induced stress during ramp-up and ramp-down cycles. Two thermal extremes were chosen for the study, namely, industry based "standard" temperature condition (for down hole drilling application) from -40ºC to 150ºC and an accelerated "high" temperature condition from -40ºC to 185ºC. Temperature cycle was designed to have a ramp up/down of 5ºC/min with 4.5 hours dwell time at maximum temperature and a 1 hour dwell at minimum temperature.

A total of 24 test boards were used in the study, each of which comprised of 18 devices (2 devices of each type) with Cu and PCC wire bonds, from 7 different manufacturers that

have 4 different package types. This ensured a wide range of parameters that contributes to failure and hence a range of failure times were expected. 10 boards were subject to the standard test condition of which 5 boards were monitored in-situ for electrical resistance change and to spot open circuit failures, while the other 5 boards were removed at intervals of 100, 200, 400, 800 and 1600 hours. 14 boards were subjected to high test condition, of which 9 boards were monitored in-situ and 5 boards were removed at the above-mentioned intervals for analysis. Figure 3.1 summarizes the plan of experiment.
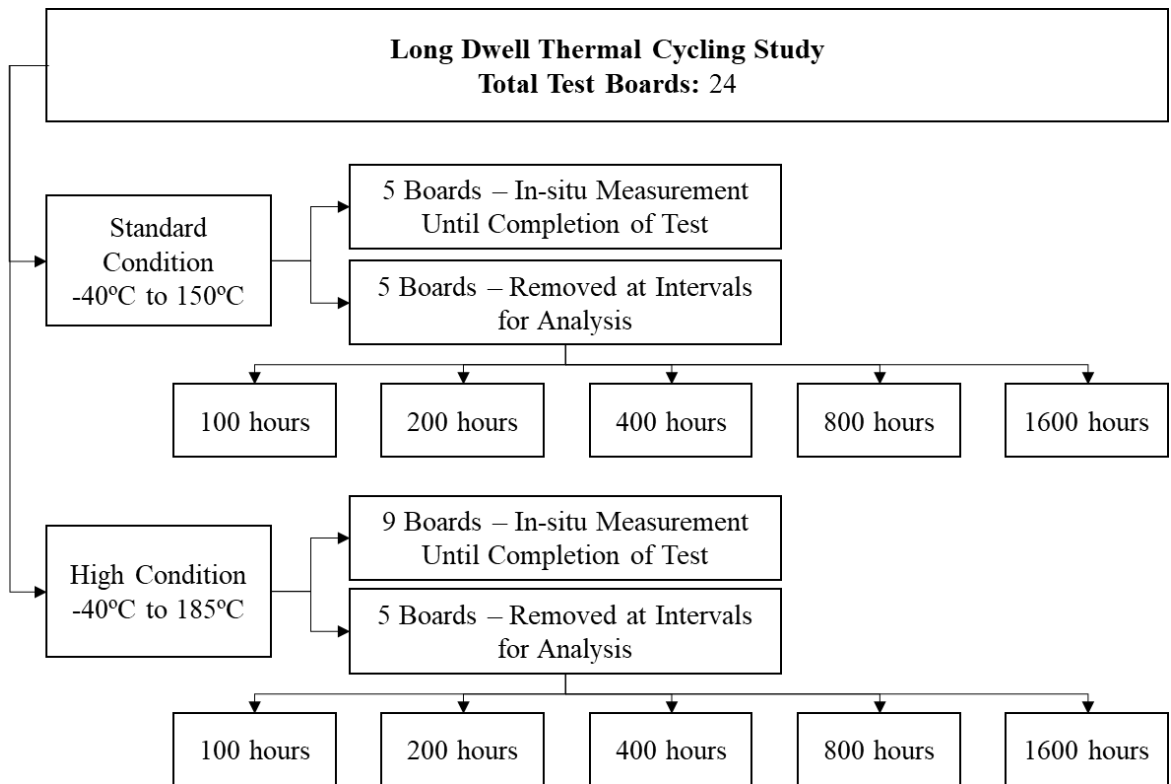
Figure 3.1: Design of Experiment (DOE) for Long Dwell Thermal Cycling Study.

Boards removed at intervals were subjected to non-destructive and destructive analysis to compare with initial measurements and assess damage on wire bonds or to identify failure time.

3.2. Test Vehicle – COTS Parts With Cu Wire Bonds

Major switch to use of Cu wire bonds were made only recently at the time of starting this work, hence there were only few OEMs that had already made the conversion to copper wire bond and whose parts would be available for purchase. Copper content varied significantly from one manufacturer to another, such as, 99% represented as 2N, 99.9% (3N) and 99.99% (4N). In addition several other materials such as Palladium (Pd) coated Cu (PCC), Ag coated Cu and Pd doped Cu are available. However, with the addition of dopants and coating material wire bond process cost has been shown to increase in addition to the complexity in the bonding condition, hence this study was restricted to only Cu and PCC which are the two widely available alternatives to Au wire bond material, in the industry.

Since COTS parts are used in this study, a wide variety of parts are available based on functionality, package type, device reliability ratings, geometrical and material characteristics. Nine devices were selected from this wide gamut of devices, which were commercially available and also represented different functionality, package type and manufactured by different OEMS as shown in Table 3.2.

Device 1 was a voltage regulator used for a wide variety of applications including local, on-card regulation. It is designed as a three pin transistor outline (TO) package and is the only through-hole component used in this study. The package was assembled on the board through bending the three leads and securing the component with an additional bolt and nut at the hold provided on the top of the device as shown in Table 3.2. This device has copper wire bonds of ~50um diameter, largest used in this study.

Device 2 was a thyristor, used for functioning as a programmable overvoltage protector. This is a surface mount eight leaded small outline integrated circuit (SOIC) type package. Eight copper wire bonds of ~45um are present in the device connecting all leads.

Device 3 was a field programmable gate array, specifically designed for meeting high volume, cost-sensitive consumer electronic applications. This is a surface mount, thin quad-flat package (TQFP) with 100 I/Os and has the largest external dimensions compared to other packages used in the study.

Device 4 was a field programmable gate array. This is a surface mount, quad flat no-leaded (QFN) package with 48 I/Os.

Device 5 was a field programmable gate array. This is a device similar to device 4 and manufactured by the same OEM. This device was expected to fail at the same time as device 4 and was included in the study to verify the correctness of running the test.

Device 6 was a single-chip Bluetooth device, used for applications such as health care sensors, smart watches, sports equipment, remote controls, etc. It is a surface mount QFN package with 32 I/Os consisting of copper wire bonds.

Device 7 was a mixed signal micro-controller, typically used for 2-wire and 3-wire single phase metering. This is a 64 leaded QFP package that consists of Cu wire bonds.

Device 8 was an interface IC. Although device 7 and 8 were manufactured by the same OEM, they perform different functions and have different wire bond characteristics that makes them unique for this study. It is also a 64 leaded QFP device.

Device 9 was a high-performance digital signal controller. This is an 80 leaded QFP with palladium coated copper wire bonds.

All of these nine devices were live parts with active circuitry inside which required identification of a baseline characteristic that could be compared to after thermal cycling. Continuity measurement was done to identify the longest chain in each of the device, which would cover maximum number of wire bonds whose degradation could be monitored. Table 3.1 shows an example of one such multi-meter measurement for device 2. Results from this analysis was used in the board design to monitor specific leads in devices that would be used to monitor failure of the device.

Table 3.1: Probing Analysis to Find Longest Internal Connection within Device 2.

Leads	1	2	3	4	5	6	7	8
1	-	X	X	✓	X	X	✓	✓
2	✓	-	✓	✓	✓	X	✓	✓
3	✓	✓	-	✓	✓	X	✓	✓
4	X	X	X	-	✓	X	✓	X
5	✓	X	X	X	-	X	✓	✓
6	X	X	X	X	X	-	X	X
7	X	X	X	X	X	X	-	X
8	✓	X	X	X	✓	X	✓	-

Table 3.2: DUT Characteristics and Non-Destructive Analysis Results.

Device No.	Device 1	Device 2	Device 3	Device 4	Device 5	Device 6	Device 7	Device 8	Device 9
Package Type	TO	SOIC	TQFP	QFN	QFN	QFB	QFP	QFP	QFP
Part Category	Voltage Regulator	Thyristor	FPGA	FPGA	FPGA	Buletooth	Micro-Controller	IC	Digital Signal Controller
Length (mm)	30	5	15.8	6	6	7.5	12	12	13.7
Width (mm)	10	3.9	15.8	6	6	7.5	12	12	13.7
Thickness (mm)	4.7	1.3	1	0.8	0.8	0.9	1	1	1
Input/Output Pins	3	8	100	48	48	32	64	64	80
Wire Bond Material	Cu	Cu	PCC	PCC	PCC	Cu	Cu	Cu	PCC
Package Image									
X-Ray Analysis									
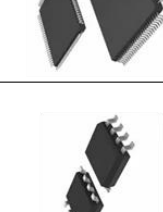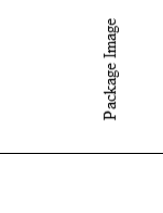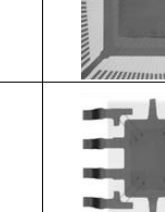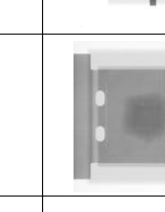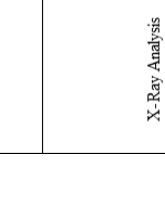
3.3. Printed Circuit Board (PCB) Design and Assembly

This study was done with high temperature (maximum of 150ºC and 185ºC) hence PCB material selection was done appropriately to reach such temperature without damage to the board. Polyimide was used as the PCB fabrication material due to its high temperature capability, that includes high glass transition (Tg) of 260ºC and capability to withstand high temperature without early degradation. Electroless Nickel Immersion Gold (ENIG) was used as the final finish on solder pads in the board due to its capability to retard interfacial intermetallic compound (IMC) with SAC 305 solder. The cross-sectional structure of the board is shown in Figure 3.2.
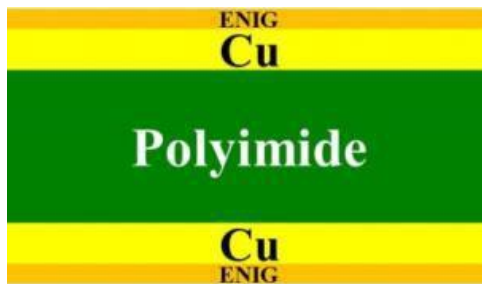
Figure 3.2: Cross-section View of PCB.

A total of 24 test boards were used in this study with each board consisting of two of the nine different devices. These eighteen packages were placed at symmetric locations on the board. Each device was provided with several locations for probing, in addition to monitoring two pins determined by the longest internal chain connection for each device. Trace lines from each device terminated at the bottom of the board at plated through holes (PTH), where one end of Teflon coated wires were soldered manually which would be used for in-situ monitoring. Other end of wires was connected to a 34923T 80 Channel Reed MUX card which in-turn was connected to data acquisition instrument. Wire connection at

the board was additionally secured through use epoxy based potting material at the primary

and the secondary side of the board. Each of the PCBs were mounted between a top and a

bottom frame made of aluminum with 14 bold and nuts as shown in the final assembly in

Figure 3.3. Warpage from these constraints would be unique, which was the reason to place

devices symmetrically throughout the board.
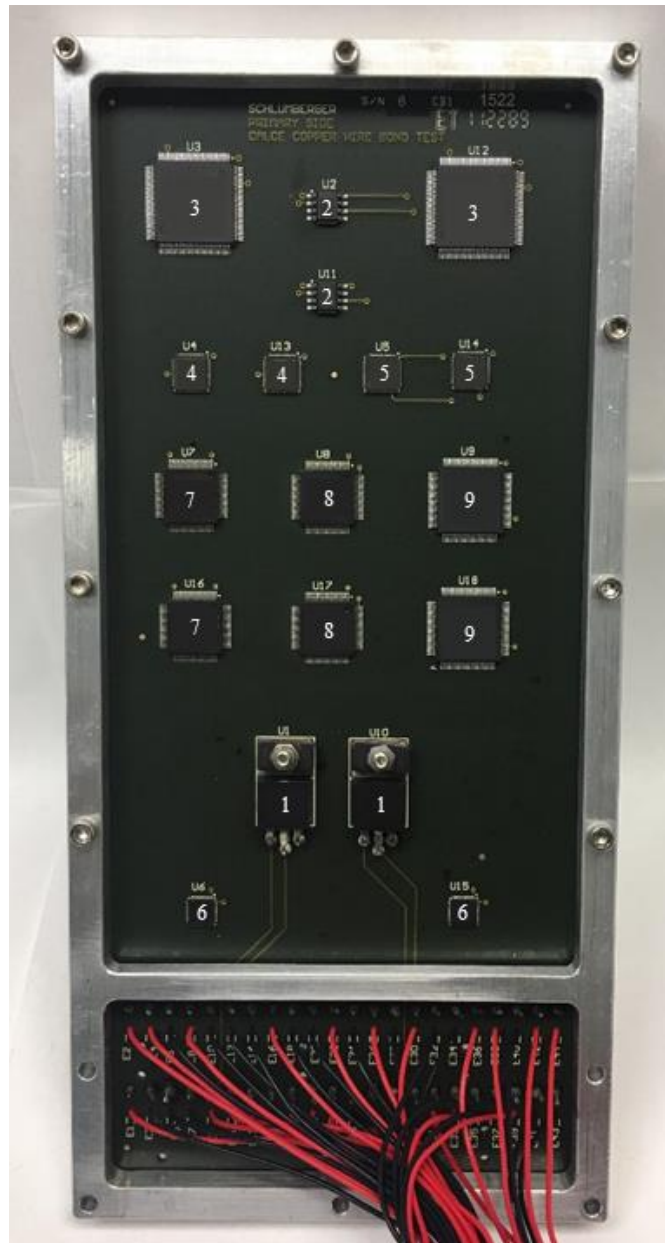
Figure 3.3: Printed wiring assembly with Al frames on both sides.

All devices were monitored through the internal connection identified from multi-meter probing as mentioned before. Table 3.3 shows lead connections in each of the devices used in study. Base line resistance measurement were carried which would be used for comparison during test to point out failure. Considering resistance increase of certain percentage would not be valid in this study due to the live nature of components used in study whose internal circuitry performance can cause variation. Additionally, solder joints were part of the electrical measurement path and their degradation/failure would also contribute to in-situ results. Hence a complete open-circuit accompanied with cross-sectional analysis was needed to be performed in order to narrow down failure to wire bonds.

Table 3.3: Pin Connections for Devices Under Test (DUT).

Device No.	Pin Connection	
	Source	Ground
1	2	1
2	2	8
	1	6
3	22	1
	95	23
4	19	1
5	35	1
6	1	32
7	16	1
8	64	1
9	1	64

3.4. Failure Criteria for Long Dwell Thermal Cycling Test

Four parameters were monitored for identification of failure, namely, (1) In-situ electrical resistance, (2) I-V characterization at intervals, (3) IMC thickness, (4) Interfacial crack at intervals and (5) Bond shear strength. However, use of in-situ and IV characterization was

not efficient in detecting wire bond failure due to solder joints that were present in the measurement path way and due to internal circuitry in these COTS parts whose failure could not be distinguished from those of wire bonds. Hence, IMC thickness, interfacial crack and bond shear analysis were the only three conditions that was able to relate to degradation/failure of wire bonds, out of which, observance of a continuous interfacial separation was defined as failure (from cross-sectional analysis). Hence failures times were detected only at the intervals when the devices were taken out for cross-sectional analysis.

4. Interfacial IMC Growth Kinetics Modelling Using Arrhenius Relationship

Intermetallic compounds (IMCs) between Cu bond and Al bond pad are formed during the ultrasonic bonding process and have shown to be around ~15-40 nm in thickness in the region of contact between Cu and Al [11]. This initial IMC formation provides the adhesion strength between bond and bond. However, with growth in thickness of the IMC a higher electrical resistance, oxidation and interfacial cracking has been observed. Hence modeling to growth in thickness of these IMCs are of utmost importance in reliability analysis.

4.1. Introduction

As shown in the Chapter 2, the test vehicle consisted of COTS parts that comprises of Cu and Palladium (Pd) coated Cu, various bond pad thicknesses and bond parameters. These differences lead to change in interfacial reaction and affect growth rates of interfacial IMCs. Cross-sectional analysis and subsequent electron microscopic imaging provided a means to measure these IMCs, data from which was used to derive growth constants and activation energy through use of Arrhenius modelling.

Currently available studies on Cu wire bonded interface shows a wide range of growth constants and activation energies as listed in Table 4.1. These variations arise from the different bonding conditions that were used to make the bonds which result in different grain sizes, grain boundary densities and defects such as dislocations, which all contribute to short-cut paths for Cu diffusion in Al as compared to bulk diffusion. Most of these studies uses lab made wire bonds with unknown bonding parameters on test chips whose bond pad material and geometrical characteristics may not match to that of COTS parts, used in the industry. Thus due to a combination of the wide range in IMC characteristic

60

values and non-conformity with COTS parts, this IMC study was performed to aid in obtaining realistic results to estimate IMC growth kinetics and therefore reliability.

Table 4.1: Cu-Al IMC Activation Energy and Growth Constant Present in Literature.

IMC	HTS Temperature (°C)	E_a (KJ/mol)	$K_0(m^2s^{-1})$	Reference
Cu-Al	175, 200, 250	60.79	1.21×10^{-7}	[1][2]
Cu-Al	200, 250, 300	97.45	1.21×10^{-7}	[3]
Cu-Al	150, 200	129.29	1.63×10^{-4}	[4]
Cu-Al	175, 200, 225, 250	121.57	3.70×10^{-5}	[5]
Cu-Al	150, 180, 200	121.57	Unknown	[6]
Cu-Al	150, 250, 300	109.99	1.39×10^{-8}	[7][8]
Cu-Al	150, 175, 200	113.85	1.43×10^{-8}	[9]
Cu-Al	150, 200, 250	44.38	1.64×10^{-6}	[10]

4.2. IMC Growth Rate in Cu-Al Wire Bonded Joint and Arrhenius Modelling

IMC growth is diffusion controlled which in turn arises from a concentration gradient between Cu and Al at the bonded interface. Diffusion occurs in response to a concentration gradient expressed as the change in concentration due to a change in position, $\partial C / \partial X$. The local rule for movement or flux J is given by Fick's 1st law of diffusion:

$$J = -\chi \frac{\partial C}{\partial X}$$

in which the flux J [cm^{-2} s^{-1}] is proportional to the diffusivity χ [cm^2/s] and the negative gradient of concentration, $\partial C / \partial X$ [cm^{-3} cm^{-1}] or [cm^{-4}]. The negative sign indicates that J is positive when movement is down the gradient, i.e., the negative sign cancels the negative gradient along the direction of positive flux [12].

Fick's second law of diffusion predicts how the concentration gradient changes with time due to inter-atomic movement. Mathematical representation of which is given in Eq 2.

$$\frac{\partial C}{\partial t} = D \frac{\partial^2 C}{\partial t^2}$$

The above equation can be solved in many ways based on the initial boundary conditions. In most cases, it is fair to assume a plane with constant composition due to which diffusion is $\propto \sqrt{t}$. An extrapolation of this would mean that IMC thickness is also $\propto \sqrt{t}$. This results in a parabolic growth model expressed as,

$$h = D_o t^{0.5}$$

D0 here is obtained from the well-known Arrhenius equation represented by,

$$D_o = A_o e^{\left(\frac{-Q}{RT}\right)}$$

IMC thickness plot for device 1 of aging time up to 2100 hours at maximum temperature of 150°C and 185°C is shown in Figure 4.1. Time and temperature dependence of IMC thickness as shown in the above equations is clearly visible, with a 58% higher thickness at 185°C than at 150°C. A parabolic relationship is also visible, especially with 185°C

condition that is used in the Arrhenius modelling as shown above. A higher thickness at 100 hours compared to un-aged condition is attributed to measurement error at the un-aged conditions, where thickness anywhere less than 500nm was not clearly visible.
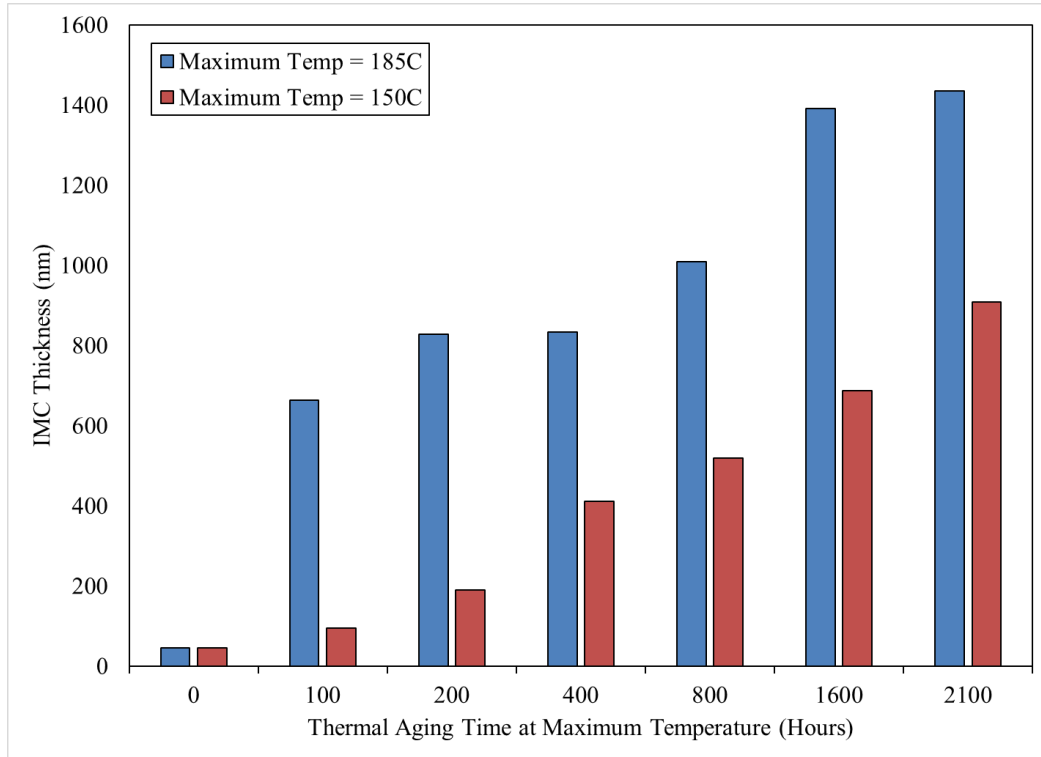
Figure 4.1: IMC Thickness for Device 1 for 150C and 185C Conditions.

Representative cross-sectional images of bonds aged to different times are shown in Figure 4.2. Growth of $CuAl_2$ and Cu_9Al_4 IMC phases (dark and light colored region) and interfacial crack between Cu_9Al_4 and Cu can be seen in the case of 185°C while not present in 150°C. However, crack at 185°C condition was not continuous throughout the bonded interface even at 2100 hours. Such an analysis was used to develop failure times which will be discussed in more detail in the following chapters.

STC Device 1 100 Hours

HTC Device 1 100 Hours

STC Device 1 200 Hours

HTC Device 1 200 Hours

STC Device 1 400 Hours

HTC Device 1 400 Hours
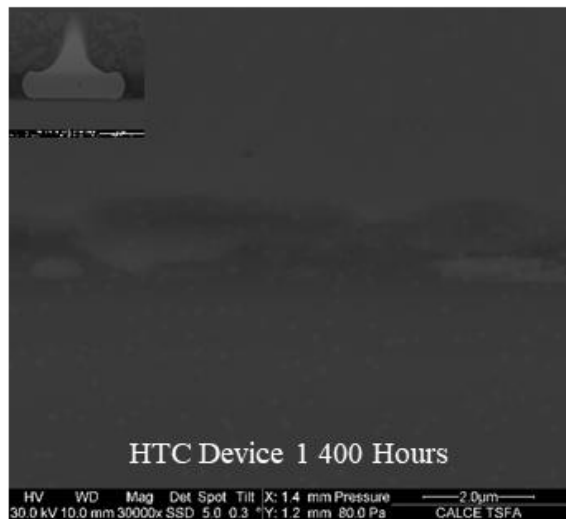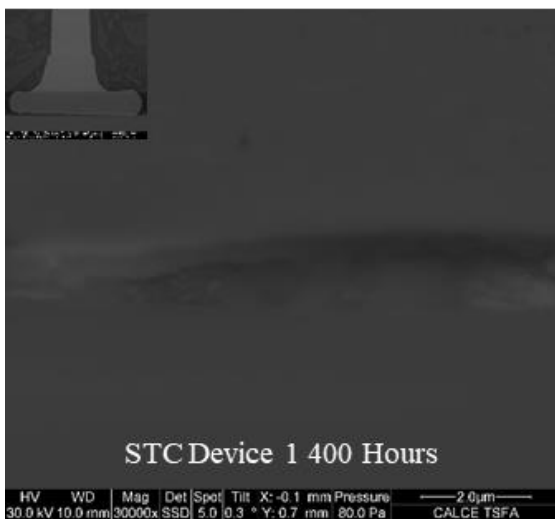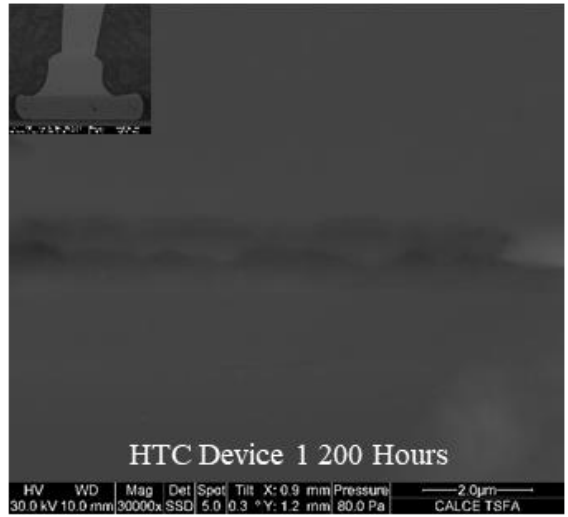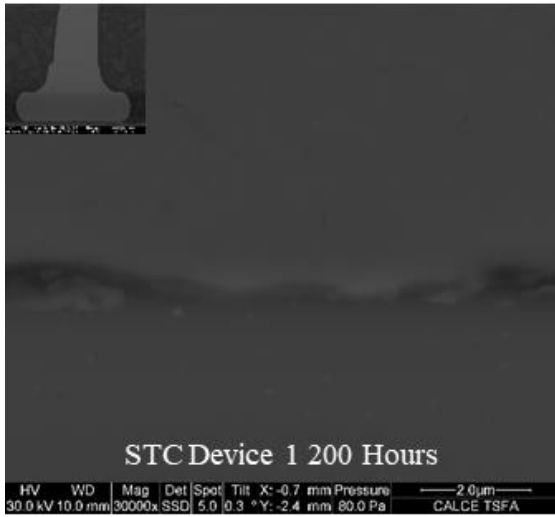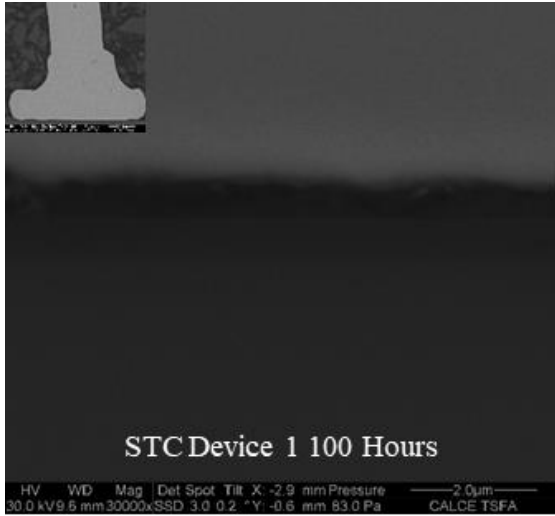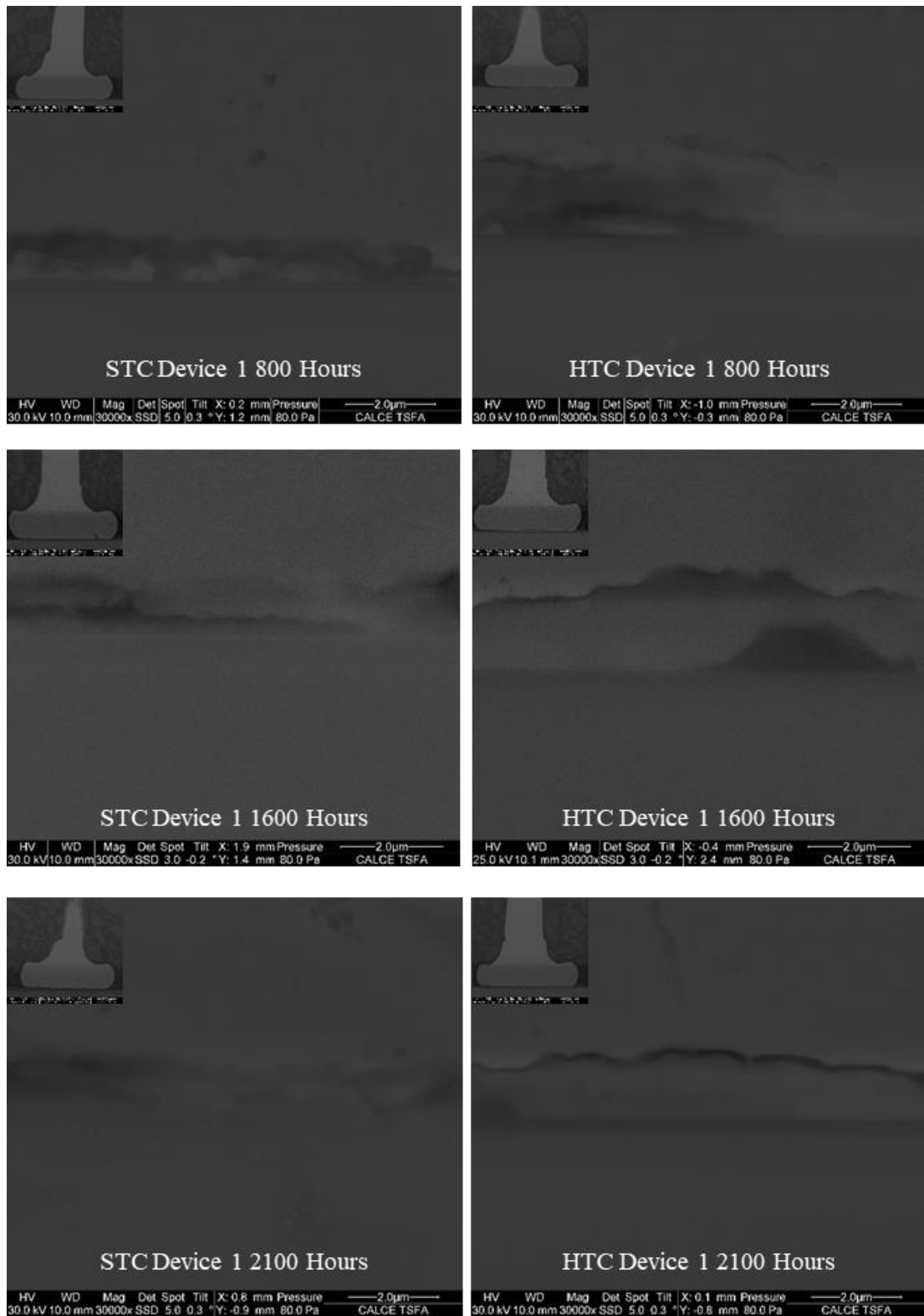
Figure 4.2: Representative Images of Device 1 Aged to Different Times at STC (150 °C) and HTC (185 °C) Condition.

IMC thickness measurements were performed on at least one bond at each aging condition by obtaining high magnification images at 20,000X to 30,000X of the entire interface and by using an open source tool, Image J. Area of IMC was measured first and then divided by the length over which the area was measured as shown in equation below,

$$\text{Interfacial IMC Thickness} = \frac{IMC\ Area}{IMC\ Length}$$

This method was preferred over others due to the non-uniform nature of the IMC growth in Cu-Al joints. Figure 4.3 explains the measurement process.
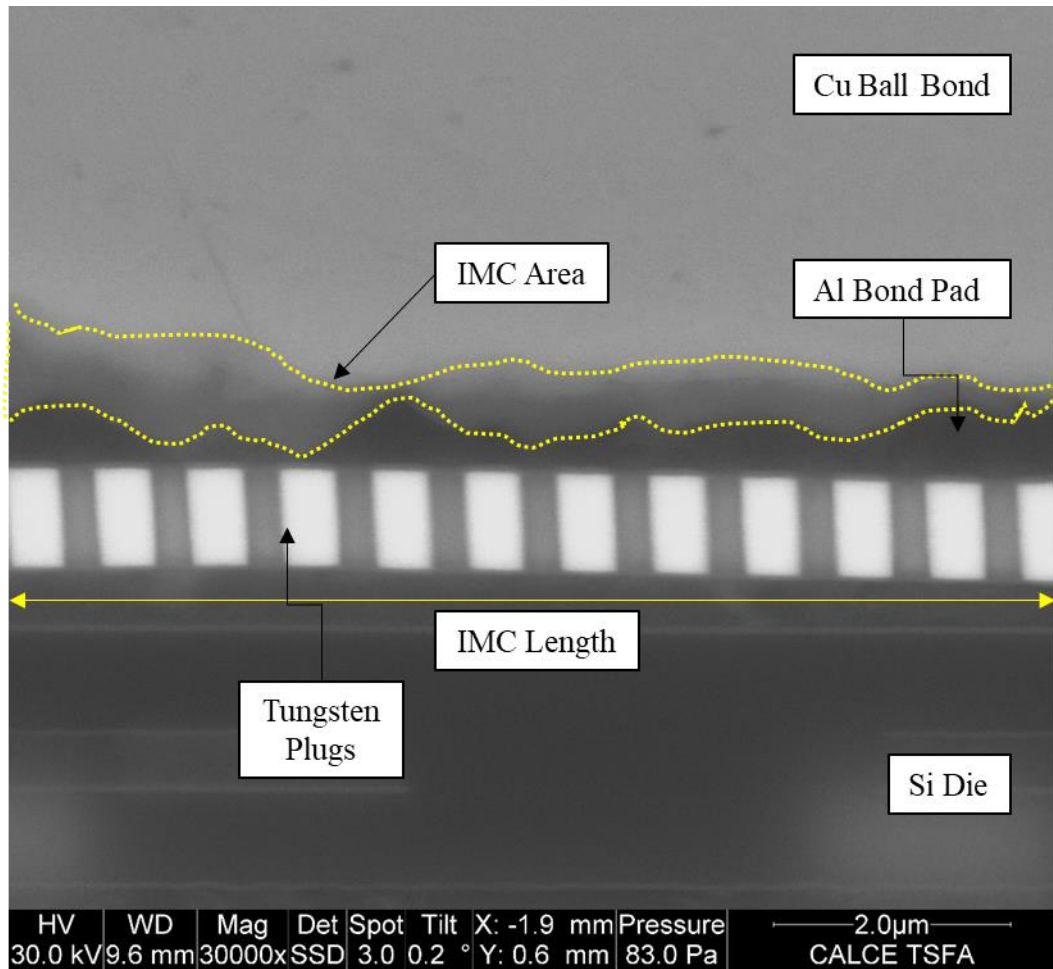
Figure 4.3: Interfacial IMC Measurement

Results from measurement of IMCs at different aging conditions for all of the devices are presented in Figure 4.2, which was used for the growth constant estimation at 150°C and 185°C as well as calculation of activation energy for Cu-Al IMC.

Table 4.2: IMC Thickness Measurement for all Nine Devices under Study

Aging Condition	IMC Thickness								
	Device 1	Device 2	Device 3	Device 4	Device 5	Device 6	Device 7	Device 8	Device 9
Un-Aged	45.6	64.0	87.0	56.2	44.4	46.4	48.6	57.6	51.8
100 Hours at 150°C	95.5	211.0	229.4	134.6	198.2	114.4	197.4	143.9	172.7
200 Hours at 150°C	189.2	275.3	243.3	186.1	234.5	130.9	403.7	214.6	232.8
400 Hours at 150°C	410.8	380.4	354.4	312.7	305.2	249.8	451.2	378.6	307.6
800 Hours at 150°C	520.0	510.0	424.0	358.5	382.6	553.2	553.7	385.2	464.6
1600 Hours at 150°C	686.6	982.0	876.0	646.5	541.9	746.6	832.6	716.4	524.6
2100 Hours at 150°C	908.5	993.4	1038.0	753.3	947.4	871.2	873.6	764.7	617.3
100 Hours at 185°C	662.9	501.3	285.6	465.5	541.4	288.3	477.9	275.9	263.5
200 Hours at 185°C	828.3	732.8	314.5	532.2	619.4	345.9	495.6	332.1	429.1
400 Hours at 185°C	832.9	1236.3	894.4	706.6	690.7	445.0	755.4	552.3	531.5
800 Hours at 185°C	1008.9	1441.9	963.3	889.2	1020.9	1089.5	864.9	615.1	544.3
1600 Hours at 185°C	1391.1	2115.0	1125.0	995.9	983.7	1399.0	1026.7	772.5	698.6
2100 Hours at 185°C	1435.8	1950.0	950.0	1206.1	1026.9	1495.9	1130.3	846.8	800.1

Figure 4.4 shows the bar charts of the measurements that are similar to the trend seen with Device 1 as shown above. In some cases, IMC thickness was found to be larger than that at an earlier time, which is due to several factors such as different device used for cross-section, non-uniformity of IMC growth and the plane of the wire-bonded interface in which these measurements were made.
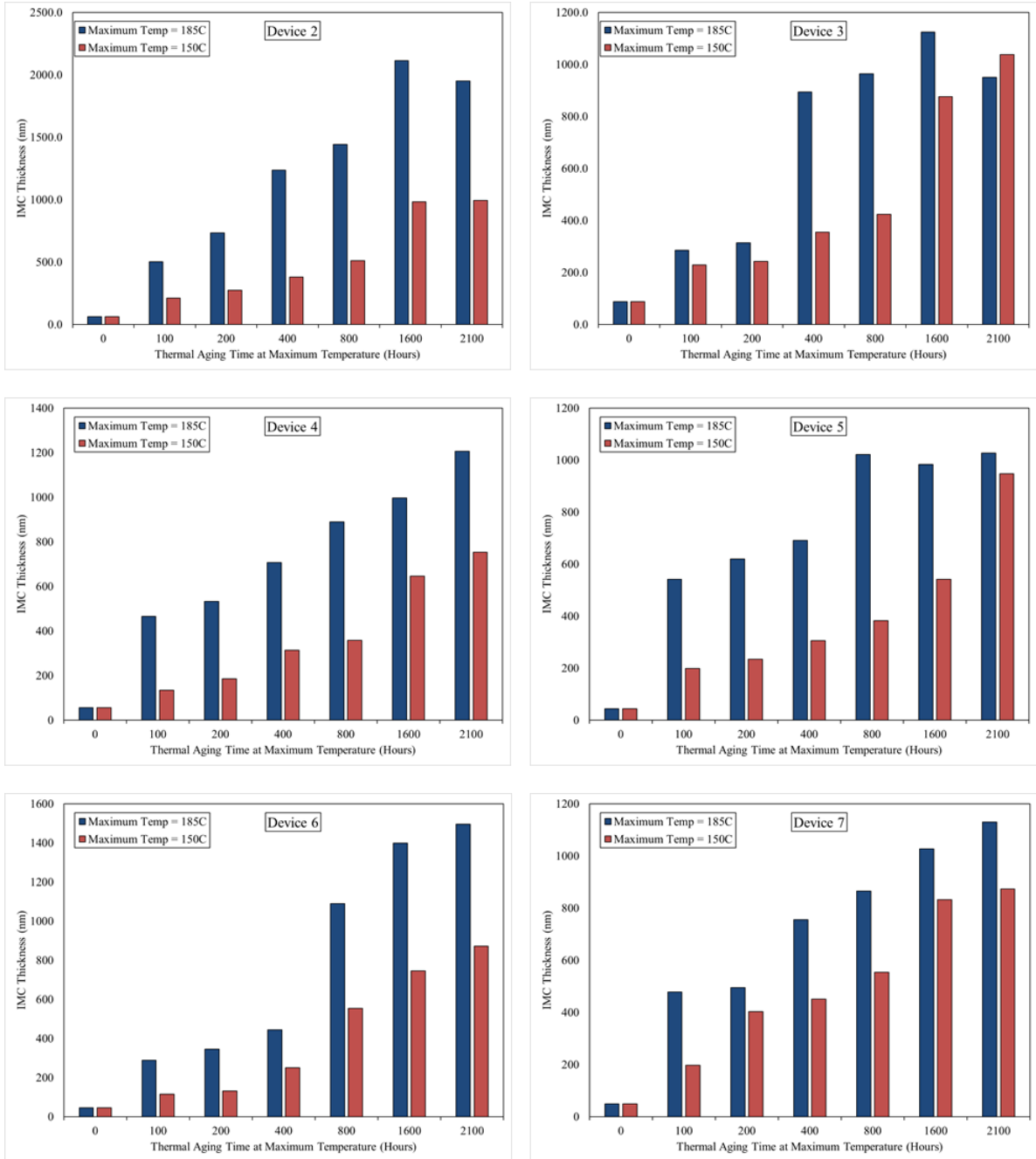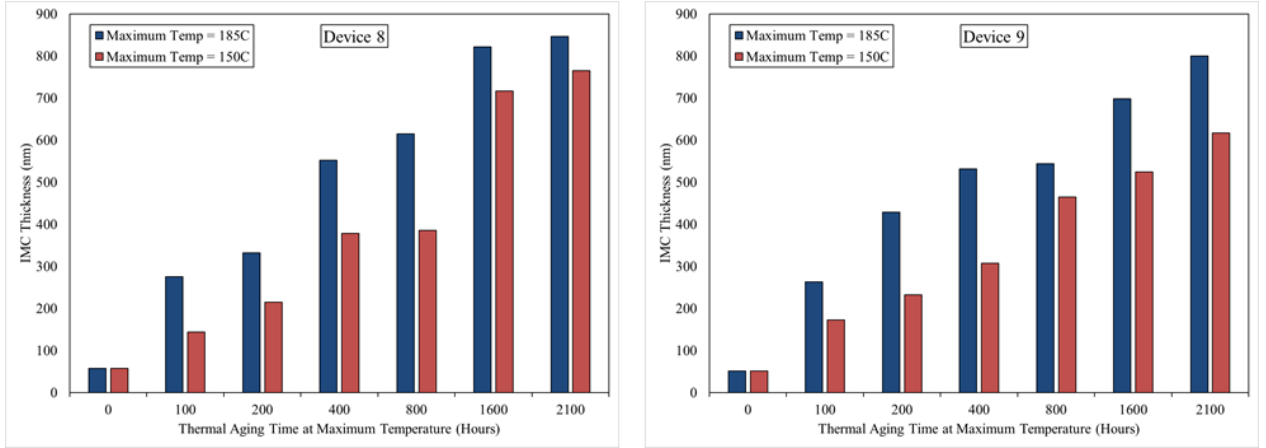
Figure 4.4: Bar Chart Showing IMC Thickness for all Devices under Study.

Using the above values, IMC thickness vs time$^{1/2}$ chart was plotted to obtain slope of the curve in order to calculate the reaction rates as given in the equation below.

$$X^2 = K \times t$$

$$K = K_0 \times e^{\left(-\frac{Q}{RT}\right)}$$

Using slope from two of the aging conditions 150°C and 185°C, ln(K) vs 1/T plot was made to find K_0 and Q as shown in Figure 4.5 (chart represents Device 1). From the bottom plot, K_0 is calculated to be $2.6 \times 10^{-6}\,(m^2 s^{-1})$ and Q is found to be 31.8 (KJ/mol).
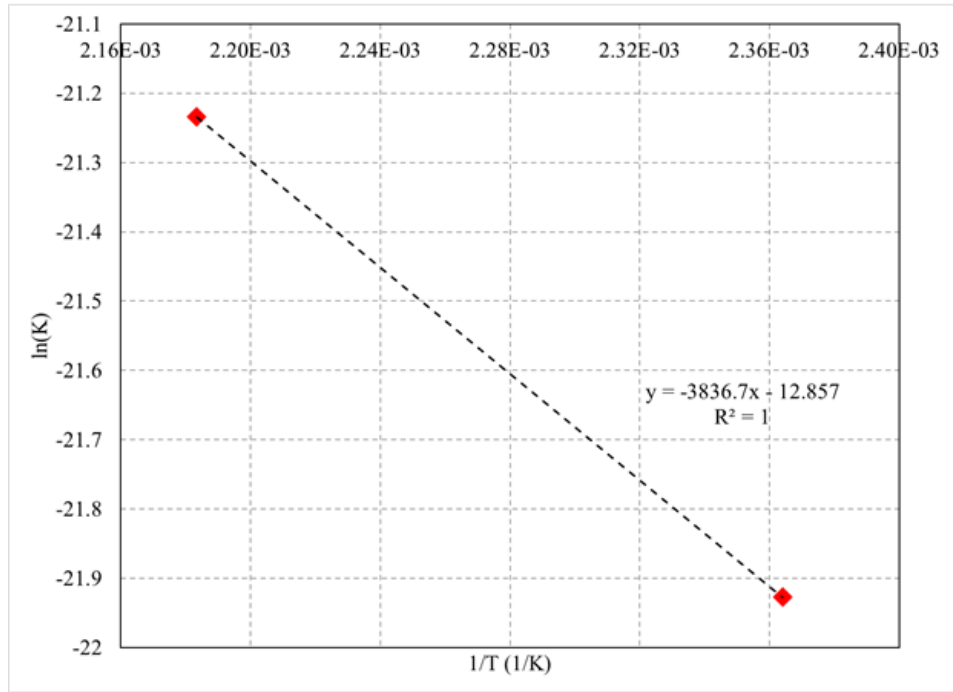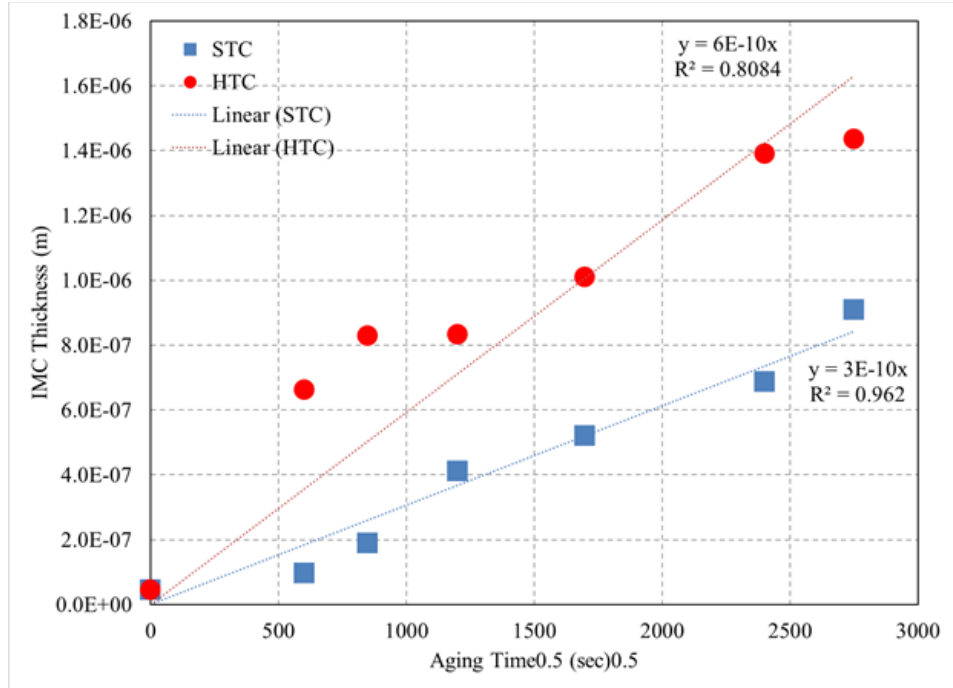
Figure 4.5: Arrhenius Modelling for IMC growth in Device 1.

Table 4.3 shows K_0 and Q values for all of the nine devices under study. Although the

devices consisted of Cu and PCC wire bonds on Al bond pad, variation in K_0 and Q were

observed. This change could arise from the different diffusion paths such as grain boundary

and dislocations that exists at these interfaces as discussed above. Two distinct groups were observed, one with power devices which has an activation energy between 30 to 41.4 KJ/mol and the other with small signal devices with activation energy between 11 to 27.5 KJ/mol.

Table 4.3: Activation Energy for Difference COTS Parts used in Study.

Package Type	Device No.	Slope at 150°C	Slope at 185°C	K_0 (m^2/s)	Q (eV)	Q (KJ/mol)
Cu Wire Bond – Power Device	Device 1	3.065×10^{-10}	5.928×10^{-10}	1.7×10^{-6}	0.314	30.354
	Device 2	3.619×10^{-10}	8.896×10^{-10}	4.6×10^{-5}	0.428	41.39
Cu Wire Bond – Small Signal Device	Device 6	2.994×10^{-10}	5.355×10^{-10}	6.0×10^{-7}	0.243	26.757
	Device 7	3.387×10^{-10}	4.622×10^{-10}	1.9×10^{-8}	0.148	14.306
	Device 8	2.684×10^{-10}	3.458×10^{-10}	7.3×10^{-9}	0.120	11.66
PCC Wire Bond – Small Signal Device	Device 3	3.443×10^{-10}	5.238×10^{-10}	8.3×10^{-8}	0.200	19.309
	Device 4	2.585×10^{-10}	4.695×10^{-10}	6.3×10^{-7}	0.284	27.463
	Device 5	2.798×10^{-10}	4.591×10^{-10}	1.8×10^{-7}	0.236	22.788
	Device 9	2.343×10^{-10}	3.160×10^{-10}	1.1×10^{-8}	0.142	13.766

Comparison between these devices shows a correlation between activation energy and bond pad thickness as with Device 2 (pad thickness 5µm) in Figure 4.6 and Device 6 (pad thickness 2 µm) in Figure 4.7. Failure time, as will be shown in the next chapter, is also different for both cases, with 1600 hours for Device 6 and no failure for Device 2. Interfacial (ball bond-bond pad) images were obtained for both devices as shown in Figure 4.6 and Figure 4.7. It can be seen that the 2nd phase of IMC, Cu_9Al_4, is much thinner in the case of Device 2 than in Device 6. Also, an interfacial failure at the region between Cu_9Al_4 and Cu is observed in the former case. Although such a correlation between pad thickness and life time exists, there may other variables contributing to failure time since COTS parts were used in this part of the study.
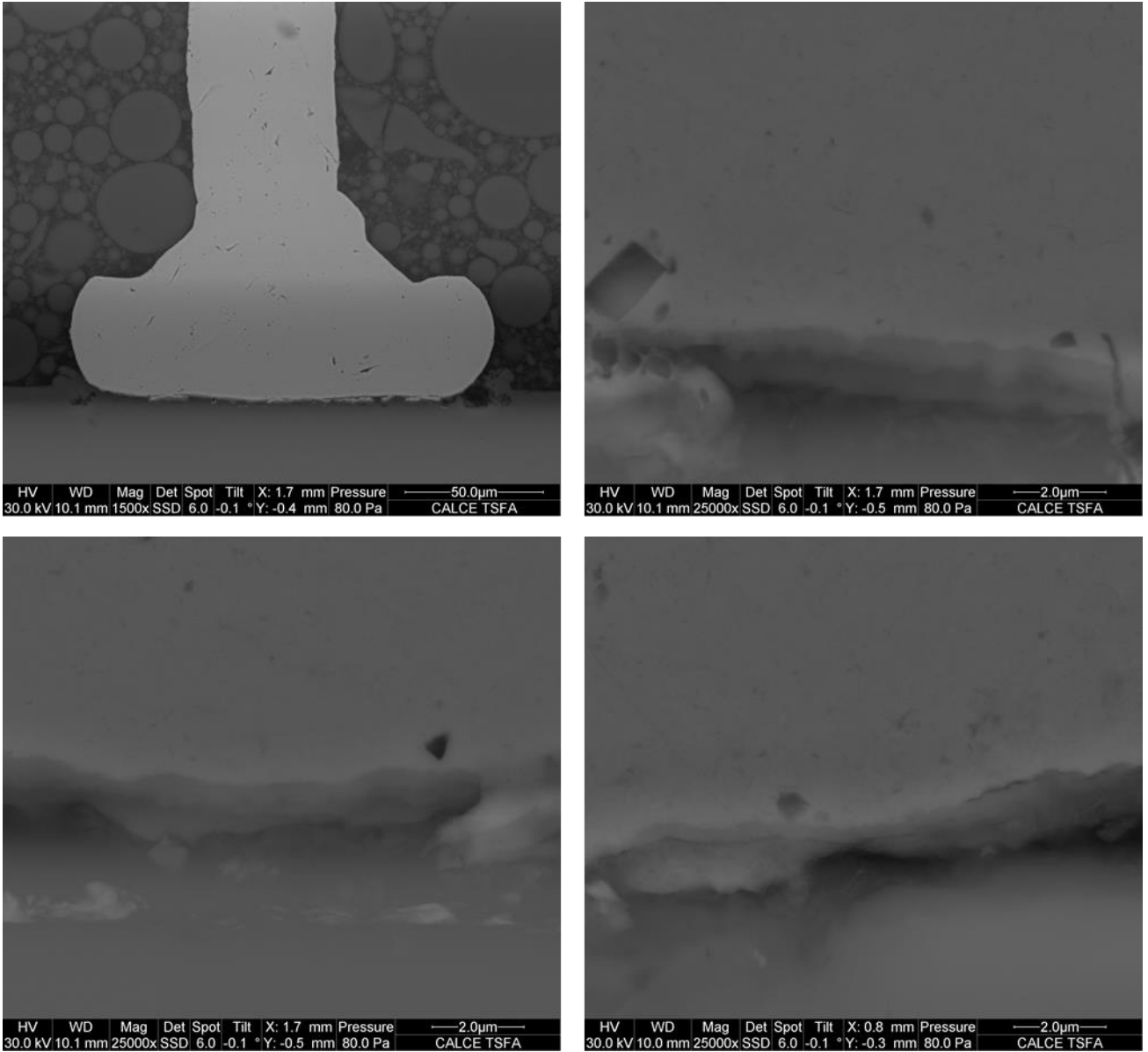
Figure 4.6: Device 2, 1600 hours at HTC (-40°C to 185°C).
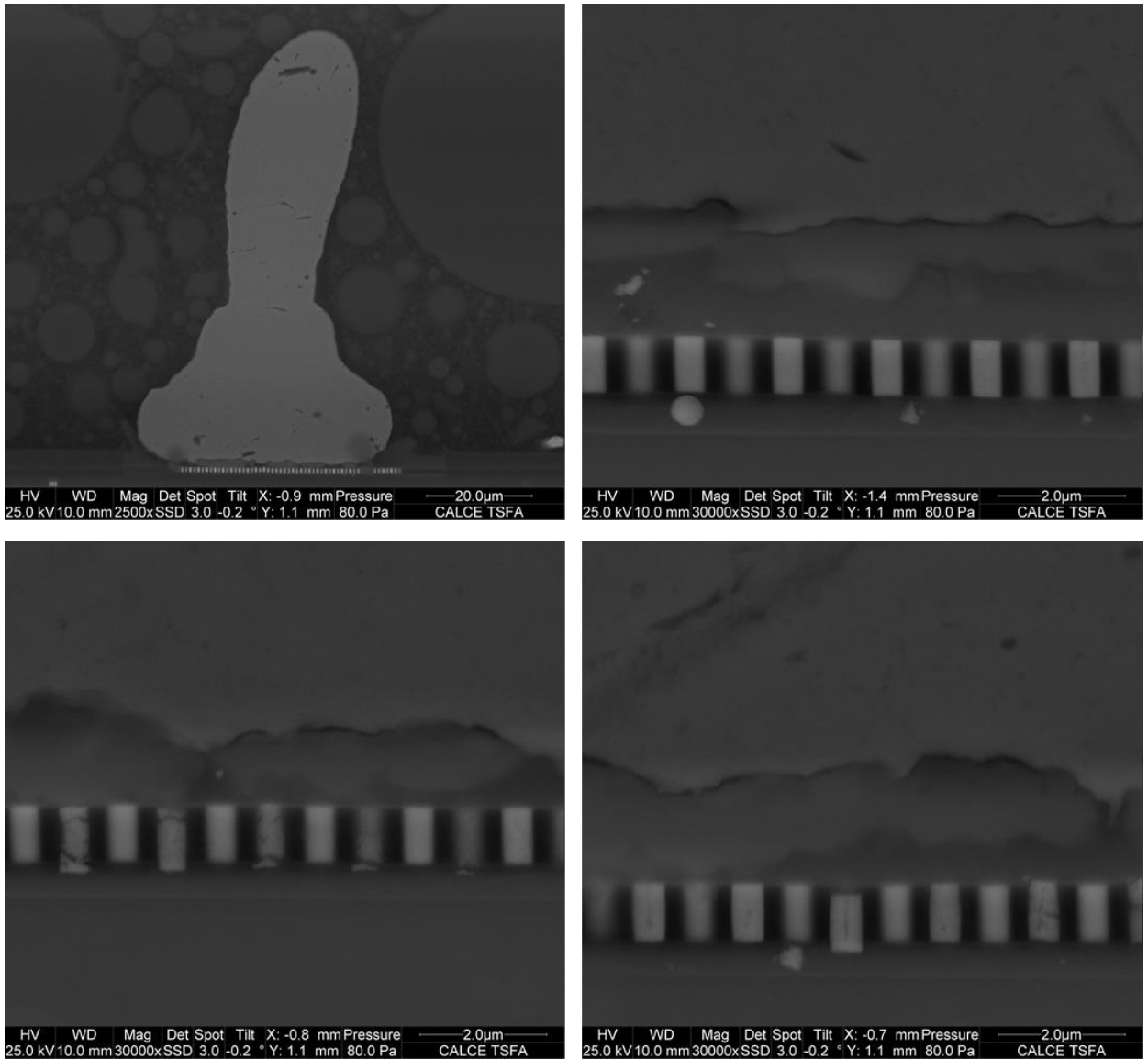
Figure 4.7: Device 6, 1600 hours at HTC (-40°C to 185°C).

Although these two devices show significant difference as stated above, there are several factors that vary between each other, apart from bond pad thickness, but this study supports the necessity to study the effect of bond pad thickness on the reliability of Cu wire bonds, which was adopted in the Part II of this research.

4.3. Summary

Cross-sectional analysis of all 9 devices under two test conditions namely, -40°C to 150°C and -40°C to 185°C, was performed in order to measure interfacial IMC thickness at un-aged, 100 hours, 200 hours, 400 hours, 800 hours, 1600 hours and 2100 hours aging condition. These measurements were used along with Arrhenius equation to model the growth of Cu-Al IMC and establish a predictive model to identify IMC thickness at different time and temperature for all 9 devices. Variation in growth constant and activation energy was observed amongst Cu and PCC devices, and in some cases even within Cu devices and PCC devices. Activation energy was found to be high with the power devices than with the small signal devices.

Comparison between device 2 (Cu wire bond, pad thickness 5 µm) and device 6 (Cu wire bond, pad thickness 2 µm) shows, thicker Cu_9Al_4 phase with the latter. A continuous separation is observed in the interface of device 6 at 1600 hours and this is not seen even at 2100 hours (end of test) for device 2. Both above observations indicate the importance of bond pad thickness in failure of Cu wire bonds; however, both devices are COTS parts and hence there could be other factors that contribute to the observed trend. These observations along with results from data-based modelling as shown in Chapter 5, were the driving factors for studying bond pad thickness effect in Part II.

4.4. Reference

[1] H. Xu, C. Liu, V. V. Silberschmidt, S. S. Pramana, T. J. White, and Z. Chen, "A reexamination of the mechanism of thermosonic copper ball bonding on aluminium metallization pads," Scripta Materialia, vol. 61, pp. 165–168, Jul 2009.
[2] H. Xu, C. Liu, V. Silberschmidt, and Z. Chen, "Growth of intermetallic compounds in thermosonic copper wire bonding on aluminum metallization," Journal of Electronic Materials, vol. 39, pp. 124–131, 2010.

[3] H. Xu, C. Liu, V. V. Silberschmidt, S. S. Pramana, T. J. White, Z. Chen, and V. L. Acoff, "Behavior of aluminum oxide, intermetallics and voids in Cu–Al wire bonds," Acta Materialia, vol. 59, pp. 5661–5673, 2011.

[4] T. C. Wei and A. R. Daud, "The effects of aged Cu-Al intermetallics to electrical resistance in microelectronics packaging," Microelectronics International, vol. 19, pp. 38–43, 2002.

[5] R. Pelzer, M. Nelhiebel, R. Zink, S. Wöhlert, A. Lassnig, and G. Khatibi, "High temperature storage reliability investigation of the Al–Cu wire bond interface," Microelectronics Reliability.

[6] J. Onuki, M. Koizumi, and I. Araki, "Investigation of the reliability of copper ball bonds to aluminum electrodes," Components, Hybrids, and Manufacturing Technology, IEEE Transactions on, vol. 10, pp. 550–555, 1987.

[7] H. J. Kim, J. Y. Lee, K. W. Paik, K. W. Koh, J. H. Won, S. H. Choi, J. Lee, J. T. Moon, and Y. J. Park, "Effects of Cu/Al intermetallic compound (IMC) on copper wire and aluminum pad bondability," in Electronic Materials and Packaging, 2001. EMAP 2001. Advances in, 2001, pp. 44–51.

[8] H.-J. Kim, J. Y. Lee, K.-W. Paik, K.-W. Koh, J. Won, S. Choe, J. Lee, J.-T. Moon, and Y.-J. Park, "Effects of Cu/Al intermetallic compound (IMC) on copper wire and aluminum pad bondability," Components and Packaging Technologies, IEEE Transactions on, vol. 26, pp. 367–374, 2003.

[9] C. L. Gan, E. Ng, B. Chan, F. Classe, T. Kwuanjai, and U. Hashim, "Wearout Reliability and Intermetallic Compound Diffusion Kinetics of Au and PdCu Wires Used in Nanoscale Device Packaging," Journal of Nanomaterials, vol. 2013, 2013.

[10] S. Na, T. Hwang, J. Park, J. Kim, H. Yoo, and C. Lee, "Characterization of Intermetallic Compound (IMC) growth in Cu wire ball bonding on Al pad metallization," in Electronic Components and Technology Conference (ECTC), 2011 IEEE 61st, 2011, pp. 1740–1745.

[11] H. Xu, C. Liu, V. V. Silberschmidt, Z. Chen, and V. L. Acoff, "Effect of ultrasonic energy on nanoscale interfacial structure in copper wire bonding on aluminium pads," Journal of Physics D-Applied Physics, vol. 44, Apr 13, 2011.

[12] https://omlc.org/classroom/ece532/class5/ficks1.html

[13] Servin, J. (2013, February). Method to measure intermetallic layer thickness and its application to develop a new equation to predict its growth. In IPC APEX EXPO technical conference (pp. 19-21).

5. Data Based Reliability Modelling for COTS Parts

In addition to interfacial IMC analysis as shown in Chpater 4, IV characterization at different time intervals was also performed. They were obtained to find out the resistance of the leads in the devices and to spot discontinuities in the internal circuit (wire bond). The IV sweep is performed with an Agilent 4155C semiconductor parameter analyzer, which plotted the IV curve within the specified voltage range as shown in Figure 5.1. Maximum and minimum voltage used in these tests, were kept below the absolute maximum ratings of the parts. Slope of the curve can be used to obtain resistance across different leads, which represents degradation of the circuitry in addition to wire bonds.
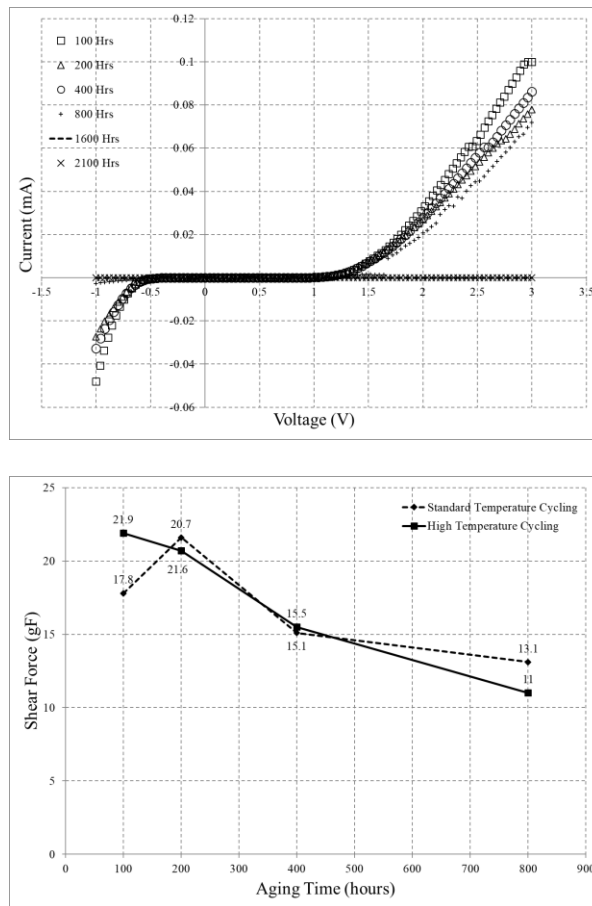
Figure 5.1: Damage parameter, I-V sweep (left) and bond shear force (right).

The other device, out of the two replicates from the board, was decapsulated to reveal the ball bonds which were then sheared using a DAGE 2400 to find out the shear strength degradation with thermal cycling. Devices aged to greater than 800 hours were not able to be decapsulated due to growth of oxidation layer on the periphery of the encapsulant that prevented acid etching, hence results only up to 800 hours are presented. Shear strength showed an initial increase at standard cycling conditions after which there was a drop, which is attributed to the increase in coverage of IMC laterally and then growth in thickness (more work on change in shear force due to aging is presented in Chapter 6). High cycling conditions showed a direct drop in force with time indicating that the maximum shear force could have been before 200 hours. Very low shear values observed in both cases at 800 hours indicates severe degradation of interface leading to poor adhesion. Such a trend was observed in most of the devices. Shear force can also be affected by the decapsulation procedure, especially because the acids used in the process can adversely affect bond wire and interface. Thus, cross sectional analysis followed by electron microscope imaging was performed to support all the measured degradation factors. Presence of full crack in the wire bond-bond pad interface was considered as failure as until then electrical connectivity exists. Specimen preparation was done with silicon carbide abrasive sheets and polished with diamond suspension as low as $0.05\mu m$ to obtain defect free surfaces that show the bond interface.

Results from one of the device (device 6) is shown in Figure 5.2, where growth in IMC and separation between Cu_9Al_4 and Cu (from 200 hours) is clearly visible.
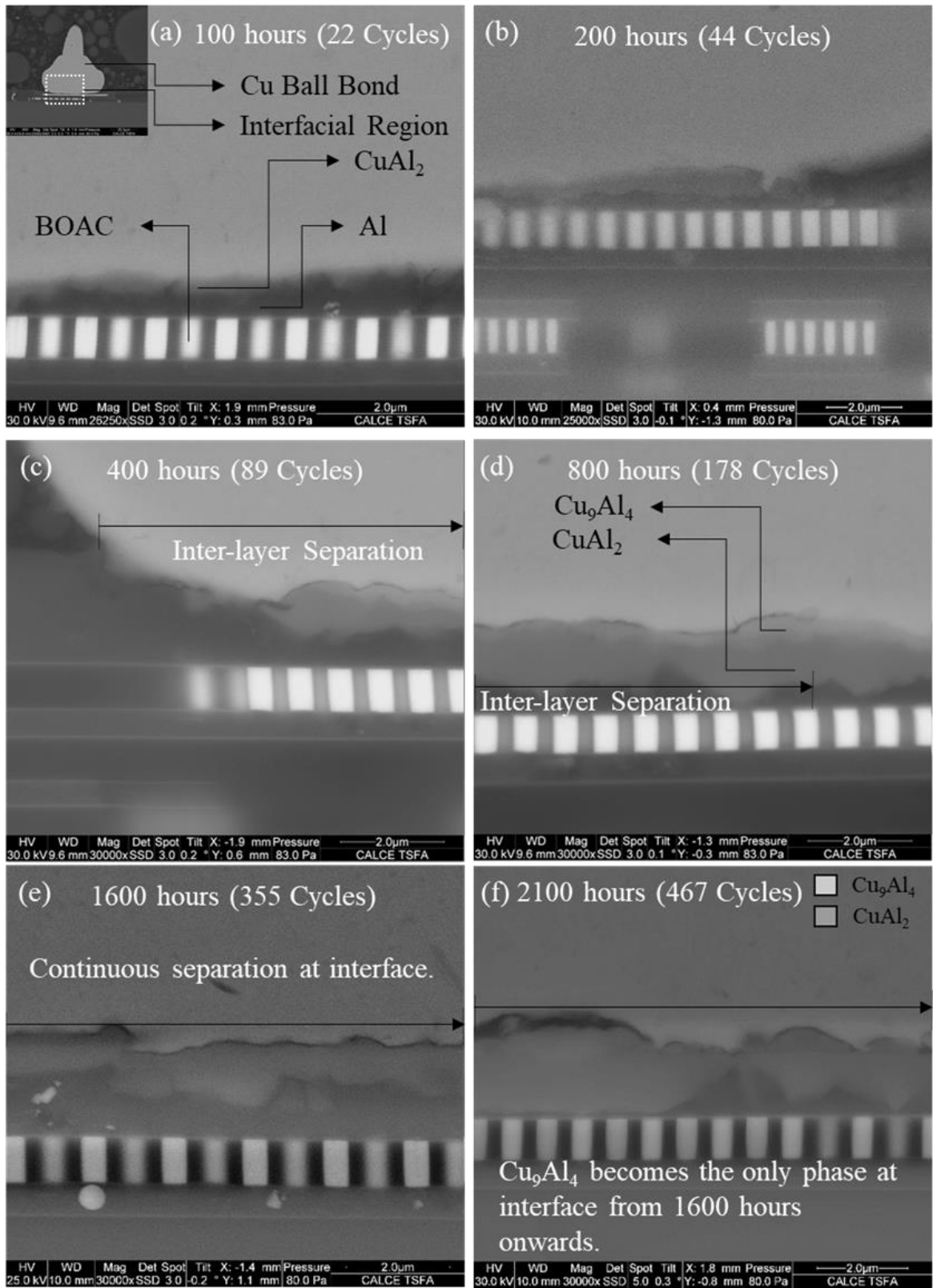
Figure 5.2: Interfacial failure at 1600 hours of device 6 under high temperature cycling condition.

A combination of thermal stress and stress from γ phase formation is believed to be the cause of separation, which occurs at region above Cu_9Al_4. From such analysis, failure time was defined as complete separation at interface and was found for all nine devices as shown in Table 5.1.

Such a complete interfacial separation was not observed with all devices, for example, Figure 5.3, shows images of interface of device 8, where separation is found to be discontinuous at even at 2100 hours. Thus, a failure time of 2100+ is mentioned for device 8 in Table 5.1. Difference in failure times are expected as these devices are completely different from each other and experience different stress based on package characteristics and the materials used in them.
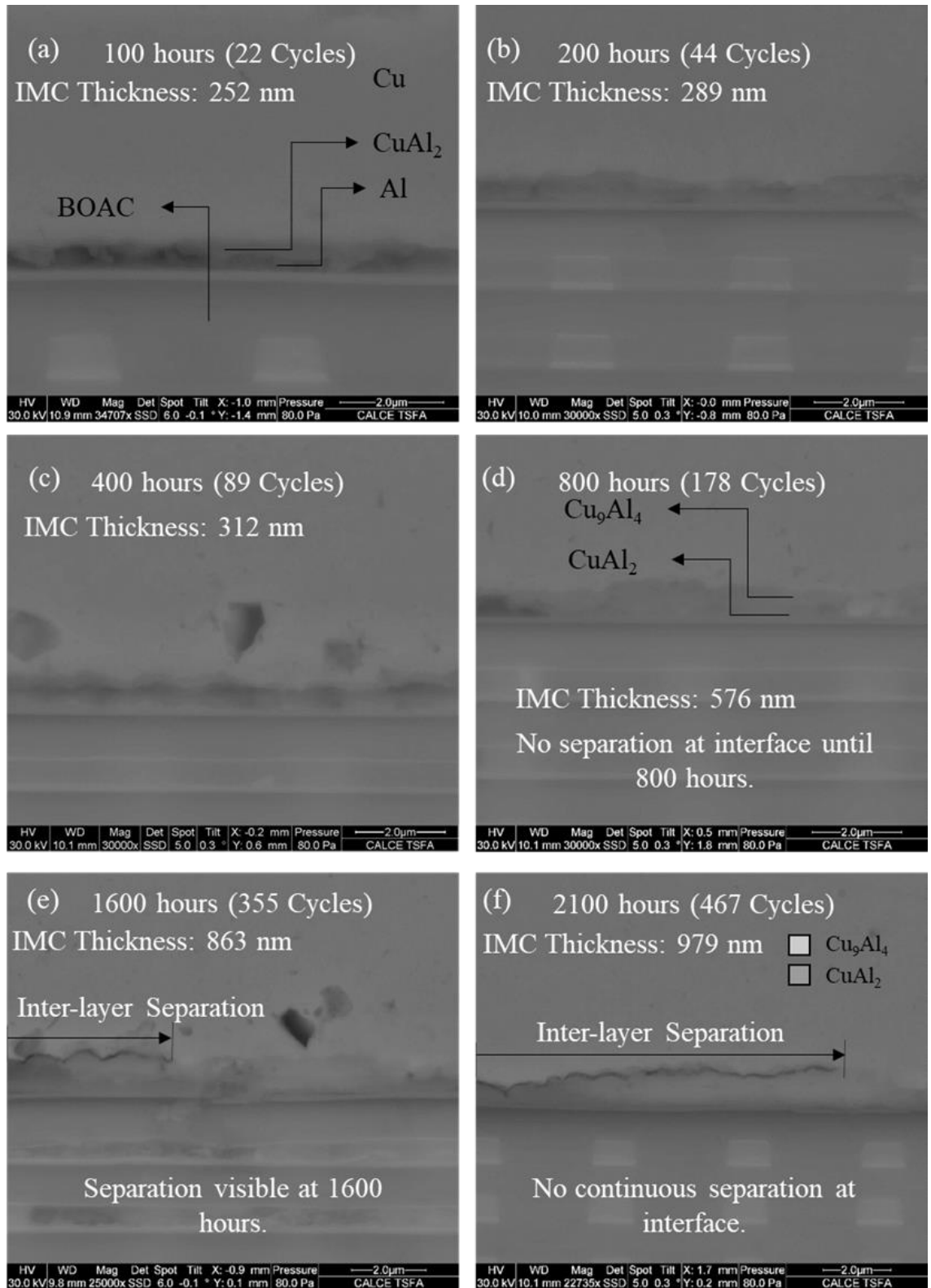
Figure 5.3: Interface of device 8 showing no continuous separation even at 2100 hours at high temperature cycling condition.

Similar procedure for specimen preparation was performed to obtain interfacial region of wedge bonds, where failures typically occur. In the case of device 6, under high temperature cycling, separation was observed to initiate at 1600 hours from the underside of bond. This device consists of Cu wire bonded on Ag coated Cu lead. Interfacial degradation is seen at 1600 and 2100 hour, through which a separation is observed. Such failure was not observed in all devices, for e.g., in the case of device 3, where PCC wire is bonded on Ag coated Cu lead. Difference in wire material and processing parameters affect failures at wedge bond.

In each case, only few bonds from the device, for ball and wedge, were analyzed and were considered representative of other bond-pad-lead pairs. This research focuses on building a failure prediction model using the obtained failure time data. Table 5.1, summarizes failure times from observation for ball and wedge bonds. Devices that did not show failure even at the end of test (2100 hours) are represented as 2100+ hours.

Table 5.1: Summary of failure time from cross sectioning of device.

Device No.	Ball Bond Failure Time (hours)	Ball Bond Failure Time (Cycles)	Wedge Bond Failure Time (hours)	Wedge Bond Failure Time (Cycles)
1	2100 +	466 +	2100 +	466+
2	2100 +	466 +	2100 +	466+
3	1600	355	2100 +	466+
4	2100	466	800	177
5	2100	466	1600	355
6	1600	355	1600	355
7	2100	466	2100 +	466+
8	2100 +	466+	2100 +	466+
9	2100 +	466+	2100 +	466+
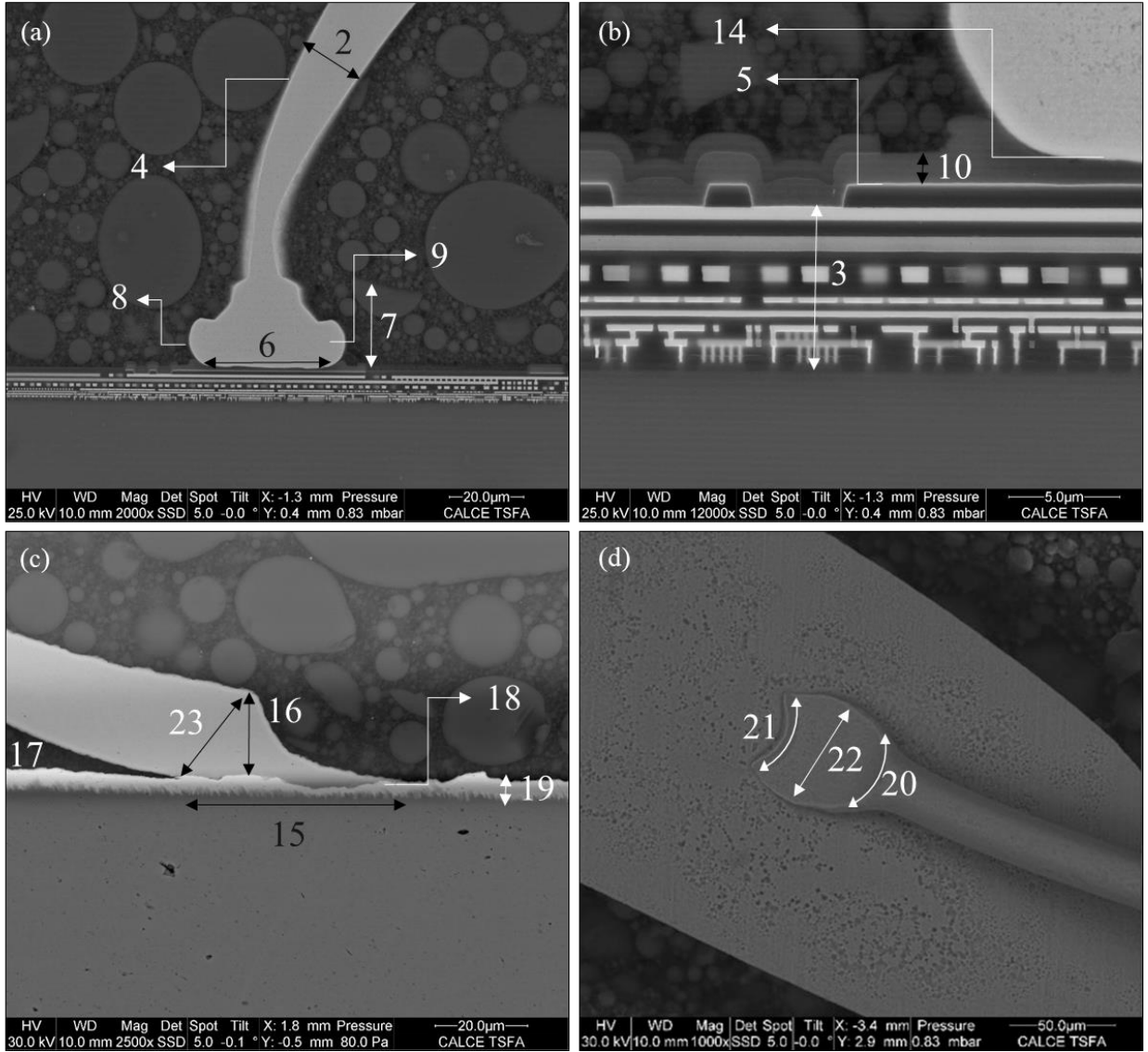
Figure 5.4: Ball and Wedge Bond Parameters.

Time to complete failure at these interfaces depends on various geometrical and material

parameters which were identified and presented in Table 5.2.

Table 5.2: Device Parameters and Measure Values.

Device Parameters	Device 1	Device 2	Device 3	Device 4	Device 5	Device 6	Device 7	Device 8	Device 9
Wire material (1)	Cu	Cu	PCC	PCC	PCC	Cu	Cu	Cu	PCC
Wire diameter (µm) (2)	25.4	48	20	18	18	20	18	20	20
Bond-over-active-circuitry (BOAC) thickness (µm) (3)	0	0	6	8	8	6	4.4	7.5	7.5
Pd coat thickness (µm) (4)	0	0	0.51	0.41	0.33	0	0	0	0.35
Passivation layer thickness (µm) (5)	0	0	0.2	0.25	0.25	0.2	0.42	0.32	0.23
Ball bond length (µm) (6)	86	123	34	30	30	36	47.3	44.6	54.9
Ball bond height (µm) (7)	43	70	25	24.5	24.5	30	34.5	35.1	34.3
Ball bond curvature1 (µm) (8)	12.11	22.5	5.9	8.2	6.7	12.2	11.0	10.4	13.8
Ball bond curvature2 (µm) (9)	17.3	21.7	5.9	8.0	6.6	14.3	16.8	13.1	15.5
Bond pad thickness (µm) (10)	2.5	5	1.1	1.1	1.1	2	0.8	1.5	0.8
Epoxy mold compound (EMC) CTE1 (ppm/°C) (11)	12	12	8	6	6	12	8	8	12
EMC Coefficient of thermal expansion (CTE2) (ppm/°C) (12)	47	45	37	51	51	49	33	33	49
EMC Glass transition temperature (Tg) (°C) (13)	150	150	130	140	140	130	125	125	130
Interfacial Pd thickness (µm) (14)	0	0	0	3.1	2.2	0	0	0	4.4
Wedge length (µm) (15)	95	115	50	30	30	33	100	55	30
Wedge height (µm) (16)	18.4	20.9	19.7	18.8	17.1	9.8	24.5	23	5.5

Wedge angle (degree) (17)	10	10	20	30	28	15	10	20	10
Lead coat material (18)	Cu	Ag	Ag	Ag	Ag	Ag	Ni	Ni	Ag
Lead coat thickness (µm) (19)	0	5.5	5	5.5	5.5	4.5	1.5	1.5	4.5
Upper radius (µm) (20)	17.4	48.5	14	18	18	20	16.3	15.9	15.7
Lower radius (µm) (21)	22	37.4	33.5	15.	15	22.4	20.7	32.1	45.1
Wedge width (µm) (22)	135	125.2	34.3	36.6	38.5	37.5	52.6	50.8	39.6
Shortest wedge distance (µm) (23)	19	14	10.4	8.4	7.4	8.6	19	15.6	17.5

To judge the susceptibility of a component to failure from a knowledge of the value of a few measurable parameters which can be obtained by analyzing a small sample of the device a Principal Component Analysis (PCA) based approach was adopted. It is widely used in data modelling to extract critical features and reduce the dimensionality of the parametric space, without losing significant information in the process. It becomes ubiquitous in applications with large data set and is a unique way to identify critical factors that affect copper wire bond failure times in commercial devices. There is a large amount of data (14 parameters for ball bond and 9 parameters for wedge bond) which are related to each other and ultimately the TTF. Correlation coefficients among 14 variables for ball bond and 9 variables for wedge bond indicate several significant relationships as shown in Table 5.3. Wire material shows positive correlation with Pd coat thickness and interfacial Pd thickness. Wire diameter is directly related to ball bond geometry such as bond length, height and curvature. Additionally, wire diameter and bond pad thickness shows positive correlation indicating that manufacturers tend to use thicker pad for thicker wires, possibly to prevent BOAC crack. From wedge bond coefficients, geometry of wedge is found to be

closely related to each other such as wedge length and wedge width, which arises out of bonding process.

Table 5.3: Correlation coefficients of ball bond (top) and wedge bond (bottom) variables.

	Wire Material	Wire Diameter	BOAC Thickness	Pd Coat Thickness	Passivation Layer Thickness	Length of Ball Bond	Height of Ball Bond	BB LFT Curvature	BB RHT Curvature	Bond Pad Thickness	EMC CTE 1	EMC CTE 2	EMC T$_g$
Wire Diameter	-0.341												
BOAC Thickness	0.6	-0.75											
Pd Coat Thickness	0.993	-0.341	0.598										
Passivation Layer	0.201	-0.719	0.727	0.2									
Length of Ball Bond	-0.377	0.921	-0.88	-0.381	-0.739								
Height of Ball Bond	-0.415	0.953	-0.807	-0.418	-0.629	0.972							
BB LFT curvature	-0.282	0.871	-0.66	-0.283	-0.533	0.884	0.935						
BB RHT curvature	-0.447	0.665	-0.733	-0.451	-0.382	0.823	0.843	0.895					
Bond Pad Thickness	-0.43	0.961	-0.78	-0.425	-0.78	0.885	0.913	0.831	0.656				
EMC CTE1	-0.378	0.516	-0.607	-0.396	-0.609	0.654	0.606	0.724	0.761	0.551			
EMC CTE2	0.645	0.071	0.062	0.643	-0.45	0.032	-0.049	0.092	-0.102	0.133	0.185		
EMC Tg	0.085	0.642	-0.646	0.094	-0.853	0.661	0.551	0.418	0.269	0.686	0.256	0.57	
Interfacial Pd	0.946	-0.305	0.555	0.945	0.181	-0.288	-0.334	-0.146	-0.285	-0.426	-0.164	0.588	-0.007

	Wedge length	Wedge Height	Wedge Angle	Lead Finish Thickness	Average Inner Radius	Average Upper	Wedge Width
Wedge Height	0.589						
Wedge Angle	-0.646	0.142					
Lead Finish	-0.474	-0.348	0.46				
Average Inner	0.566	0.16	-0.299	0.33			
Average Upper	0.124	-0.318	-0.546	0.093	0.274		
Wedge Width	0.808	0.271	-0.548	-0.401	0.606	0.123	
Shortest Wedge	0.626	0.155	-0.783	-0.763	-0.015	0.419	0.495

Relating these variables to failure time can be done by grouping devices from three-dimensional scatter plots, which becomes cumbersome for analysis as there will be 1771 plots for a set of 23 parameters ($^{23}C_3$). Principal component analysis is as a dimensionality reduction tool here that can be used to eliminate parameters that does not show higher variance and group parts that are similar. This is done by finding the line (eigenvector) that has maximum variance with the parameters. The direction of the first such line is not constrained. A second line can be found that has the next maximum value of variance (eigenvalue) with the data however, this line must be perpendicular to the first line. These lines or eigenvectors are called principal components and their eigenvalues give the value of variance with the data. Principal components with the high eigenvalues are chosen, which accounts for the largest spread in data. From this 'spread' some of the devices form groups based on their similarity with one another. These groups of devices are anticipated to have the same (or nearly the same) TTF, based on which a life time estimation can be obtained for a device that falls within a parametric space.

In this study, grouping of the nine devices under study into sets was done based on the ball bond parameters collected above that contribute to interfacial separation. It is anticipated that the TTF of the ball bonds in the temperature cycle test will be close to each other for devices in the same set. With inclusion of failure time data, this method can be used to predict failure time of a new device by determining its parameters, and using it along with the training set of data to find the nearest neighbor group whose failure time is known from experimental testing. TTF of the new device is expected to be similar to that of the devices in the neighboring groups. This method can be used to assess failure time without

conducting extensive accelerated tests. However, the test is valid only for the specific failure mechanism mentioned in this study and under the similar test conditions.

5.1. Data-Based Failure Time Modelling Principal Component Analysis

Principal component analysis is used to identify patterns and similarities within a large list of parameters that contribute to a part. Such identification of patterns in high dimensions become cumbersome using graphical representation. Another great advantage of the method is that it can reduce the high dimension to lower dimension with negligible information loss. Consider a data set, represented by a vector 'x', where,

$$X = (x_1, x_2, \dots, x_n) \qquad (6)$$

From the given data vector, the mean can be found,

$$\mu = \frac{1}{n}(x_1 + \dots + x_n) \qquad (7)$$

and the covariance matrix of the data can be calculated by,

$$C_x = \frac{1}{n-1}\sum_{i=1}^{n}\{(x - \mu)(x - \mu)^T\} \qquad (8)$$

The components of C_x, denoted by $c_{i,j}$, represents the covariance and $c_{i,i}$, the variance between the random variable components x_i and x_j. Simply put, the variance determines the spread of values around the mean values and the covariance determines how much each of the dimensions vary from the mean with respect to each other.

The eigenvectors e_i and corresponding eigenvalues λ_i are the solutions to the equation given by,

$$C_x e_i = \lambda_i e_i \qquad (9)$$

From here, the equation can be solved to find λ_i by solving the characteristic equation,

$$| C_x - \lambda I | = 0 \qquad (10)$$

where, I is the identity matrix of order same as that of C_x

From comparing the values of different eigenvectors, an ordered orthogonal basis is created, with the first eigenvector having the direction of largest variance. This way is used to reduce the data, comprised of higher dimensions, into lower dimensions, that have significant variance.

Principal component analysis reduces the parameters for ball bond by combining and choosing the most important ones based on the principal component values for each. A higher principal component value represents a parameter that is more important while the lower ones can be eliminated. This is done by finding the eigenvector which shows the maximum variance with the data. The eigenvalue is amount of variance that is obtained with each of the eigenvector. Thus, higher eigenvalue indicates larger variance.
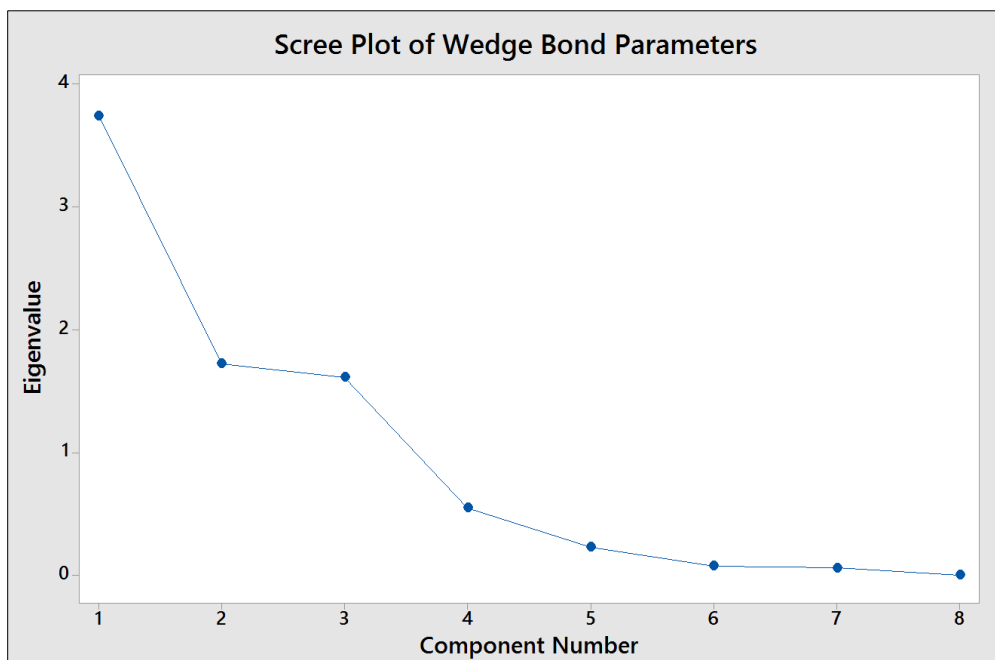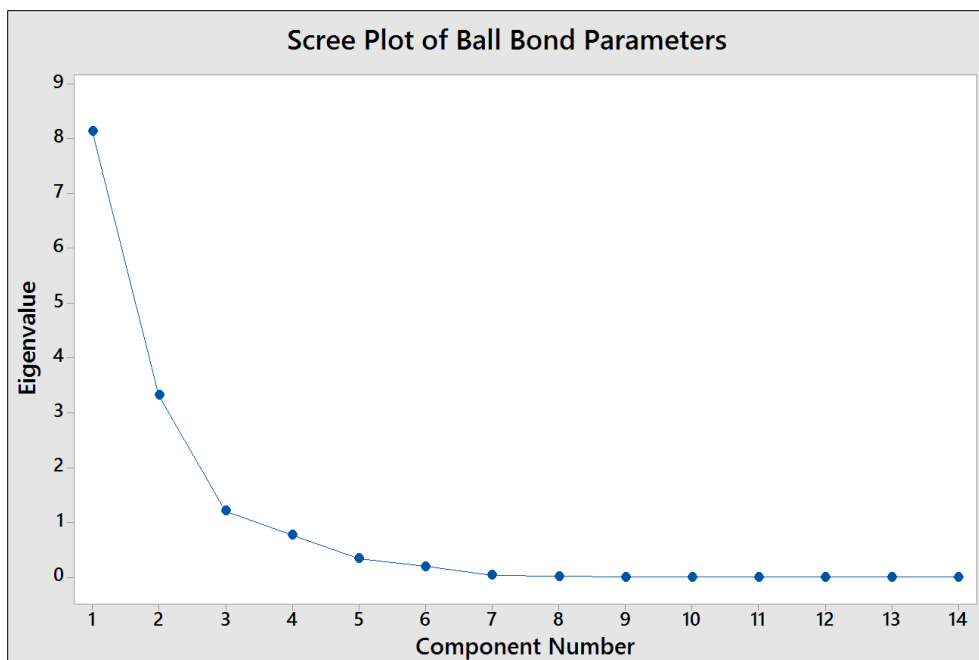
Figure 5.5: Scree plot showing eigenvalues of different principal components for ball bond parameters (top) and wedge bond parameters (bottom).

Scree plot, Figure 5.5 (top), shows eigenvalues for different components and it can be seen that the first three parameter components (NOTE: these are parameter components NOT

electronic components) have high eigenvalues compared to the others, for ball bond as well as wedge bond, hence only the first three are chosen. Score plot, Figure 5.6, shows the devices in groups plotted on the chosen three principal components, PC1, 2 and 3. From the score plot devices 1-9 can be grouped as highlighted and devices that fall in the group have similar failure times found from experiments. Device 3 and 6 that fail before 1600 hours, device 4 and 5 that fail before 2100 hours and device 1 and 2 that did not fail for 2100 hours lie within the same groups. Although device with same failure times fall within the same group, the group itself do not align in space based in TTF. For e.g. device 1,2 and 9 does not fail even after 2100 hours, but 1 and 2 form a group, while 9 is far away from forming a separate group. This is attributed to parameter that contributed to failure of these bonds, which may be different. Device 9 does not fail because it is a PCC wire bond with interfacial Pd thickness of 4.4µm that inhibits IMC growth and leads to longer life, while device 1 and 2 do not fail because they have thick wire bonds that results in reduced bond stress in addition to high T_g mold compound material that contributes to less thermal stress on wire bonds.
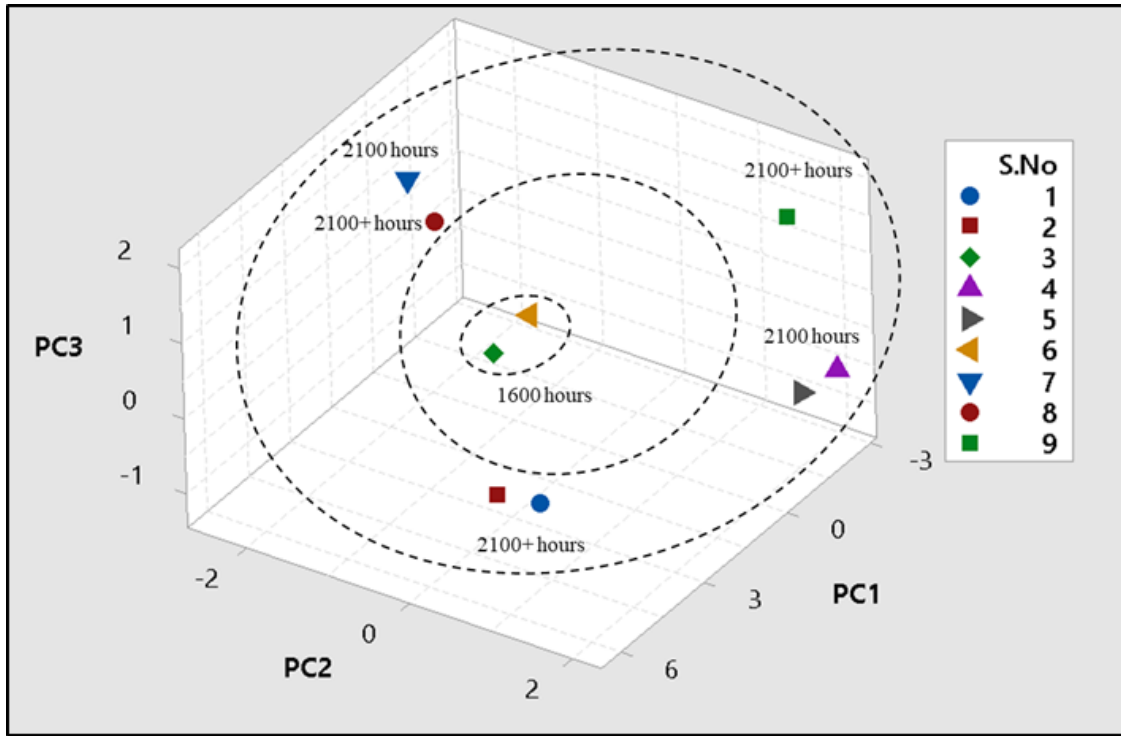
Figure 5.6: Result of PCA showing groups of devices based on its variables.

Score plot of device based on wedge bond parameters is shown in Figure 5.7, where a distinct group comprising of 4 and 5 is observed. An extended group of 4, 5 and 6 is labelled, where failure times (from Table 5.1) are close to each other. Other devices are scattered and do not form groups as well as those in ball bond parameters. Reason for lack of organization is due to lower number of parameters that are considered for the wedge bond in comparison with ball bonds and lower number of failed wedge bonds. Only 9 parameters are considered for wedge bond PCA as not many exclusive ones exist, that is instrumental for device failure. However, with more device failure, a better relationship is expected. Although variations in bonds were considered to be low, the cross-sectioned plane for wedge bonds has a significant effect on the measured parameters due to the un-symmetry in wedge bonds as compared to ball bonds. The focus of this research is on the

bi-metallic ball bonded interface. Although wedge bond modelling is shown here for applicability of the method, studying its failure was not part of this research.
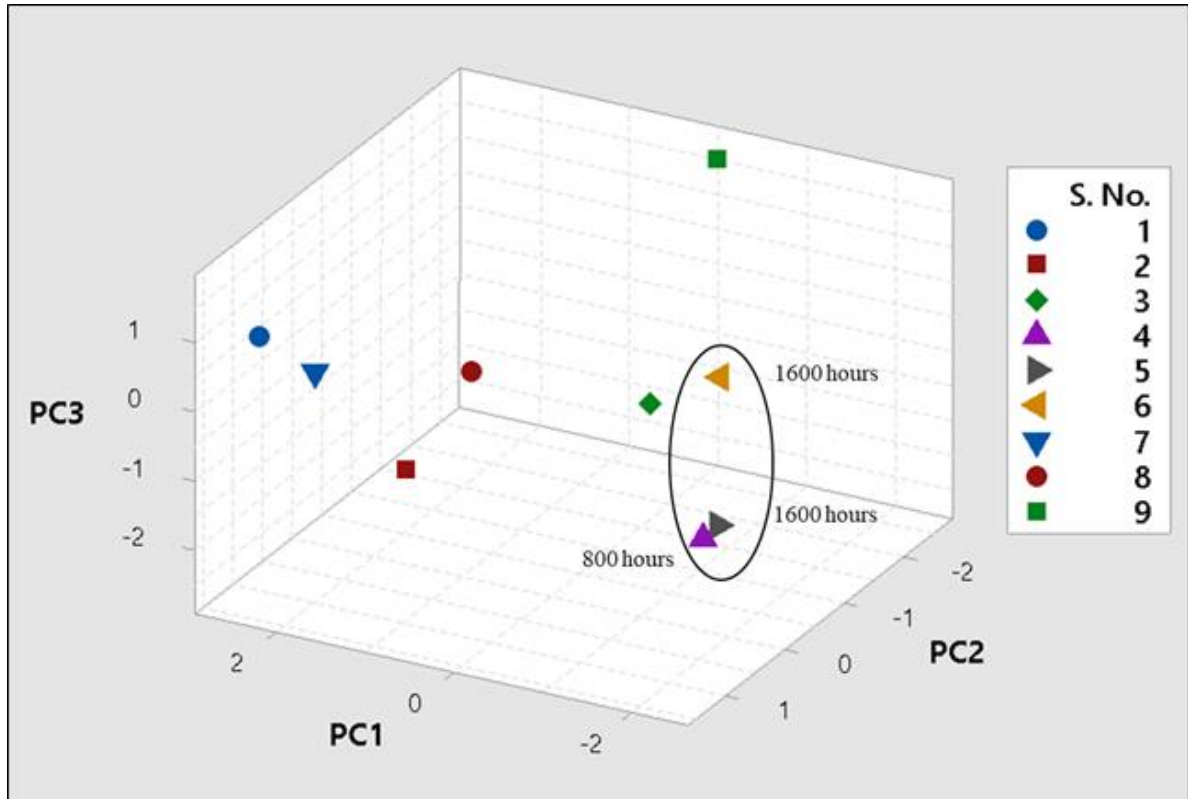
Figure 5.7: Score plot (top) showing groups of devices based on wedge bond parameters.

To estimate failure time of a new device (not part of the above test DOE), material and geometrical characteristics needs to be evaluated by cross-sectional analysis and this information needs to be used to find its location on the component axes along with the training data devices. To show the working of the technique, a hypothetical device of characteristics such as the one shown in Table 5.3.

Table 5.3 Material and geometrical characteristics of device 10.

Device Parameters (Ball bond)	New Device 10
Wire material	PCC
Wire diameter	20
BOAC thickness	5
Pd coat thickness	0.5
Passivation layer thickness	0.25
Ball bond length (6)	35
Ball bond height (7)	18
Ball bond curvature1(8)	10
Ball bond curvature2(9)	10
Bond pad thickness (10)	2
EMC CTE1 (11)	12
EMC CTE2 (12)	45
EMC Tg (13)	130
Interfacial Pd thickness (14)	3

Using these values component coordinates are identified and device 10 is plotted along with the training set of 9 devices as shown in Figure 8. Distance of device 10 is calculated from other groups, from which it is expected that failure time of device 10 will be close to that of device 9. This is also evident from values presented in Table 5.3, which are similar to device 9.
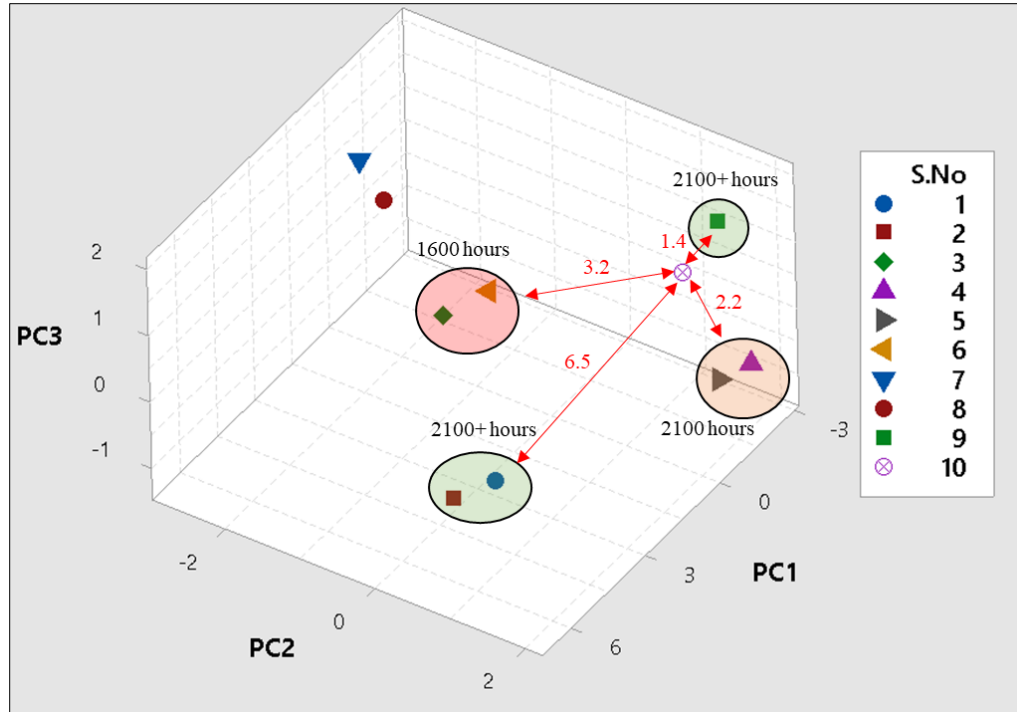
Figure 5.8: Identification of failure time of new device 10.

The nine different devices are categorized into three major groups based on the principal parameter components 1, 2 and 3. PCA can also identify the parameters based on which the devices were split into groups; this is given by higher values of principal component as shown in Figure 5.9.
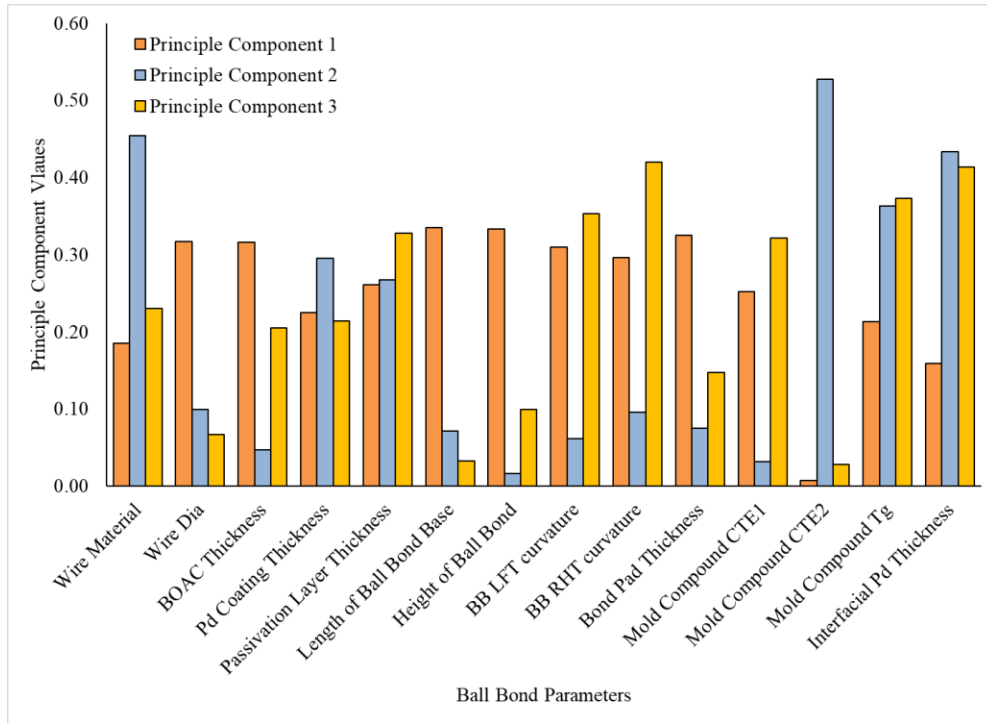
Figure 5.9: Principal Component Values of Ball Bond Parameters.

Length of ball bond base, bond height and bond pad thickness have higher PC1 values compared to the others, which makes them a determining factor in grouping the components in the PC1 axis. From this analysis the independent factor in PC1 that has the highest contribution is the bond pad thickness and is chosen for further analysis. Palladium coating thickness, EMC CTE2 and wire material are the other determining factor that is chosen to categorize components along PC2 direction and bond curvature and EMC Tg contribute to categorizing in the PC3 direction. It must be noted that the palladium coating thickness parameter also includes the wire material type parameter because the pure copper wire material by definition has a Pd coating thickness of zero.

5.2.Summary

Twenty-three parameters of wire bond that is critical for its failure in thermal cycling condition was identified and used to build a data-based model to estimate failure time of a new device. Failure times obtained from accelerated thermal cycling test was used as training data for this model and a method to estimate lifetime of a new device was shown. This method can aid in part selection, where lifetime can be estimated just by the knowledge of the initial parameters. The confidence of results from this model can be improved with addition of training data from more devices.

Additionally, this data-based method was used to identify contribution of bond parameters in reliability of the wire bonds. Al bond pad thickness was found to be a critical parameter from this analysis, based on its principal component value (loading). Thus, from this analysis, effect of pad thickness is chosen for further investigation as presented in Part II of this work.

6. Dependence of Bond Shear Strength on Pad Thickness and Interfacial Changes due to Aging of Bonds

Shear force analysis have been widely accepted as an important criterion for bond quality assessment and is followed by most of the OEMs today. Standards such as AEC Q-100-001, ASTM F1269-13 and JESD 22-B116 are typically used for judging bonding quality, but these standards were mainly developed for Au wire bonds and does not reflect change in wire material to Cu (except JESD 22-B116 Rev). Additionally, all of these standards does not consider the effect of bond characteristics, except wire diameter, on the shear force of the bonds. This chapter aims to study one such parameter, bond pad thickness, which was found to be a critical factor affecting the shear force.

6.1. Effect of Pad Thickness on Initial Bond Shear Analysis

6.1.1. Bond Shear Analysis

Bond shear testing is the process of measuring the bond adhesive strength by performing a destructive test. Figure 6.1 illustrates the process, where a shear tool, much wider than the ball bond to be tested, is used to apply force in the lateral direction (parallel to the substrate).
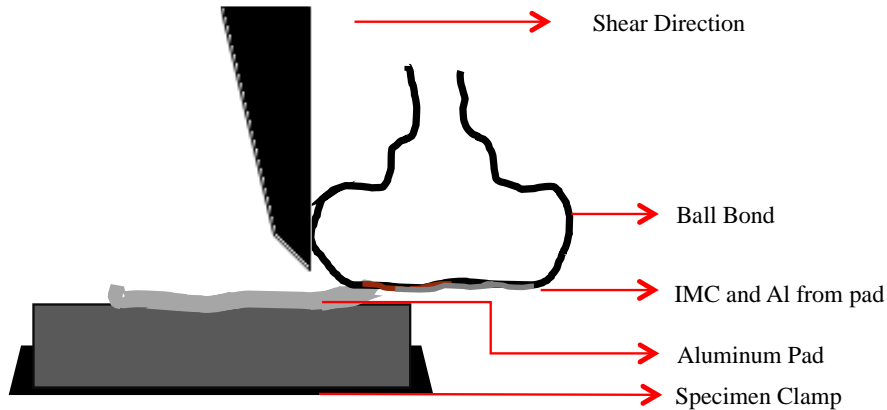
Figure 6.1: Bond shear testing showing bond yielding at the interface.

The shear tool is set to move at a constant speed, while the force encountered to move the tool in its path is noted. As the tool hits the bond and stops, the force is increased until the bond breaks. Peak force that causes the break is recorded as the shear strength of the bond. Bond shear testing is primarily used to optimize the bonding process and then to qualify and monitor wire bonds on production samples. It can also indicate the stress tolerance of the bond, such as stress from thermal expansion of mold compound during thermal cycling conditions.

Bond shear strength depends on several factors that are listed below:

1. Bonded materials

2. Area of bonding

3. Surface roughness of bond pad

4. Oxidation of Al pad surface

5. IMC strength

6. IMC area

7. IMC % area coverage

8. Cracks or voids in the bond interface

9. Pad film ductility and strength

Thermosonic ball bonding of Cu wire utilizes power, time, and force in the bonding "recipe", controlling the process to break native oxide on the Al pad surface and cause increase in temperature, promoting formation of a solid-solid solution of Cu-Al IMC. Wherever oxide remains intact on the Al surface, IMC will not form, hence no bonding in that area. IMC area is most significant in determining bond strength, with increased IMC coverage hence higher strength preferred.

Bond strength can be measured in a pass/fail sense in the bond *pull* test. If the wire breaks mid-span while the bond ball is still intact, then the bond is considered strong. However, this doesn't predict the bond's reliability once it is packaged, surrounded by molding compound with a different thermal coefficient of expansion. The bond *shear* test is used on these strong bonds to provide a value that may be more indicative of bond reliability.

IMC area is most significant in determining bond strength, with increased IMC area resulting in higher shear strength. IMC coverage as percentage of bond area can be measured in a destructive test. Companies may decide to set a lower limit for IMC coverage such as 80%, below which reliability may be assumed to be questionable.

Several wire bond shear testing standards are in use, such as JEDEC, ASTM, AEC, etc. [1][2][3]. These have been developed to perform standard shear tests facilitating the results to be compared. Only the JEDEC JESD22-B116 most recent version that addresses Cu wire bonds, while the other standards are primarily meant for Au wire bonds. Shear strength values increase with ball diameter, and ball diameter increases with wire diameter. This is due to larger IMC area, from increased free air ball (FAB) diameter in larger diameter wires. Ball bond diameter is typically 2 to 3 times the wire diameter.

A non-destructive bond shear test (NDBS) can be used in cases where 100% screening is required. In NDBS testing the shear tool stresses the bond only up to a preset value, which is kept much below the predetermined force required to shear a "good bond", and then retracts. It has been shown that NDBS does not affect ultimate destructive shear strength (for 25.4um bonds with bond diameter greater than or equal to 2.5 times the diameter). Usually NDBS limit of about 50-60% is used. ASTM (F1269-06) recommends different limits for NDBS tests based on the bond conditions.

This study shows the importance of considering bond pad thickness effect on the shear force analysis through an experimental and finite element analysis study.

6.1.2. Test Vehicle and Design of Experiment

Four different bonding process recipes on four different Al bond pad thickness were used in the experiment to study the bond pad thickness effects on bond shear results. Thermosonic ball bonds were made with Cu wire of diameter 18 µm on Al integrated circuit test pads. Pad thicknesses of 0.5, 1 and 4 µm Al were included, to cover a wide range of thickness used in integrated circuit and power electronic devices. Power and time were varied in the bonding recipe to purposely create bonds that are strong, yet exhibit a range of IMC coverage in the bonds. Table 6.1 lists the experimental bonding recipe main parameters.

Table 6.1: Bonding process recipes used in the experiment

Bonding Parameters	Recipe 1	Recipe 2	Recipe 3	Recipe 4
Power (Watts)	94% (1.78)	97% (1.84)	97% (1.84)	100% (1.9)
Time (ms)	67% (37)	75% (41.5)	84% (46)	100% (55)
Force (gF)	100% (47.5)	100% (47.5)	100% (47.5)	100% (47.5)

Recipes with reduced energy are formulated to create strong bonds having less IMC coverage. Lower energy than this results in "non-stick on pad" (NSOP), where the Cu ball pulls off the pad during the wire shaping motions. It's not feasible to go to higher energy in the experiment because the bond ball diameter begins to exceed the pad width.

After wire bonding, the assemblies were aged at 185°C for 4 hours to promote small IMC growth in the region where IMC had already formed, to enhance IMC visibility later. Then the Cu balls etched away with the use of nitric acid to expose the Cu-Al IMC following the method mentioned in. Optical microscope, and scanning electron microscope (SEM) with electron dispersive spectroscopy (EDS), were used to identify coverage of IMC at the interface, which was then measured and tabulated. Figure 6.2, shows the presence of Cu in the central region which corresponds to the $CuAl_2$ IMC.
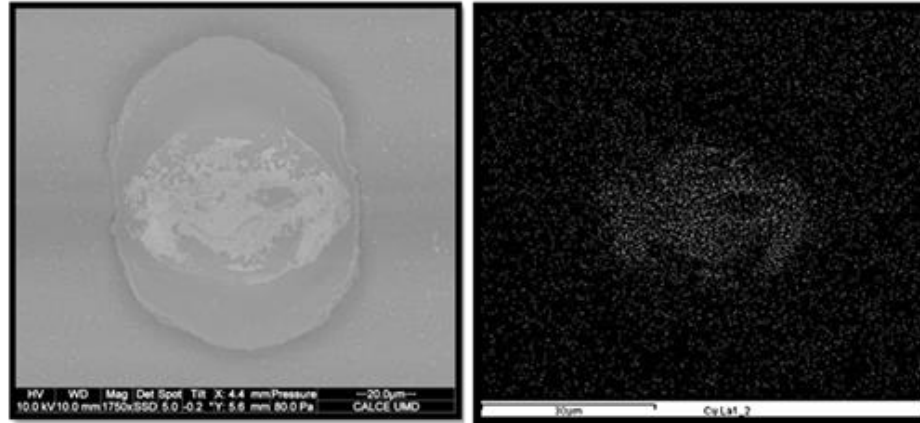
Figure 6.2: EDS analysis of the ball bond-bond pad interface region after etching. (Left) SEM image and (Right) Cu map indicating the Cu-Al IMC region.

6.2. Results

Bonding area was measured from inspection of pad Al deformation after etching away the Cu ball bonds. Figure 6.3, shows the bond area versus experimental bond recipe for each of the pad Al thicknesses. Bonding area increases with higher bonding power and time as

expected. But at lower power and time, thicker pads caused smaller bonds. We attribute this to the fact that more US energy is being absorbed into the malleable thick Al pad film instead of causing more Cu ball deformation. However, with increased power and time the bond ball shape and bond area became essentially constant at the largest diameter, regardless of pad thickness. This indicates an apparent robustness against pad thickness changes in the optimal bonding recipe.
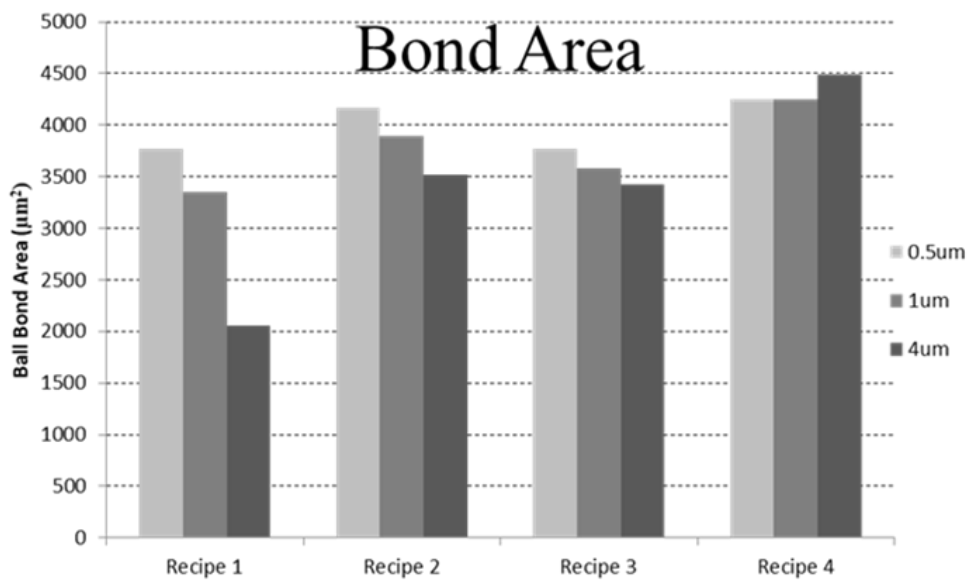
Figure 6.3: Ball bond area measurement for all pad thickness with different bonding recipes.

Figure 6.4 shows the IMC area measured after etching the bond. It shows an increase in IMC area with higher energy bonding recipes, as expected. The error bars show the range measured from 0.5 to 4 µm pad thickness. Maximum area of IMC coverage is limited by the bond area. There does not appear to be a relationship between IMC area and pad thickness.
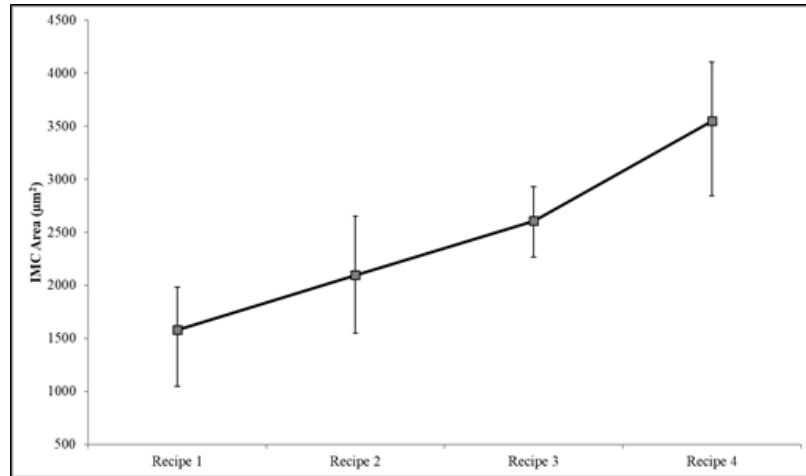
Figure 6.4: IMC area in different pad for different bonding recipes.

%IMC coverage (with respect to bond area) in Figure 6.5 increases from about 50% to over 80% as bond recipe energy increases. Error bars show the range of measurements made from 0.5 to 4 µm pad thickness. %IMC coverage also becomes consistent at the highest energy recipe similar to the ball bond area.
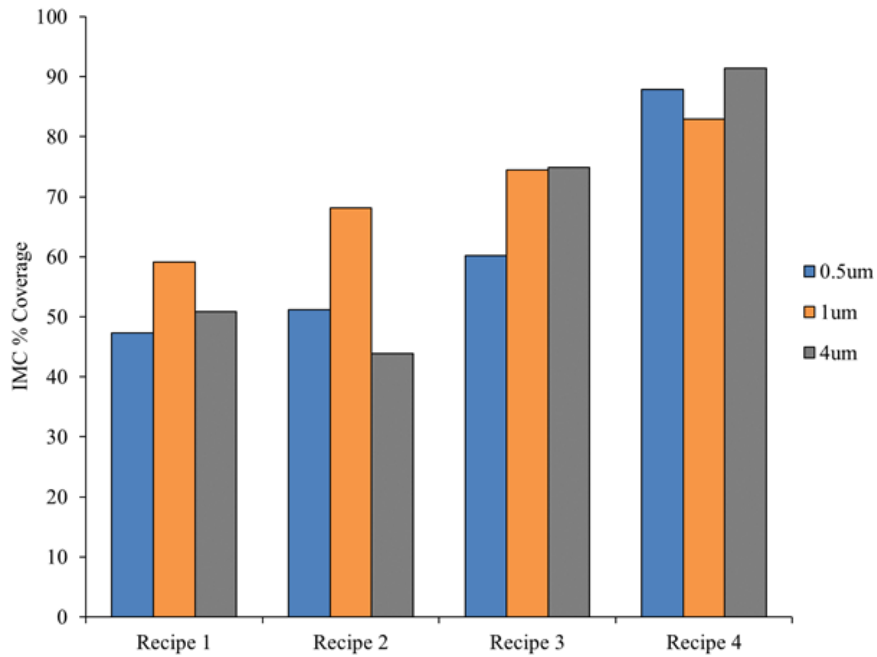
Figure 6.5: IMC percent coverage measurement for all bond pad thicknesses with different bonding recipes.

Shear strength and shear mode was tabulated for about 10 bonds for each recipe on each of the pad thicknesses. Figure 6.6 shows example micrographs of bonds after shear test for the 4 pad thicknesses. All sheared in the Al below the bond as expected. In this case, the shear mode tells us that Al strength is being exceeded, and that all other aspects of the bond are therefore stronger than the Al shear strength, including pad films adhesion to the silicon-dioxide below, IMC adhesion between Al and Cu, and the Cu ball itself.
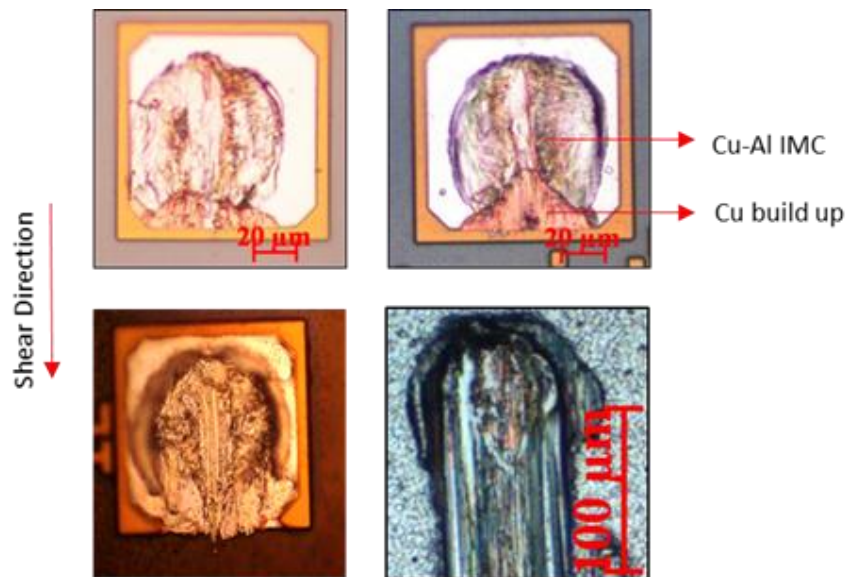
Figure 6.6: Shear mode for bonds on different pad thickness. (Clock wise from top left) 0.5um, 1um, 4um and 3um.

Figure 6.7 is example optical micrographs showing IMC after etching away the ball bonds, for all bond recipes for one of the pad thicknesses.
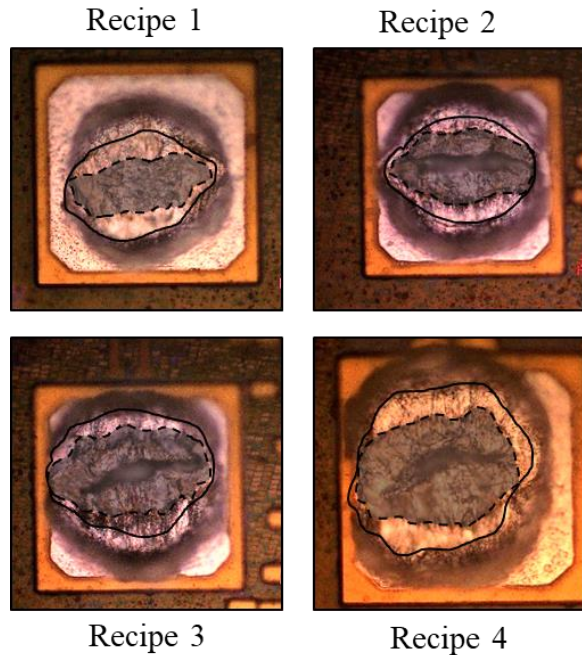
Figure 6.7: Images of ball bond-bond pad interface post etching. IMC region is highlighted in grey shade and the ball bond area is also marked.

6.2.1. Pad Thickness Effect – Experimental Results

Shear force measurements are shown in Figure 6.8, which shows a trend of increased shear force with thicker pad for the same bonding recipe. An average of 33% more shear force is required to shear the ball bond off 4 µm Al pad as compared to 0.5 µm pad thickness. Higher power and time (obtained by changing recipe from 1 to 4) in bonding caused an increase in shear force due to increased IMC area, as expected. It is hypothesized that the apparent increase in shear force with increased pad Al thickness is due to higher stress absorption in the thicker pad Al beneath the bond prior to shearing the Al film.
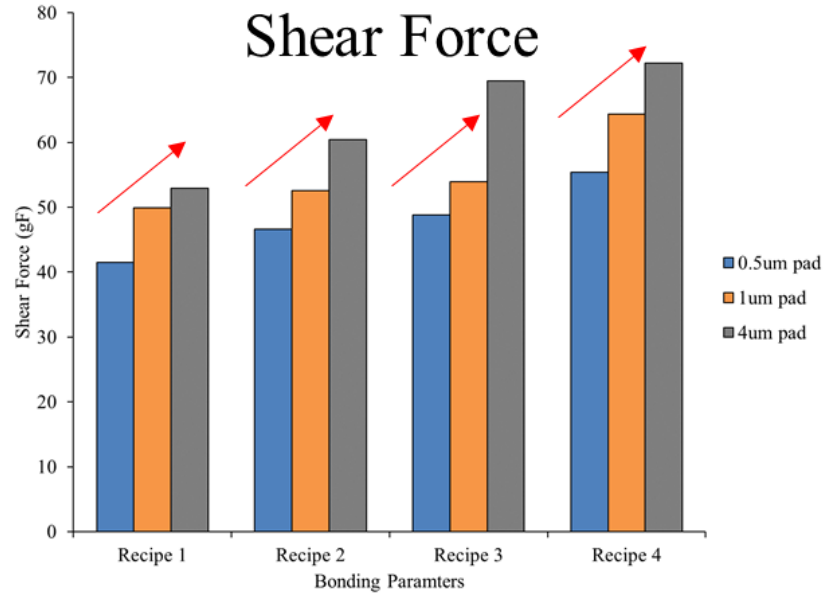
Figure 6.8: Shear force values for bonds on different pad thickness with different bonding recipes.

A recently revised standard, JEDEC JESD47J for qualification of integrated circuits, states that each Au or Cu ball bond on Al bond pad shall have shear force per bond area greater than 0.0062 gram force/μm^2 to be considered reliable. The shear strength of bonds in this study were above the limit specified by the standard.

6.2.2. Pad Thickness Effect – FEA Results

Finite element analysis (FEA) was performed to investigate stress in the pad Al due to the force of a shear tool, to try and match the physical data and to gain more understanding from the shear test. Figure 6.9 shows the model of a bond ball attached to the bond pad used in this analysis. The wire diameter is and bond diameter roughly match experimental conditions. Force was applied on the shear tool (rectangular block), shown with red arrow.
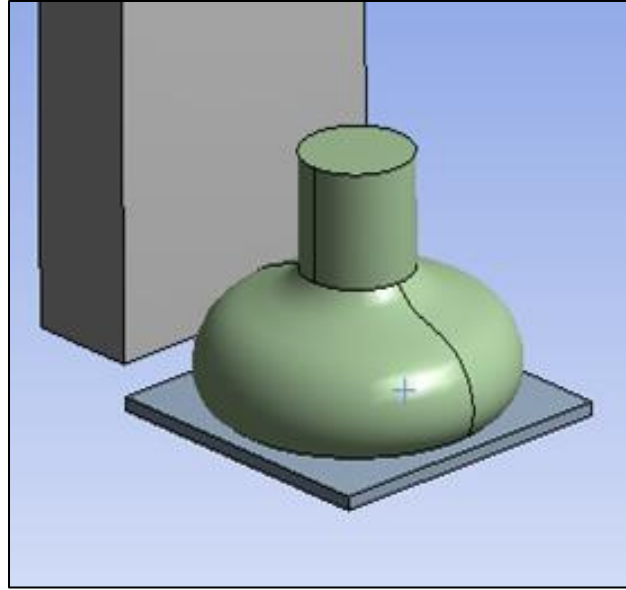
Figure 6.9: Finite element model of ball bond on bond pad.

The pad Al bottom face was implemented as a bonded "fixed support". Von-Mises stress is monitored to observe stress distribution in the Al pad. Thick pads show lower stress than thinner pads for the same applied force. In other words, it will require higher shear stress on the Cu ball to cause the Al film below it to yield, when the Al is thicker. Table 6.2 summarizes data for an applied shear force of 12 gF, for FEA models of 4 different Al pad thicknesses. For the same applied shear force on the Cu ball, FEA predicts much more stress in the thinnest pad Al film, with a 43% increase in stress with the thickest pad at the same point below the Cu bond (comparable to the 33% average increase observed experimentally).

Table 6.2: Relative shear stress for different pad thickness

	FEA Relative Shear Strength in pad Al for stress on Cu ball of 12gF			
Pad Thickness (μm)	0.5	1	3	4
Von-Mises Stress (MPa)	283	252.6	212	198
Relative Change (%)	43	27.6	7.1	0

FEA helps explain why higher force is required to shear the Al film apart on thicker pads. Four to five times the amount of force (12 gF) is actually required experimentally to cause the whole bond to shear from the pad, but FEA has sufficiently validated the effect of shear force on pad thickness by this simple modeling. Lower stress in thick pads is due to the increased stress dissipation through the malleable Al. Figure 6.10 shows aerial views of stress in the pad beneath the Cu ball bond. As mentioned, the applied 12 gF on the Cu ball causes highest stress below the yield point for Al (240 MPa) in the case of thick pad. The thin pad, in the same location, has 283 MPa stress (red region), already far above the yield point. This is another view illustrating that results of shear testing predicts higher shear values for Cu bonds on thicker pad Al.
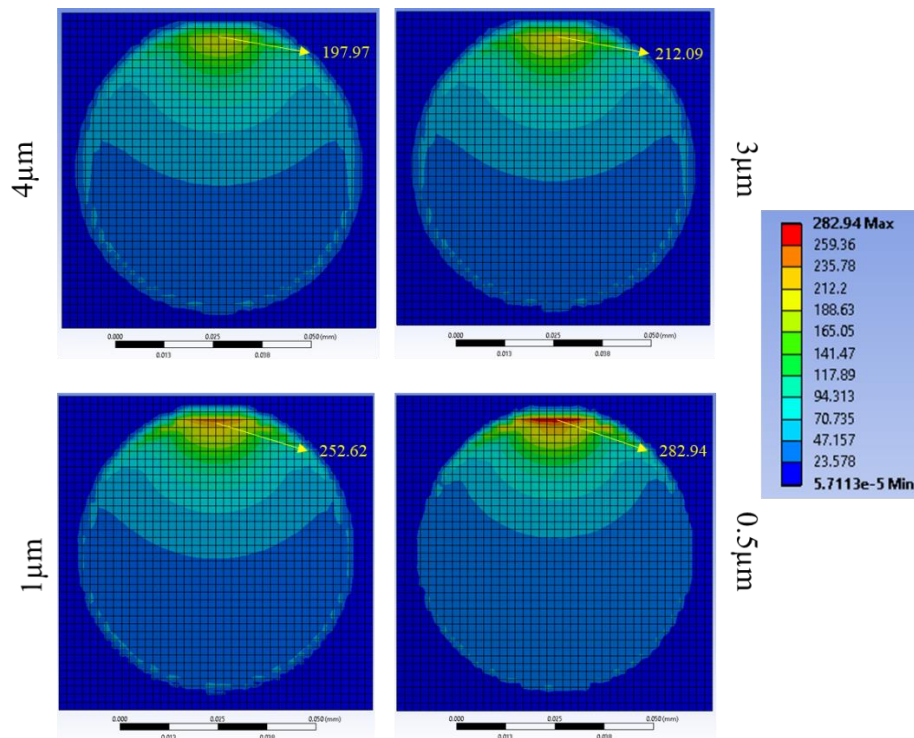

Figure 6.10: Von-Mises stress at a section 0.25μm under the bond pad for an applied force of 12gF.

6.3. Effect of Interfacial Changes on Bond Shear Analysis

The contact region of Cu bond, through IMC formation, governs the area of Al pad that experiences the shearing load. Thus the shear load indicates adhesion between bond and pad. With conditions such as non-optimized bonds, pre-existing defects in die pad, and incorrect shear method, location of shear and magnitude of force could be different, which needs to be addressed in order to obtain consistently correct shear force values that can be compared between different bond samples. JESD22B-116B specifies six shear mode types, which are presented in Table 6.3, of which type II is the desired shear mode.

Table 6.3: Shear Mode Types as Presented in JESD22B-116B [1].

S. No.	Shear Mode	Characteristics of Fractured Region	Cause
1	Type I: Bond lift	Separation of wire bond from pad. Unreasonably low shear force	Poor IMC coverage Non-optimized bonding conditions
2	Type II: Correct shear	Shear at the bonding surface (Al)	Lower strength of Al
3	Type III: Cratering	Chip out of die material	Pre-existing cracks in die Crack of ILD layer due to bonding
4	Type IV: Invalid shear	Shearing of pad before the bond observed	Low tool height Debri under tool
5	Type V: Shear skip	Tool passes over the bond	Large tool height Squished bond due to non-optimized parameter
6	Type VI: Pad lift	Removal of Al, exposing die material	Poor Al adhesion to die Non-optimized bonding condition

The standard does not explain the mechanics of shear testing and its effect on bond degradation. Such an explanation would aid in understanding the effect of shear force on bond reliability. With the growth in thickness of IMC, the interface changes due to emergence of new phases of material and thus a change in the material properties, affecting

shear force. Cross-sections of destructively sheared bonds after aging at 200°C show some regions under the bond that have $CuAl_2$ and no Al remaining. These regions experience failure in Cu bulk or at interface between Cu and $CuAl_2$ IMC as shown in Figure 6.11. This is different from initial condition, where shearing occurs only at the Al interface. To correlate change in shear force to the mode of shear, sheared region from different aging conditions were analyzed.
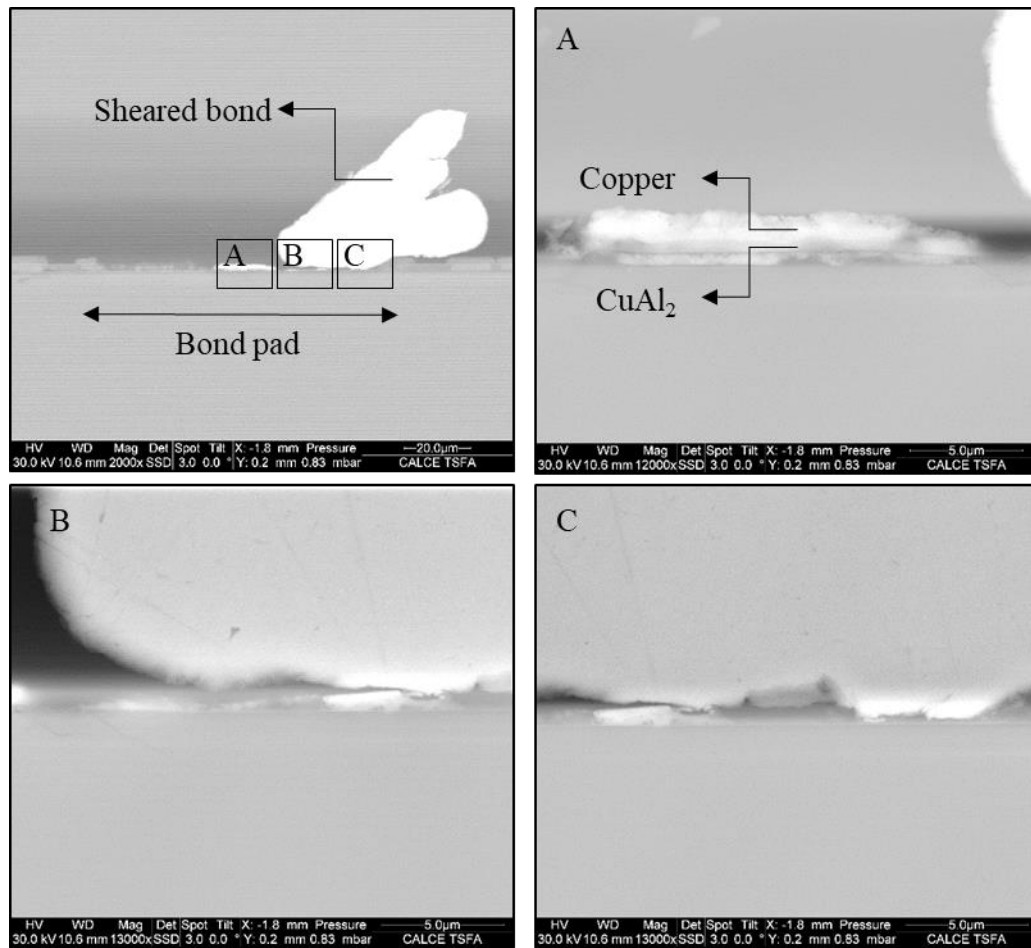
Figure 6.11: Destructive shear analysis showing failure at Cu, Al and $CuAl_2$.

6.4. Results

We observe that shear force and failure mode at bond interface varies with interfacial degradation. To study this, four Cu wire bond recipes (Table 1) were formulated that would each give shear mode of type II at initial condition as shown in Figure 6.13. All of the measured shear forces are well above the limit set by JEDEC standard JESD-B116B for a good quality bond.

Shear force increases with recipe bonding energy due to larger area of IMC coverage. Additional factors include thicker IMC formation, and the change in shear failure region in locations where all the pad Al is consumed, as mentioned above.
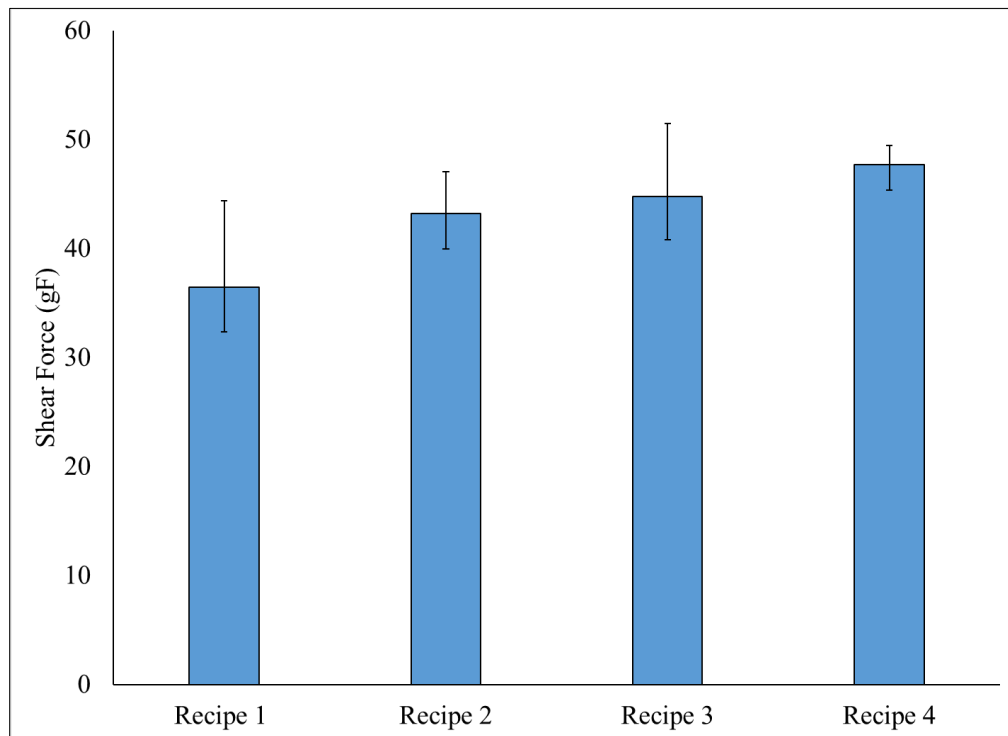
Figure 6.12: Shear force for different bonding conditions used in this study.

For all of the recipes, aging to 24 hours shows a significant increase in shear force (Figure 6.13). This is due to greater IMC coverage at the interface thus improving adhesion

of bond to pad. Post shear images show remaining Cu in some regions, which is absent in the case of un-aged shear samples. Traces of $CuAl_2$ (brown region) are observed with higher energy bond recipes, 3 and 4, which is verified to identify the correct phase of IMC as shown in Figure 6.14.
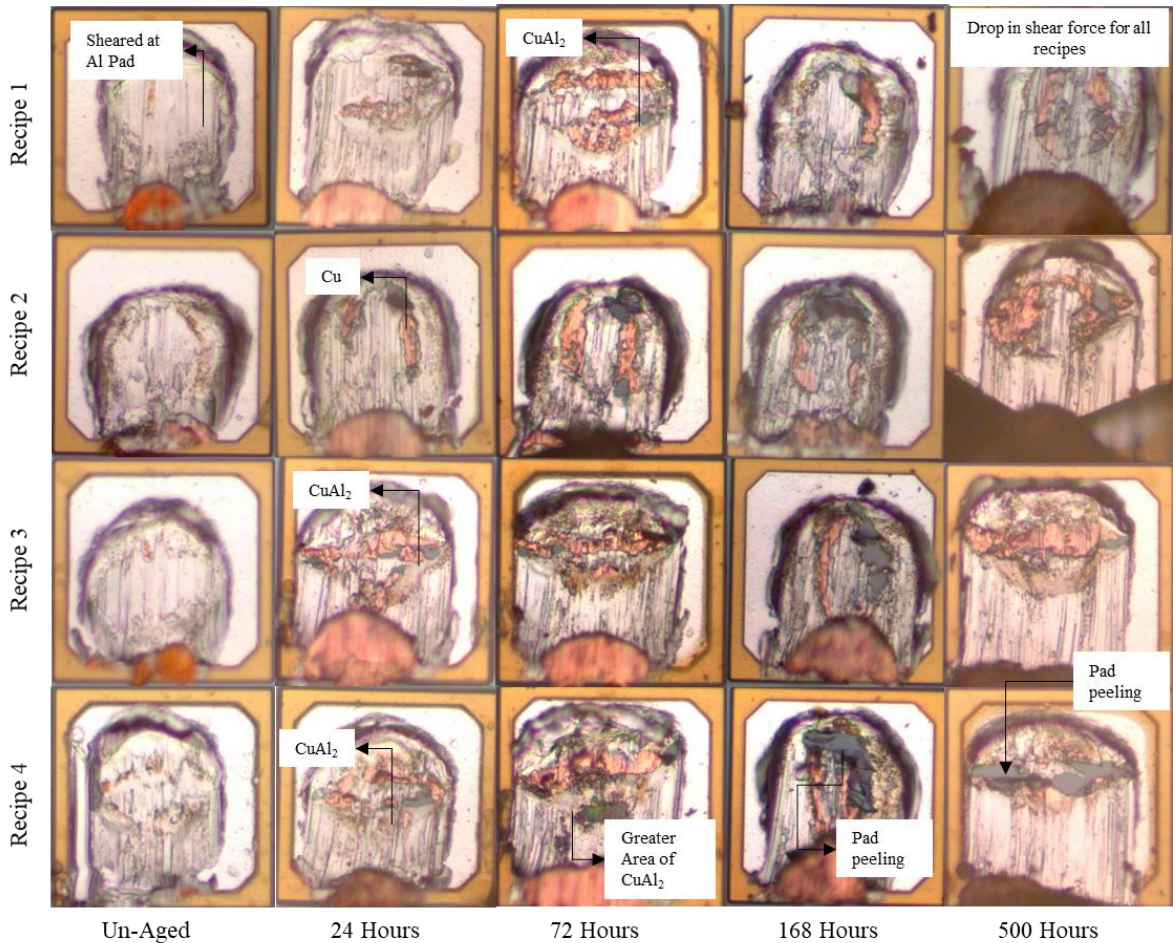
Figure 6.13: Post shear analysis for four bond recipes after different aging times.

Aging to 72 hours at 200°C causes a drop in shear force for recipe 2 and 3, but an increase for recipe 4. This is attributed to the fact that larger bonding area, such as in recipe 4, leads to greater IMC coverage area thereby reaching greater peak force later, as compared to the

lower energy recipes. Sheared region of bond recipe 3 after 24 hours at 200°C shows indications of remaining Cu and $CuAl_2$ (brown region).
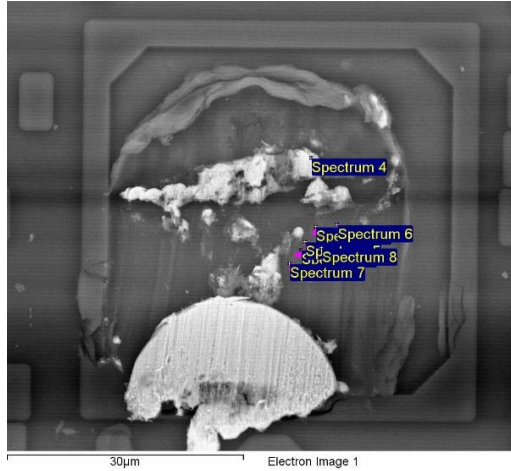
Spectrum No.	Al	Cu
Spectrum 1	77.39	22.61
Spectrum 2	75.59	24.41
Spectrum 3	73.75	26.25
Spectrum 4	77.14	22.86

Figure 6.14: EDS scan showing $CuAl_2$ on post sheared region.

In addition, some areas of pad peeling are also observed, which is caused by complete consumption of Al in the pad material by $CuAl_2$ IMC. This is especially noticeable in recipe 4, where remaining Al starts out thin due to harsh bonding conditions.
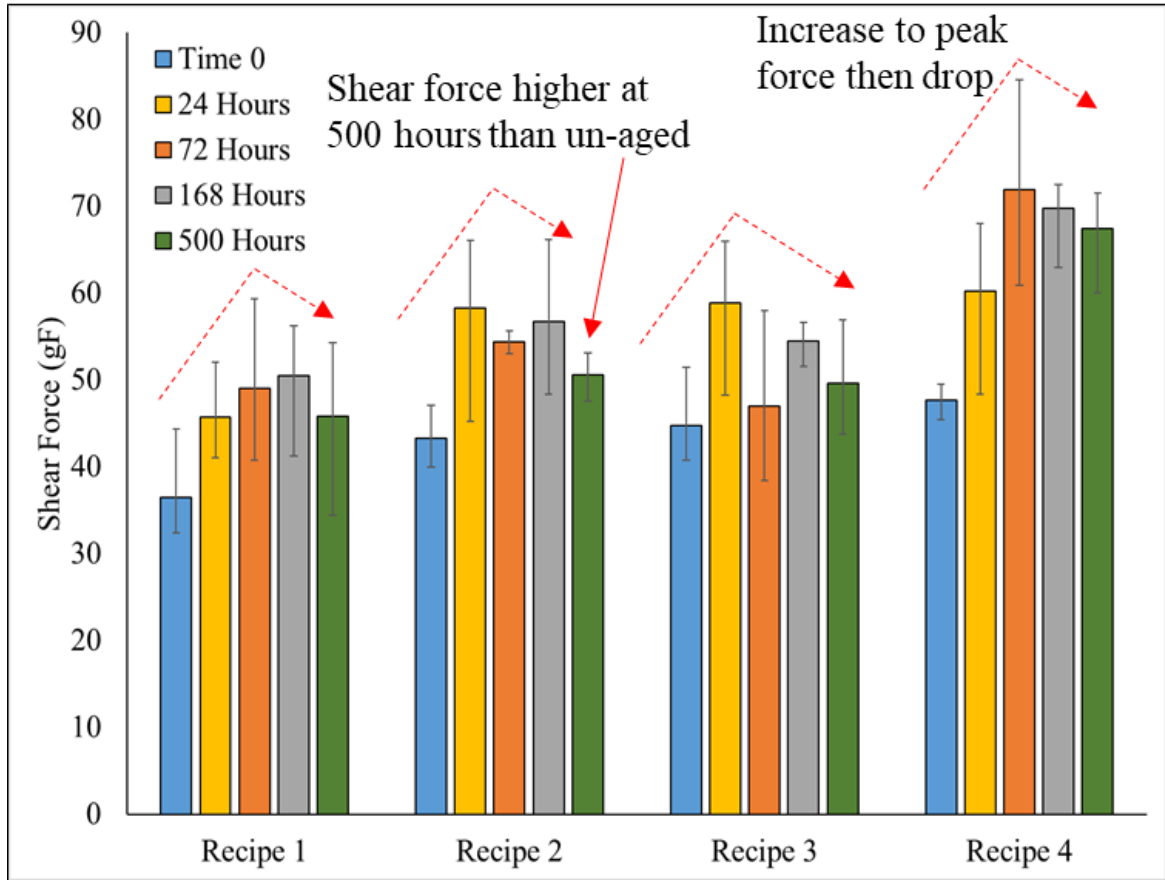
Figure 6.15: Shear force for all bonding recipes with thermal aging.

Aging to 168 hours, shows significant drop in shear forces and a change in shear mode for 3 out of 4 bond recipes (recipe 2, 3 and 4). Post shear analysis shows failure predominantly in the interface between Cu and IMC, leading to a significant drop in shear force. A larger area of pad peeling is also observed, which contributes to reduced shear force compared to 24 and 72 hours.

After aging to 500 hours at 200°C, bond force still shows higher values compared to initial conditions, especially high in the case of recipe 4 where bond area is largest, indicating a possibility of lateral coverage along with growth in thickness of IMC. However, compared to 168 hours, a drop in force in all 4 bond recipes is observed, owing to the growth in

thickness of $CuAl_2$ IMCs and an adverse change in shear mode. Sheared region shows Cu, $CuAl_2$ (brown region) and underlying Si. Thus 500 hours of aging at 200°C marks the onset of bond force reduction.

6.5. Conclusion

Bond shear testing is an important evaluation process that is used to categorize good quality bonds from bad ones. Several factors contribute to the shear force. We have shown that Al bond pad thickness is a significant factor in shear test results, with Cu bonds on thicker pads producing higher shear strength values than for thinner pads, even for non-optimized Cu wire bond recipes. Shear mode is consistent throughout the experiment, shearing in the pad Al beneath the bond at the non-aged condition. IMC% coverage was measured and it was concluded that it did not cause the increase in shear force. A hypothesis that the thick Al pads absorb higher stress than thin pads is proven by performing FEA on a simplified model of the ball bond-bond pad interface. For the same applied lateral stress to the Cu bond ball, calculated stress developed in the Al pad film is significantly less for thick pads compared to thin pads. This implies that shear test limits in manufacturing should take pad Al thickness into account when comparing bonds from different devices.

With exposure to high temperature, bond interface undergoes changes through IMC growth that is reflected by the bond shear analysis. Four recipes were used in the study to understand effect of aging on shear force analysis. Results show a trend of initial increase in the shear force for the bonds due to lateral IMC growth. The peak force reached by the bonds take a longer time in the case of Recipe 1 (lowest values of bond parameter settings used in study) compared to others. Extended time of 500 hours of aging at 200ºC shows pad peeling which causes a reduction in shear force. Although it is higher than in the un-

aged condition, interfacial IMC has consumed most of Al pad and hence at this state, other failures of the bond can occur. Hence shear force analysis must include the study of aging conditions and shear mode along with the force values in order to study wire bonded interface.

6.6. Reference

[1] JEDEC Solid State Technology Association, VA, USA (2017), *Wire Bond Shear Test Method*, (JESD22-B116B).

[2] ASTM International, PA, USA (2018), *Standard Test Method of Destructive Shear Testing of Ball Bonds*, (ASTM F1269-13).

[3] Automotive Electronics Council, USA (1998), *Wire Bond Shear Test*, (AEC Q-100-001 Rev-C).

[4] Davoudi, K. (2017). Temperature dependence of the yield strength of aluminum thin films: Multiscale modeling approach. Scripta Materialia, 131, 63-66.

7. Effect of Aluminum Bond Pad Thickness on Cu Wire Bond Reliability.

Aluminum bond pad thickness was shown to be a critical parameter in the device classification that led to reliability modelling as well as from the results shown in Chapter 4, where IMC activation energy was different with devices from different pad thicknesses. With these preliminary results on pad thicknesses, detailed review of literature was performed to identify the effect and need to study it from a perspective of understanding Cu wire bond characteristics and reliability.

7.1. Introduction

Bond pad related failures have been widely studied in the past [6][7], of which Al pad thickness have been studied previously from the stand point of manufacturing to ensure good bendability of Cu. Two critical concerns exists with use of Cu wire, (1) Use of thin Al pads with higher (than Au) bond force required to make the bond can cause failure in the active circuitry beneath the bond pad (BOAC), causing minor cracks that can propagate under use condition to cause failure, (2) Use of thick bond pads can lead to extrusion of the Al, known as Al "splash", which could pose risk in fine pitch devices, where unnecessary electrical contact may exist from one pad to another. Song, M. et al., [1] observed several modes of failure during the wire bonding such as pad cratering, pad metal peeling and Al push-out with non-optimized pads. They prescribed need to consider BOAC cracking and Al "splash" for optimizing pad thickness for use with Cu wire bonding. Electrical probing for circuitry verification prior to wire bonding can removed Al from material due to probe shear. This can led to areas of very less Al that can adversely affect Cu bonding. Thick bond pads are typically used with high power devices such as MOSFETs, IGBTs, etc.

where resistance to electron flow in interconnection can significantly affect device performance. On the other hand, small-signal devices such as as micro-processors, transceivers, receivers, etc. use thin pads to prevent excess "splash" of Al, which is a concern especially for these fine pitch devices.

Although such optimization is necessary from the standpoint of bondability, the effect of Al pad thickness on Cu wire bond characteristics further in the life cycle has not be evaluated thoroughly. With exposure to high temperature, Cu diffusion in Al leads to Cu-Al IMC formation. In this bi-metallic joint, Al becomes the limiting material as compared with Cu and hence controls the thickness and phases of IMC formation. To understand the effect of the limiting material, Sarabol, P., et al.,[2] studied three cases of Cu and Al ratio, namely, (1) 2 µm:0.2 µm, (2) 2 µm:2 µm and (3) 0.2 µm:2 µm at initially formed condition and after aging for several days at 50C, 100C, 150C and 200C. Interface integrity was studied through a pull test on the joint. Case (2) and (3) required significantly lower pull load than (1), indicating the poor interfacial performance with higher Cu content than Al, as present in wire bonded joints. Hence the results from the study indicate poor performance of "thin" Al pads.

Fan, S., et al.,[3] studied the effect of different Al pad thickness in interfacial IMC growth of Cu wire bonding with use of a thin pad (0.8 µm to 1.5 µm), medium pad (1.6 µm to 2.8 µm) and a thick pad (2.9 µm to 4 µm). High temperature storage at 175C and 205C was performed and devices were removed at 500, 1000 and 2000 hours from 175C and 250, 500 and 1000 hours from 205°C. Results from the study showed growth of Cu9Al4 with the thin pad at 1000 hours in 205°C and absence of Cu_9Al_4 in the thick pad at the same

aging temperature and time. This was attributed to the constant supply of Al in the thick pad that continued growth of $CuAl_2$ but not Cu_9Al_4.

Hentzell, H.T.G., et al.,[4] performed isothermal aging study on Cu-Al bimetallic thin-film to study interfacial diffusing species and identify phase kinetics. Vapor deposition of both Cu and Al were done up to a thickness of 2700 Å and 5000 Å respectively and were aged for time interval from 5 minutes to 160 hours. X-Ray diffraction showed the first forming phase was θ-$CuAl_2$, which was reported to grow until all Al is consumed and near the end of Al depletion after which a η_2-$CuAl$ phase was identified. Finally a γ_2-Cu_9Al_4 phase was identified after most of θ-$CuAl_2$ was consumed. This 'single compound growth' phenomenon was further strengthened with the results from aging of thicker Al (much thicker than Cu), where θ-$CuAl_2$ is the first and last phase that is said to exist at the interface.

On the other hand, IMC growth in bulk specimen as presented in the study by Kouters, M.H.M., et al.,[5] shows multiple phases that grow simultaneously at the Cu-Al interface. Hence, thickness of Al in the case of Cu-Al system has a significant effect on the time of formation of different IMC phases.

Interfacial reaction between interacting elements in wire bond-bond pad configuration are different from that of materials prepared by methods such as vapor deposition, bulk-specimen welding, etc. due to the following factors:

(1) Grain boundary to grain volume ratio

(2) Interfacial defects (i.e. dislocation) and

(3) Limiting volume of one or both of diffusing elements.

With the above knowledge of studies presented in literature and the differences to Cu-Al ball bond-bond pad pair, this study is conducted to understand the IMC growth and interfacial failure with different bond pad thickness conditions.

A plan for studying the effect of Al pad thickness is developed as shown in Figure 7.1.
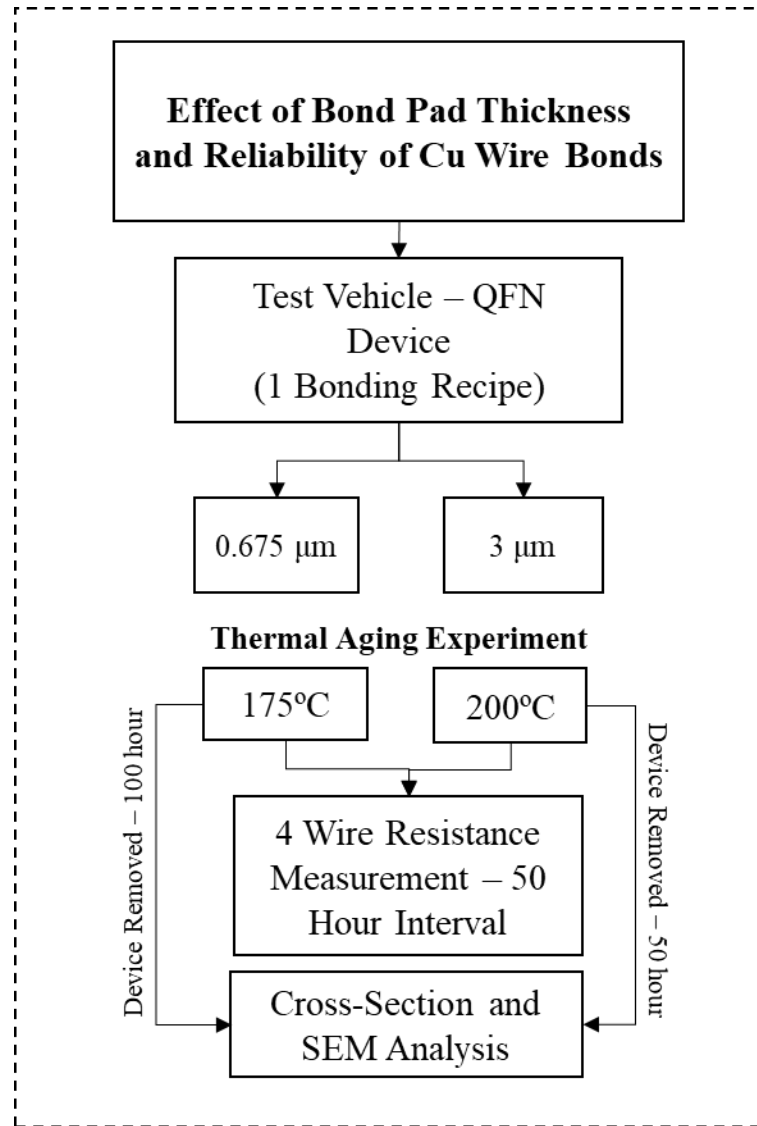

Figure 7.1 Test Plan for Studying Effect of Bond Pad Thickness on Reliability of Cu Wire Bonds.

This work will use of QFN test device on which wire bonds were bonded in-house with controlled parameters that consists of two different pad thicknesses (0.675 µm and 3 µm) as shown in Figure 7.2. These packages were encapsulated and then aged at two temperature conditions, 175°C and 200°C, during which electrical measurements and cross-sectional analysis are performed on devices taken out at an interval of 50 hours.

7.2. Test Vehicle and Design of Experiment

OFN packages was used in the isothermal aging study. These packages consisted of Si die at the center with 5 large pads and few smaller pads. 4 out of the 5 large bond pads were located at each side of the package and was used in this study. Wire bonding on these packages were done with a K&S 4524 Ultrasonic Wire Bonder using 18 um Cu wire, similar to that used in many COTS devices. A forming gas (N_2H_2) was used to prevent oxidation during free air ball (FAB) formation, which ensured good bonding between Cu and Al. Wire bonds were made in manner to be able to measure 4-wire resistance on the bonds under study as shown in Figure. This allowed for monitoring the changes due to IMC growth and interfacial cracking that occurs at the Cu-Al interface. 4 of the 5 large pads were used, with two ball bonds on one pad that connects to two different leads as shown, additionally wire bonds were made from one lead to another to form a connection to measure the 4 wire resistance. With this configuration, 4 data points were able to be obtained with each side of the package. Post wire bonding, these packages were encapsulated with HYSOL FP4450, one-part epoxy mold compound at room temperature and cured at 165°C for 1 hour. All of the 90 packages used in the study were subjected to baseline characterization to obtain electrical resistance data right after cure profile was completed. QFN test socket shown in Figure 7.2 was used for these measurements.
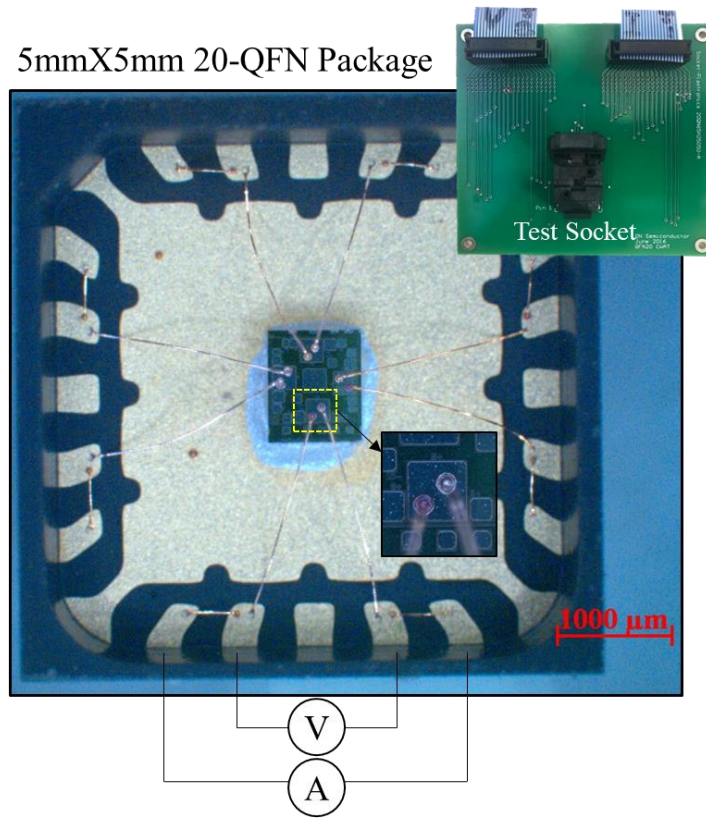
Figure 7.2: Test Vehicle – QFN device with Cu Wire Bonds.

Base line measurements shows a higher resistance with the 0.675μm pads compared to the 3μm pads, due to the larger cross-sectional area in the latter case as shown in Figure 7.3. This trend was consistent with all packages. Several data points were collected to observe if there were variations due to measurement but it was found that the measurement variations were minimal. Minor variation from one bond pad to another was observed, especially with the 0.675 μm pads, but each bond pair was marked and its aging resistance was compared to its own base line which the difference not significant.
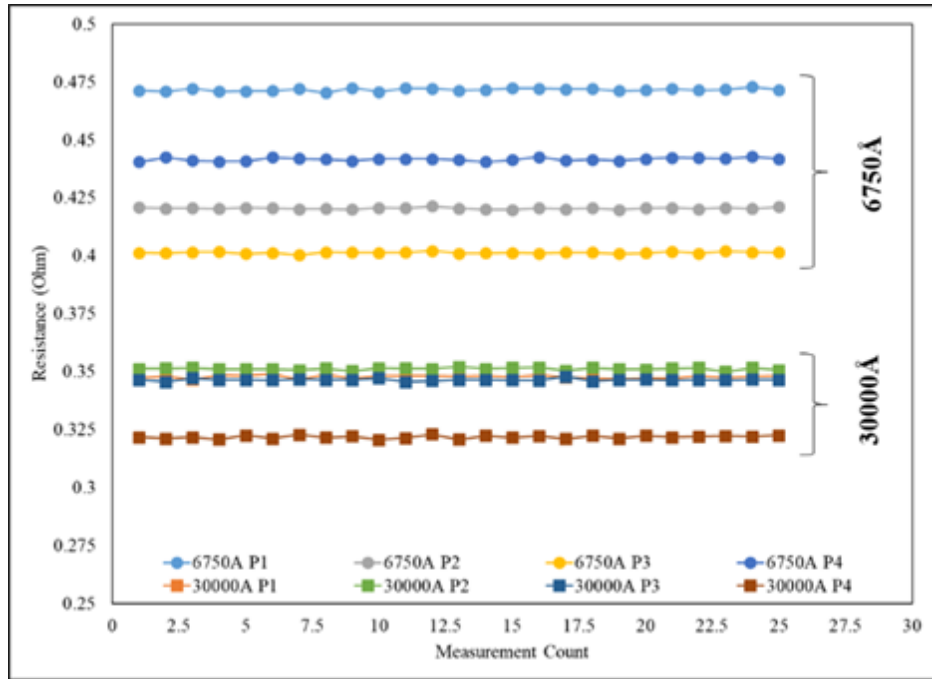
Figure 7.3: Base line Characterization Results for All Bond Pairs in QFN Package.

7.3. Results from Accelerate Thermal Aging

About 20 devices of each 0.675 μm and 3 μm devices were aged at each of 175°C and 200°C condition. These devices were removed every 50 hours for resistance monitoring for all packages. Figure 7.4 shows one device from 175°C and 200°C that was aged until 1000 hours and 650 hours respectively. In the case of 175°C, a steady increase was observed with 0.675 and 3um until about 600 hours, after which bonds on the thin pad shows a sharp increase compared to those on the thick pad. In the 200°C case, a similar trend is observed but resistance values go up to almost two orders of magnitude higher than in the case of 175°C, by the end of test.
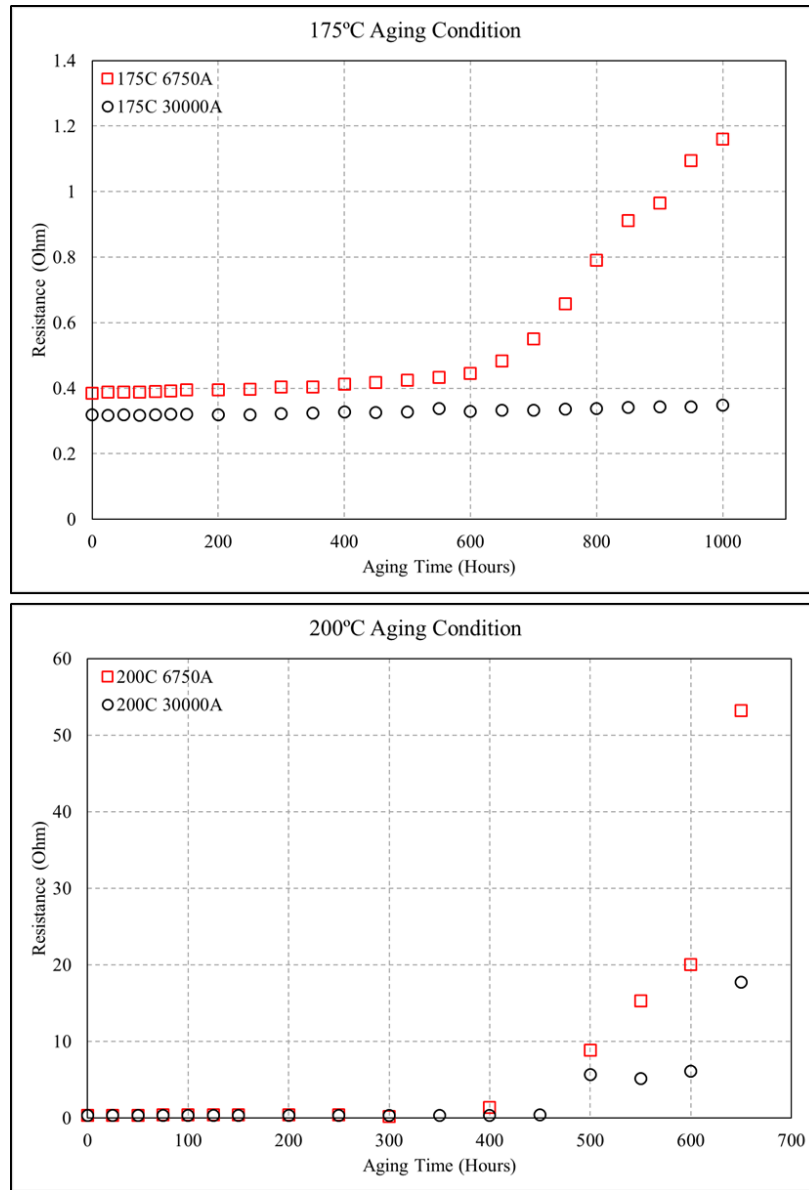
Figure 7.4: Resistance of One Bond Pair with Thermal Aging

Average values of resistance taken from multiple devices were used for analysis as significant variations were found from one device to another during thermal aging. Figure 7.5 shows the averaged values obtained from the test. Thin pad shows a higher change in resistance by completion of the test compared to the thick pad. A reasonable value of increase that can be assumed to be failure is 20%. A knee point is defined here as the time to cause greater than 20% resistance increase, which occurs sooner with the thin pad than

in the case of a thick pad. No open circuits were observed even at the end of test at 175°C condition.
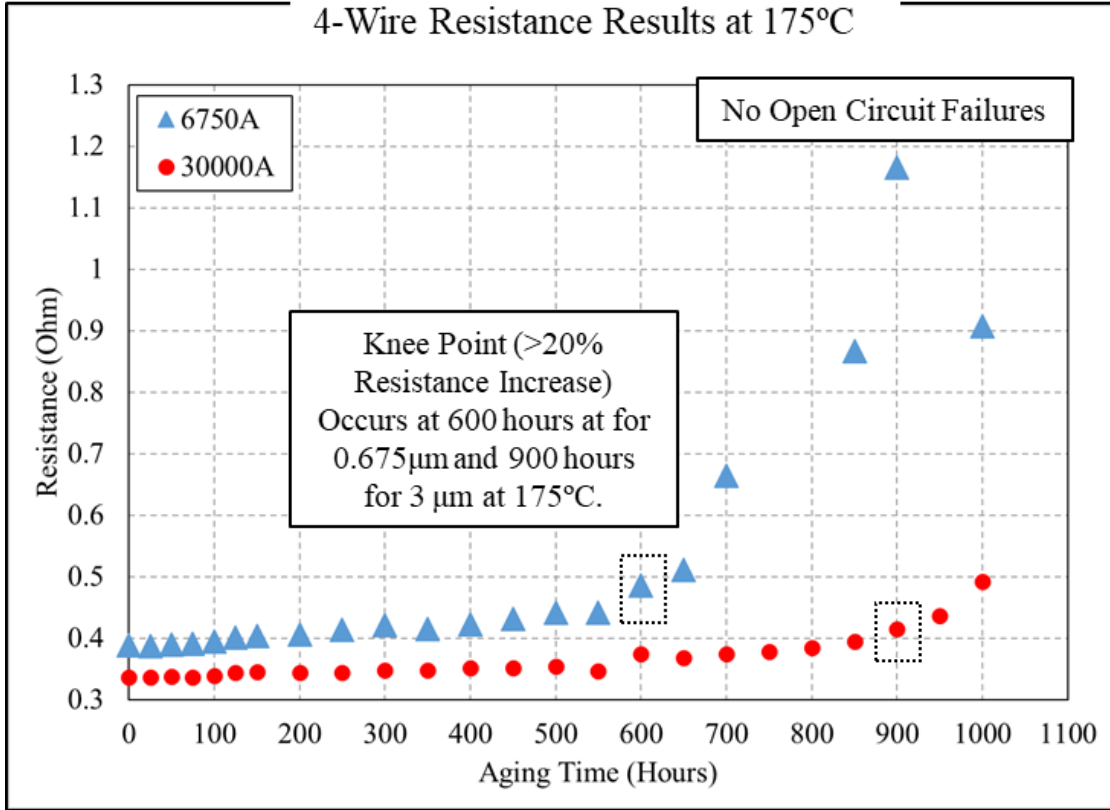
Figure 7.5: Isothermal Aging at 175C Condition.

Higher resistance increase with the thin pad is attributed to early onset of Cu_9Al_4, due to consumption of all Al from the bond pad material, which leads to long interfacial cracks as shown in Figure 7.6. Higher magnification images of the interface at selected tim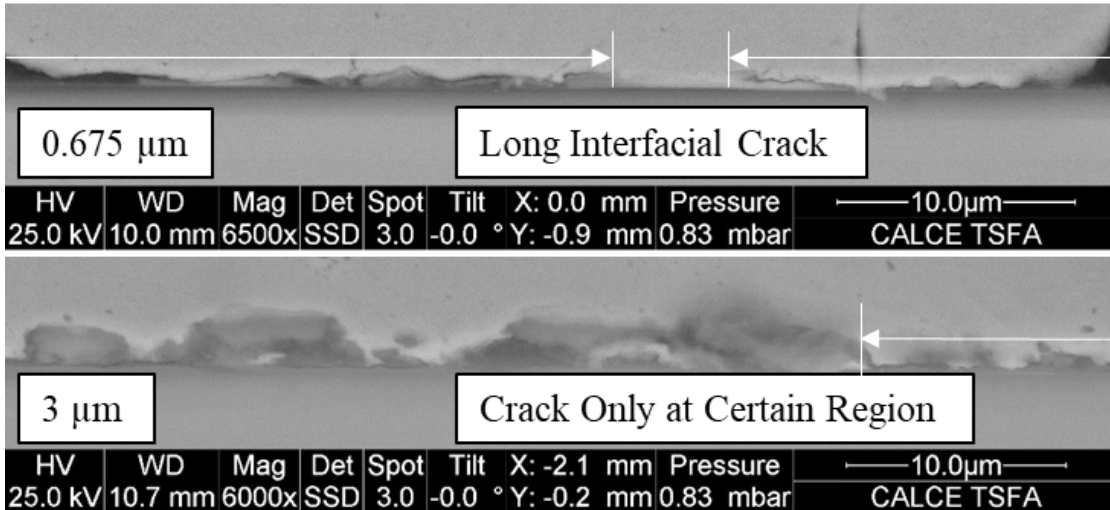e intervals are shown in Figure 7.6, where interfacial cracks between IMC and Cu are visible. To confirm the growth of Cu_9Al_4 at the thin pad interface and its delay with thicker pads, electron dispersive spectroscopy (EDS) analysis was performed at high magnification at the IMC region on both 0.675 and 3 um pad interface that was removed at knee point time of thin pad, at 150 hours, where resistance was >20% compared to baseline. Results of EDS analysis are shown in Figure 7.7, where atomic % of Cu is seen to be close to the range where Cu_9Al_4 phase (62.5-69%) has been identified. Spectrum locations are pointed out where the analysis was performed. At the same aging time and temperature, EDS analysis of the IMC shows atomic % of Cu to be 31-36%, close to the range of $CuAl_2$ identified phase (31.9-33%). A higher Cu is detected in both cases, which could be due to the measurement technique itself, which is not a strict surface analysis method. Thus, these conditions prove the early growth of Cu_9Al_4 with thin pad that causes a higher resistance spike, which does not happen with the case of the thick pad due to constant supply of Al.

0.675 μm   **3 μm**

Cu Bond

Cu-Al Interface

100 Hours

Al pad

Si Die

400 Hours

1000 Hours

Interfacial
Crack

No Continuous Crack
even at 1000 hours in
both pad thickness.
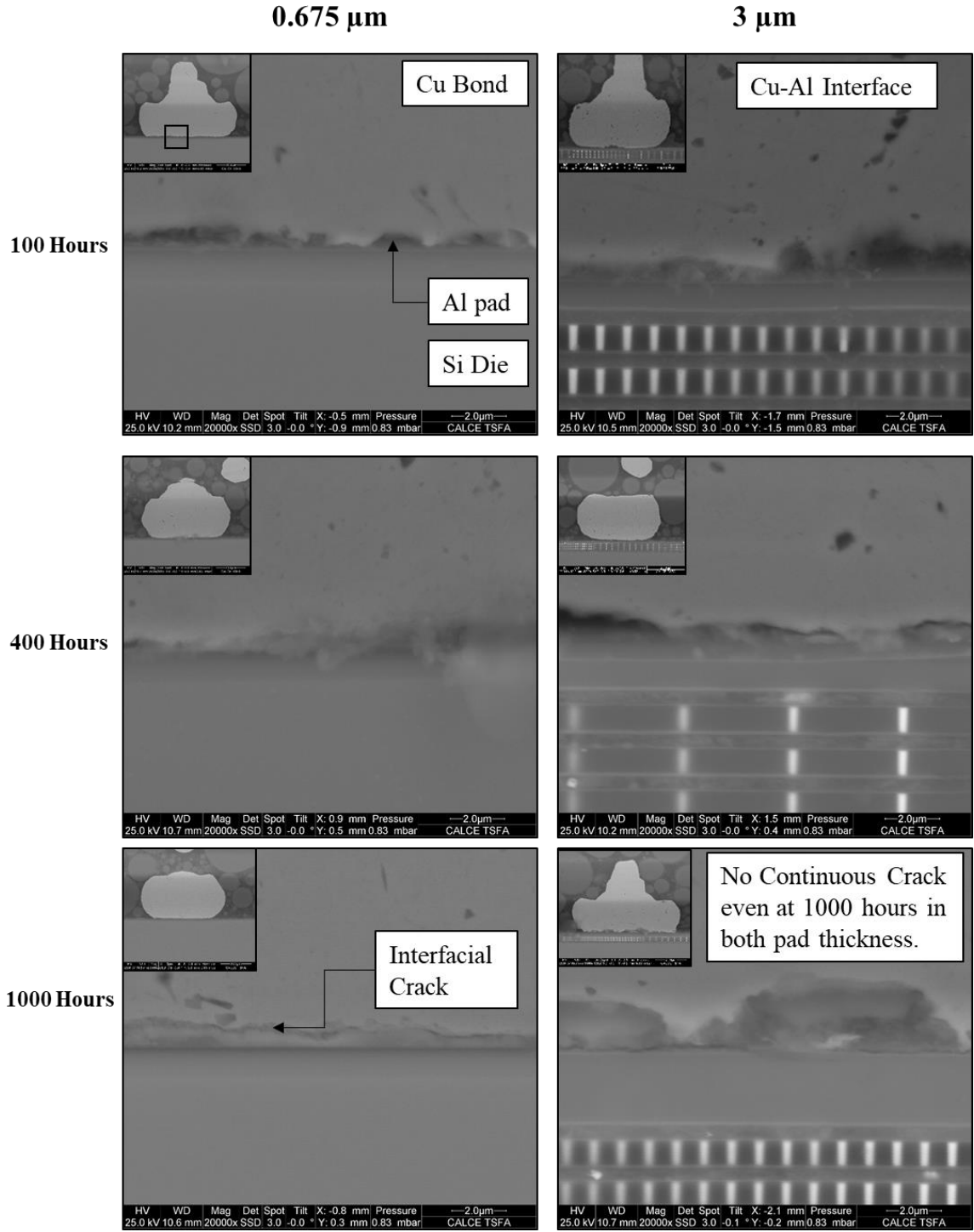
Figure 7.6: Interfacial Damage from 175℃ Isothermal Aging.

Phase	At. % Cu
Al	0 – 2.84
$CuAl_2$	31.9 – 33
Cu_9Al_4	62.5 – 69
Cu	80.3 – 100

Spectrum	Al	Cu
Spectrum 1	29.07	70.93
Spectrum 2	28.16	71.84
Spectrum 3	18.66	81.34
Spectrum 4	21.84	78.16
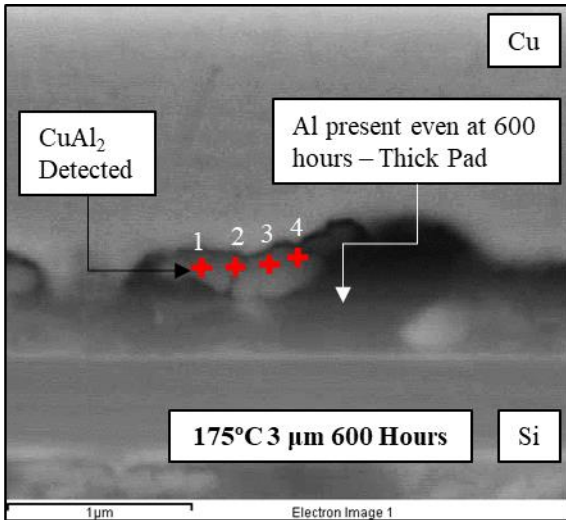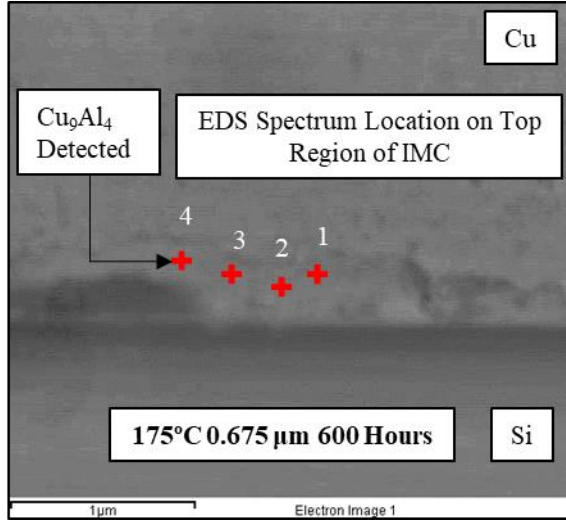
Spectrum	Al	Cu
Spectrum 1	63.45	36.55
Spectrum 2	61.17	38.83
Spectrum 3	64.67	35.33
Spectrum 4	68.51	31.49
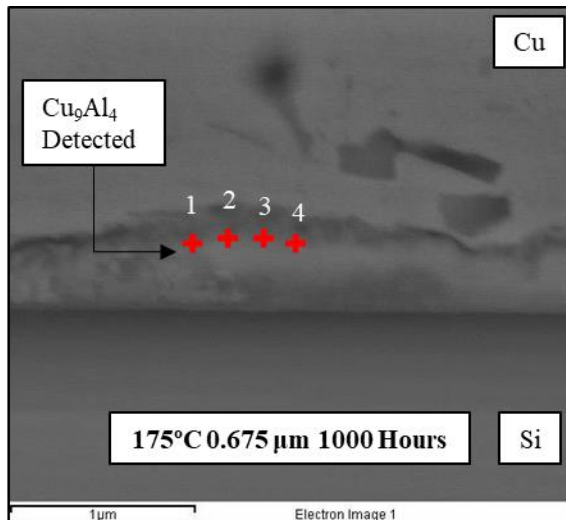
Spectrum	Al	Cu
Spectrum 1	25.52	74.48
Spectrum 2	28.24	71.76
Spectrum 3	38.9	61.1
Spectrum 4	37.97	62.03

129

Spectrum	Al	Cu
Spectrum 1	29.98	70.02
Spectrum 2	35.1	64.9
Spectrum 3	35.57	64.43
Spectrum 4	34.05	65.95
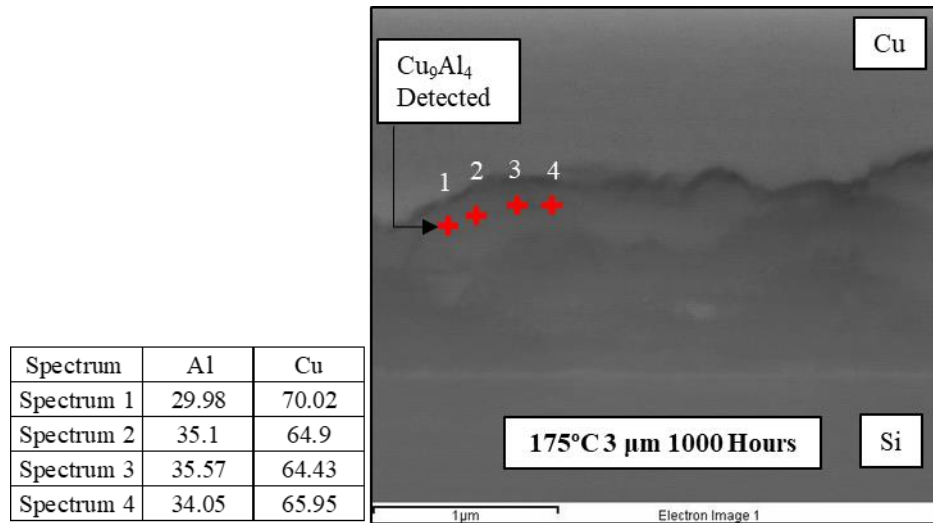
Figure 7.7: EDS Analysis Results.

Similar analysis of average electrical resistance was performed with the devices from 200°C isothermal aging condition as shown in Figure 7.8. Similar trend of early increase in resistance observed with thin pads compared to thick pad. In addition, resistance increases to about two order of magnitude than with 175°C aging condition due to accelerated IMC growth and interfacial cracking. Few open circuit failures were also observed after 350 hours of aging in the 0.675um pad condition. The knee point occurs much earlier in the case of 200°C aging, at 75 hours with 0.675um and at 125 hours at 3um.
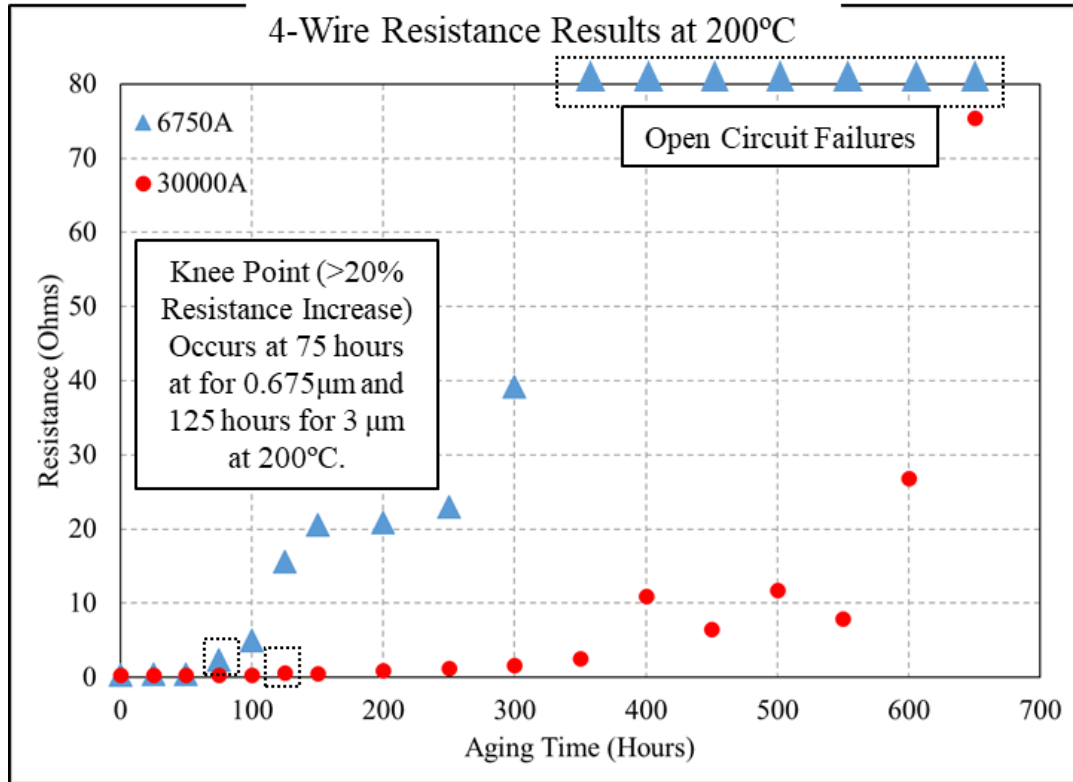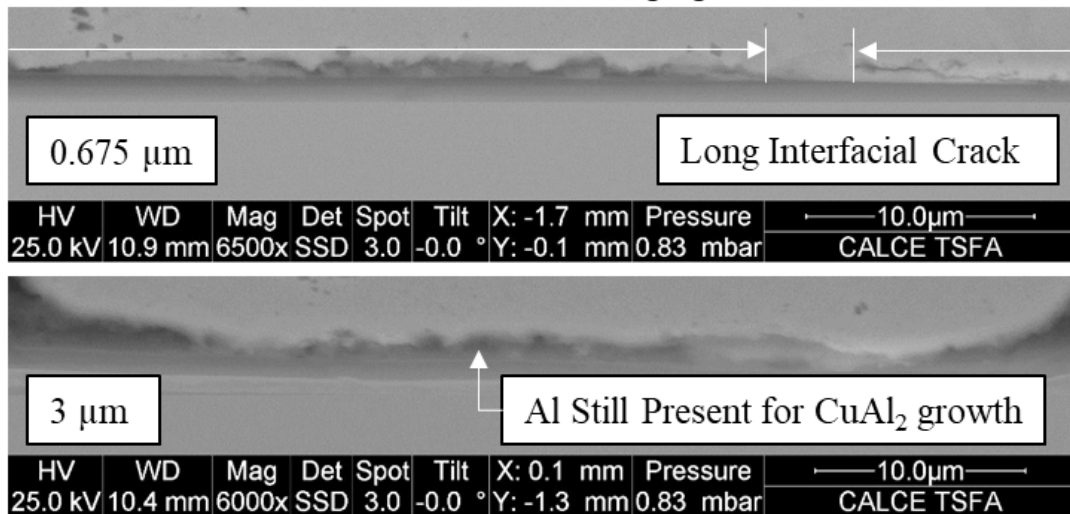
Figure 7.8: Isothermal Aging at 200C Condition.

Cross-sectional images at different time intervals are shown in Figure 7.9 for both pad thicknesses. A continuous crack at interface in 0.675um is observed at times greater than 300 hours leading to an open circuit failure. With the 3 um pad, interfacial cracks are visible

although not continuous and region of contact between bond and pad are present as shown in *Figure 7.9*.
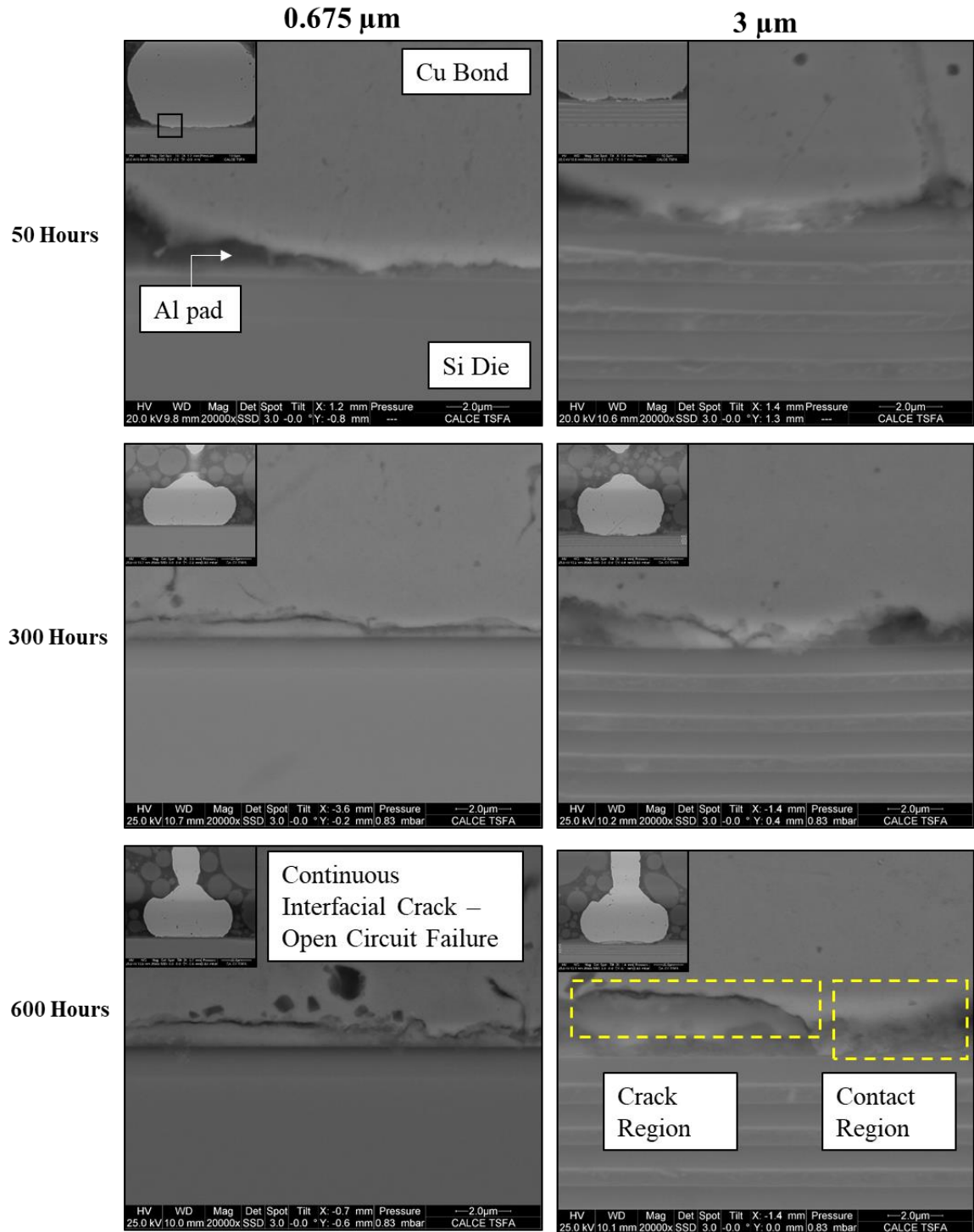
Figure 7.9: Interfacial Damage from 200°C Aging.

EDS analysis was performed on the devices removed at 150 hours. Figure 7.10 shows the result from analysis, where higher atomic % of Cu 61-69% is seen at the thin pad case, which corresponds to Cu_9Al_4 phase. In the case of the thick pad, atomic % of Cu is found to be between 36-39% that corresponds to $CuAl_2$ phase.

Phase	At. % Cu
Al	$0 - 2.84$
$CuAl_2$	$31.9 - 33$
Cu_9Al_4	$62.5 - 69$
Cu	$80.3 - 100$

Spectrum	Al	Cu
Spectrum 1	36.43	63.57
Spectrum 2	38.48	61.52
Spectrum 3	36.15	63.85
Spectrum 4	30.44	69.56

Spectrum	Al	Cu
Spectrum 1	25.15	74.85
Spectrum 2	25.98	74.02
Spectrum 3	20.8	79.2
Spectrum 4	22.93	77.07

Spectrum	Al	Cu
Spectrum 1	60.76	39.24
Spectrum 2	63.31	36.69
Spectrum 3	63.79	36.21
Spectrum 4	62.52	37.48

Spectrum	Al	Cu
Spectrum 1	36.29	63.71
Spectrum 2	33.7	66.3
Spectrum 3	34.25	65.75
Spectrum 4	29.38	70.62

Figure 7.10: EDS Analysis Results.

Thus, this accelerated thermal aging study shows better performance of Cu wire bonds with thick Al pad compared to thin ones due to the early onset of second phase of IMC in the latter case. To make the results capable of use in package design analysis and for reliability prediction, empirical relationships were derived through use of available data to identify increase in resistance as a function of aging time for two pad thickness at two temperature conditions. Figure 7.11 shows the % increase in resistance for the different test cases studied in this work.
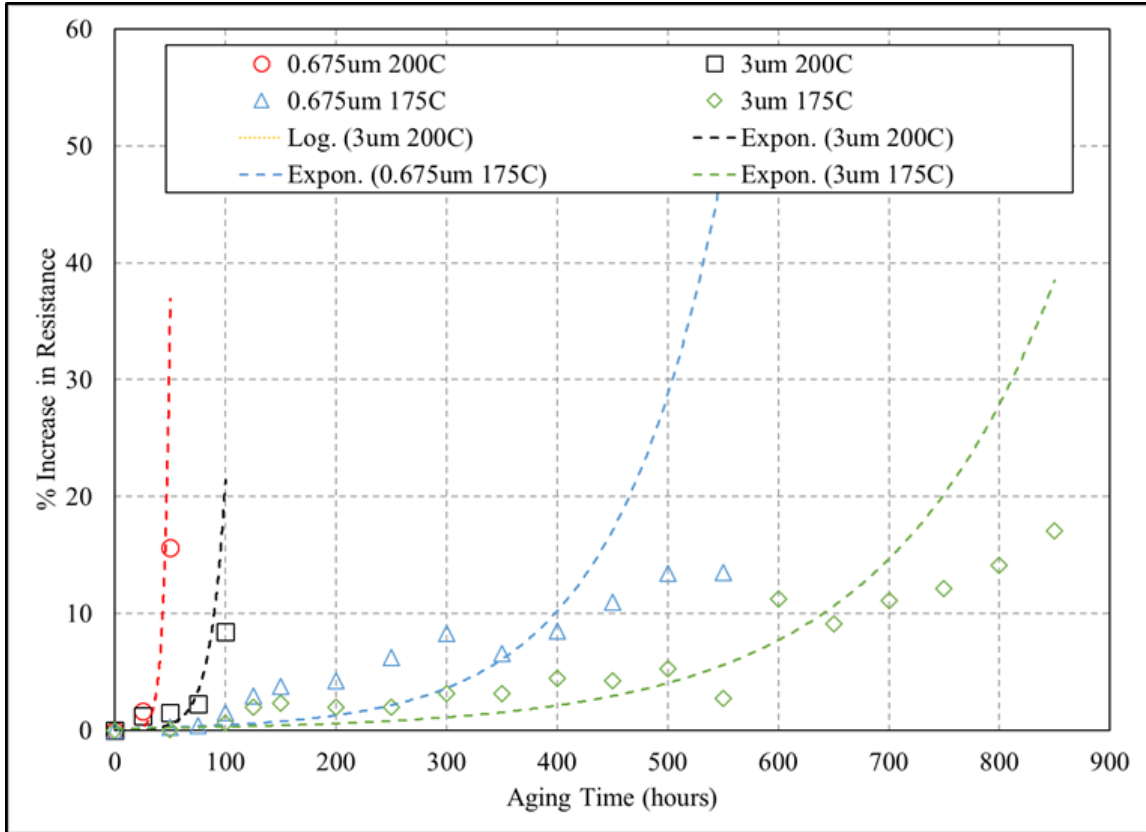
Figure 7.11: % Increase in Resistance as a Function of Isothermal Aging Time for Different Test Cases.

Exponential relationships were established from these data points and its coefficients are presented in the table below which can be used for estimating resistance increase in Cu wire bonds for two different pad thickness and temperature condition.

Table 7.1 Coefficients of Exponential Relationship.

Pad Thickness (μm)	Temperature (°C)	a	m
0.675	175	0.1624	0.0103
3	175	0.1622	0.0064
0.675	200	0.0024	0.1931
3	200	0.0122	0.0747

In this study, >20% increase in resistance is considered failure. Experimental time to failure values were used to obtain an empirical relationship to relate failure time and pad thickness at two different temperature conditions as shown below.

$$Time\ to\ Failure_{>20\%} = 64.663 \times e^{(0.2197 \times BPT)} \quad \text{at } 175°C$$

$$Time\ to\ Failure_{>20\%} = 533.37 \times e^{(0.174 \times BPT)} \quad \text{at } 200°C$$

Using the above relationship, failure time (20% resistance increase) of a bond for any bond pad thickness (BPT) at two different temperature can be identified. However, only two different pad thicknesses were used in the study, hence failure time estimation for any pad thickness between the two will have higher confidence than for extrapolation to other conditions. It can be observed that reliability of Cu wire bonds show an increase with the use of thick pads compared to thin pads, which helps delay growth of Cu_9Al_4 phase.

7.4. Conclusion

Bond pad thickness has a significant effect on the time to growth of Cu_9Al_4 phase, which has been identified in literature. This study is conducted with two pad thicknesses, 0.675 µm and 3 µm, while keeping all other factors constant. Results from this study shows an increased resistance with the thin pad compared to the thick pad. Rise in resistance occurs at a short time of aging with thin pad compared to the thick pad. Two isothermal aging conditions were used in this study to confirm this trend. Cu_9Al_4 formation due to lack of Al from pad material is considered to be reason for the earlier increase in resistance with the thin pad compared to the thick pad. EDS analysis was performed at both pad thickness

conditions, which showed presence of Cu_9Al_4 phase in the thin pad case and not in the thick pad case. A 20% increase in resistance is considered failure which is used to build an empirical relationship to identify failure time for different pad thickness at two temperature conditions.

7.5. Reference

[1] Song, M., Gong, G. L., Yao, J. Z., Xu, S., Lee, S., Han, M. C., & Yan, B. Y. (2010, December). Study of optimum bond pad metallization thickness for copper wire bond process. In *2010 12th Electronics Packaging Technology Conference*(pp. 597-602). IEEE.

[2] Sarobol, P., Williams, S., Rejent, J. A., Romero, J. A., Brumbach, M. T., McKenzie, B. B., & Vianco, P. T. (2016). *Understanding Cu-Al Limited-Volume Diffusion Towards Lifetime Prediction for Cu Wire Bonds* (No. SAND2016-9822C). Sandia National Lab.(SNL-NM), Albuquerque, NM (United States).

[3] Fan, S., Huang, L., Ho, M. C., & Hsieh, K. C. (2015, May). The intermetallic compound (IMC) growth and phase identification of different kinds of copper wire and Al pad thickness. In Electronic Components and Technology Conference (ECTC), 2015 IEEE 65th (pp. 1412-1416). IEEE.

[4] Hentzell, H. T. G., Thompson, R. D., & Tu, K. N. (1983). Inter-diffusion in copper–aluminum thin film bilayers. I. Structure and kinetics of sequential compound formation. Journal of applied physics, 54(12), 6923-6928.

[5] Kouters, M. H. M., Gubbels, G. H. M., & Yuan, C. A. (2012). Characterization of intermetallic compounds in Cu-Al ball bonds: mechanical properties, delamination strength and thermal conductivity (pp. 1-9). IEEE.

[6] Zhang, C., Yalamanchili, P., Al-Sheikhley, M., & Christou, A. (2004). Metal migration in epoxy encapsulated ECL devices. Microelectronics and reliability, 44(9-11), 1323-1330.

[7] Tan, C. M., Er, E., Hua, Y., & Chai, V. (1998). Failure analysis of bond pad metal peeling using FIB and AFM. IEEE Transactions on Components, Packaging, and Manufacturing Technology: Part A, 21(4), 585-591.

8. Contributions

Following are the contributions of this work.

1. First study to present the effect of combined thermal aging and thermal cycling reliability of Cu wire bonds, with two sets of accelerated test conditions namely, -40ºC to 150ºC and -40ºC to 185ºC.

    a. Combined effects of multiple variables were studied through use of COTS parts and important parameters that contribute to failure time grouping was identified.

    b. A systematic failure assessment showed interfacial separation between Cu_9Al_4 and Cu to be the governing cause of failure under long dwell thermal cycling condition.

    c. A data-based failure time model was developed to estimate failure time of a new device by evaluating 23 parameters of the wire bond at initial condition.

2. Effect of bond pad thickness on initial shear force was established. Ball bonds on thick pad was found to experience higher shear force compared to bonds on thin pad due to greater stress distribution in the former case. This was also confirmed by FEA which showed similar trend. Data from this study is used in the revision of JESD 22B116B standard.

3. A systematic approach was adopted to study effect of bond pad thickness on reliability of Cu wire bonds, which showed higher reliability with 3µm compared to 0.675 µm pad thickness under isothermal aging condition of 175ºC and 200ºC.

This was found to be caused by delayed growth of Cu_9Al_4 phase in the case of 3 µm pad.

4. Established empirical relationship between time to failure, bond pad thickness and temperature to assess reliability of wire bonds formed on different pad thicknesses.

9. Future Work

This work focused on understanding the reliability of Cu-Al interface degradation specifically for microelectronic packages. Failure mechanism in the long dwell thermal cycling study was identified as the interfacial separation between Cu_9Al_4 and Cu. However, the strength of this interface was not identified. Use of nano-indentation technique can give way to characterizing the interfacial strength which can then be used to understand what stress levels can cause propagation of this failure.

Part I of this study established a data-based failure estimation model to assess reliability of COTS parts with Cu wire bonds. 9 devices have been used in this study. Addition of more devices to this model is suggested to improve the confidence of the results from this method.

Part II of the study focused on understanding the effect of bond pad thickness on reliability of Cu wire bonds under two temperatures and two pad thickness condition. Addition of another temperature and pad thickness will provide additional data point for providing more confidence to the empirical relationship.

10. List of Publications

1. Manoharan, S., Krishnanramaswami, G., McCluskey, F. P., & Pecht, M. G. (2016, July). Failure mechanisms in encapsulated copper wire-bonded devices. In *Physical and Failure Analysis of Integrated Circuits (IPFA), 2016 IEEE 23rd International Symposium on the* (pp. 316-320). IEEE.

2. Manoharan, S., Patel, C., & McCluskey, P. (2016). Decapsulation of plastic encapsulated microelectronics with copper wire bonds. *High Temperature Electronics Conference*, *2016*(HiTEC), 000092-000096.

3. Manoharan, S., Patel, C., Hunter, S., & McCluskey, P. (2017). Effects of Bond Pad Thickness on Shear Strength of Copper Wire Bonds. *High Temperature Network Conference*, *2017*(HiTEN), 000068-000073.

4. Manoharan, S., Patel, C., & McCluskey, P. (2017, August). Advancements in Silver Wire Bonding. In *ASME 2017 International Technical Conference and Exhibition on Packaging and Integration of Electronic and Photonic Microsystems collocated with the ASME 2017 Conference on Information Storage and Processing Systems* (pp. V001T05A004-V001T05A004). American Society of Mechanical Engineers.

5. Manoharan, S., Hunter, S., & McCluskey, P. (2017, December). Bond pad effects on the shear strength of copper wire bonds. In *Electronics Packaging Technology Conference (EPTC), 2017 IEEE 19th* (pp. 1-6). IEEE.

6. Manoharan, S., Patel, C., Hunter, S., & McCluskey, P. (2018). Influence of Initial Shear Strength on Time-to-Failure of Copper (Cu) Wire Bonds in Thermal Aging Condition. *High Temperature Electronics Conference*, *2018*(HiTEC), 000032-000038.

7. Manoharan, S., Patel, C., Dunford, S., Morillo, C., & McCluskey, P. (2018, May). Aging Characteristics of Green Mold Compound for Use in Encapsulation of Microelectronic Devices. In *2018 IEEE 68th Electronic Components and Technology Conference (ECTC)* (pp. 1768-1773). IEEE.

8. Manoharan, S., Patel, C., McCluskey, P., & Pecht, M. (2018). Effective decapsulation of copper wire-bonded microelectronic devices for reliability assessment. *Microelectronics Reliability*, *84*, 197-207.

9. Gutierrez, E., Manoharan, S., Serebreni, M., & McCluskey, P. (2018, August). Mechanical Characterization of Transient Liquid Phase Sintered (TLPS) Cu-Sn. In *ASME 2018 International Technical Conference and Exhibition on Packaging and Integration of Electronic and Photonic Microsystems* (pp. V001T04A018-V001T04A018). American Society of Mechanical Engineers.

10. Manoharan, S., Patel, C., Hunter, S., & McCluskey, P. (2018). Mechanism of wire bond shear testing. *Microelectronics Reliability*, *88*, 738-744.

11. Li, N. M., Manoharan, S., Das, D., & McCluskey, P. (2018). Analysis of indentation measured mechanical properties on Multilayer Ceramic Capacitors (MLCCs). *Microelectronics Reliability*, *88*, 528-533.

12. Manoharan, S., Patel, C., Dunford, S., Beshears, J. and McCluskey, P., (2019). Life Prediction of Copper Wire Bonds in Commercial Devices Using Principal Component Analysis (PCA).

13. Manoharan, S., Li, N.M., Patel, C., Hunter, S. and McCluskey, P., (2018) Mechanics of Copper Wire Bond Failure due to Thermal Fatigue, 2018 IEEE *Electronics Packaging Technology Conference (EPTC)*.